Spring 5-31-2010

A study of probability distributions of DCT coefficients in JPEG compression

Gopal Thirumalai Narayanan
New Jersey Institute of Technology

ABSTRACT

A STUDY OF PROBABILITY DISTRIBUTIONS OF DCT COEFFICIENTS IN JPEG COMPRESSION

by
Gopal Thirumalai Narayanan

The Discrete Cosine Transform (DCT) used in JPEG compression has shown excellent energy compaction properties that rival that of the ideal Karhunen-Loève Transform. Lossy compression in JPEG is achieved by distorting 8x8 block DCT coefficients through quantization. It has been shown in literature that DC block DCT coefficients are Gaussian probability distributed and AC block DCT coefficients are Generalized Normal probability distributed.

In this investigation, three probability density models for individual modes of non-quantized AC block DCT coefficients are evaluated and are used as basis for the derivation of probability distributions for quantized block DCT coefficients. The suitability of each of the three derived models is evaluated using the Kolmogorov-Smirnov and χ^2 goodness-of-fit tests, and the moments of the best-fit model are derived. The best-fit model is applied to detect the presence and extent of JPEG compression history in bitmap images. A model for all quantized AC block DCT coefficients is derived using mixtures of individual quantized block DCT modes, and the model hence developed is used to validate the Generalized Benford's Law for leading digit distributions of quantized AC block DCT coefficients.

A STUDY OF PROBABILITY DISTRIBUTIONS OF DCT COEFFICIENTS IN JPEG COMPRESSION

by
Gopal Thirumalai Narayanan

A Thesis
Submitted to the Faculty of
New Jersey Institute of Technology
in Partial Fulfillment of the Requirements for the Degree of
Master of Science in Electrical Engineering

Department of Electrical and Computer Engineering

May 2010

APPROVAL PAGE

A STUDY OF PROBABILITY DISTRIBUTIONS OF DCT COEFFICIENTS IN JPEG COMPRESSION

Gopal Thirumalai Narayanan

4/20/2010

Dr. Yun Q. Shi, Thesis Advisor — Date
Professor of Electrical and Computer Engineering, NJIT

4/27/10

Dr. Atam P. Dhawan, Committee Member — Date
Distinguished Professor of Electrical and Computer Engineering, NJIT

04/20/2010

Dr. Jie Hu, Committee Member — Date
Assistant Professor of Electrical and Computer Engineering, NJIT

BIOGRAPHICAL SKETCH

Author: Gopal Thirumalai Narayanan

Degree: Master of Science

Date: May 2010

Undergraduate and Graduate Education:

- Master of Science in Electrical Engineering,
  New Jersey Institute of Technology, Newark, NJ, 2010

- Bachelor of Engineering in Electronics and Communication Engineering,
  Visvesvaraya Technological University, Belgaum, Karnataka, India, 2003

Major: Electrical Engineering

This thesis is dedicated to my mother and father, whose steadfast faith in my academic competence has helped me tackle the hardest trials, and to my sister, without whose constant presence, life in a foreign country would have been much harder.

ACKNOWLEDGMENT

I am deeply indebted to my thesis advisor, Dr. Yun Qing Shi, who spent many of his valuable hours in reviewing my research and my thesis document. Without his detailed critique of my work at critical points during the course of my study, this document would not have seen the light of day. I cannot thank him enough for having given me this wonderful opportunity to work in the rapidly evolving area of image forensics, and for having taught me the basics of image processing.

My gratitude goes to the members of my thesis committee, Dr. Atam P. Dhawan and Dr. Jie Hu of the Electrical and Computer Engineering Department of New Jersey Institute of Technology, for taking time from their busy schedules to critique my work. I would like to thank Dr. Dhawan for readily agreeing to be on my thesis committee and for his kind words on the days leading up to the defense. I would like to thank Dr. Hu for kindly agreeing to be on my thesis committee, despite my rather belated request.

A hearty thank you goes to Dr. Dongdong Fu, a former Ph.D student of Dr. Shi, who I have not had the pleasure of meeting, but whose paper on the Generalized Benford's Law provided the primary motivation for this thesis.

I would like to thank Dr. Ali N. Akansu of New Jersey Institute of Technology, whose excellent courses on Digital Signal Processing and Multiresolution Signal Analysis provided me with the knowledge necessary to understand the theory of transforms.

I am grateful to Dr. Ronald Kane, Dean of Graduate Studies at New Jersey Institute of Technology, whose insightful feedback on my thesis document was well complemented by his sparkling wit during the review.

Ms. Clarisa Gonzalez-Lenahan at the Office of Graduate Studies at New Jersey Institute of Technology responded promptly to my panicked queries regarding paper quality, and I am thankful to her for that.

Finally, my friend and housemate, Rahul, receives my sincere gratitude for his ready accommodation of my odd dining schedules. Without that, eating cooked food on a regular basis would have been but a distant dream.

TABLE OF CONTENTS

TABLE OF CONTENTS
(Continued)

TABLE OF CONTENTS
(Continued)

LIST OF TABLES

LIST OF TABLES
(Continued)

LIST OF FIGURES

LIST OF FIGURES
(Continued)

Figure **Page**

LIST OF FIGURES
(Continued)

LIST OF FIGURES
(Continued)

Figure **Page**

LIST OF SYMBOLS AND TERMS

Z	The set of integers.
R	The set of real numbers.
Z^+	The set of positive integers.
R^+	The set of positive real numbers.
C	The set of complex numbers.
L^2-*space*	The set of all square-integrable functions.
PDF	Probability Density Function.
PMF	Probability Mass Function.
DCT	Discrete Cosine Transform.
JPEG	Joint Photographic Experts Group.
IID	Independent and Identically Distributed.
IJG	Independent JPEG Group.
IJG Q-factor	The quality factor of JPEG compression using quantization tables specified in Annex K of the JPEG standard.
Leptokurtic PDF	A PDF that has a high value of kurtosis, leading to heavier tails.
Platykurtic PDF	A PDF that has a relatively low value of kurtosis.
Abscissa	The X-axis.

CHAPTER 1

INTRODUCTION

1.1 Objective

The objective of this thesis is to present new probability models for quantized and de-quantized block Discrete Cosine Transform (DCT) coefficients in JPEG compression, and to apply them to image forensic applications.

Three probability density functions (PDFs), i.e., Laplacian, Generalized Gaussian and Generalized Gamma distributions, are used as the basis models of non-quantized block DCT coefficients and the corresponding quantized DCT coefficient probability mass functions (PMFs) are derived. It is shown via χ^2 and Kolmogorov-Smirnov (KS) tests that the PMFs based on the Generalized Normal PDF are the most suitable distributions for both quantized and de-quantized DCT coefficients.

The most suitable PMF for de-quantized block DCT coefficients is then applied to a bitmap image to detect the presence of JPEG compression history. Further, the PMF is used to detect the level of any historical JPEG compression in the image. Finally, the quantized block DCT PMF is used to derive an approximate model for the first digit distributions of quantized block DCTs using finite mixtures and is used to validate the Generalized Benford Law [27].

1.2 Motivation

The primary motivation for this study is the scarcity of literature regarding the statistical properties of quantized and de-quantized block DCT coefficients in JPEG compression. In contrast with the large body of work available for the statistics of non-quantized DCT

coefficients, there have been very few publications discussing the statistics of quantized block DCTs, with the exception of [28], which models quantized block DCTs using a Generalized Laplace distribution. This thesis is therefore an attempt to derive such a model from the statistics of the process of quantization. The following questions will be explored.

1. What are the different kinds probability models associated with 2D DCT coefficients in JPEG compression?
2. What probability models are used for 2D block DCT coefficients in JPEG compression?
3. What are the most suitable probability distributions of quantized and de-quantized 2D block DCT coefficients in JPEG compression?
4. How may the probability distributions of quantized and de-quantized 2D block DCT coefficients be applied to image forensics?

Thus, this thesis presents novel models for quantized and de-quantized 2D block DCT distribution in JPEG compression. The latter model is shown to detect compression history in bitmaps, and is shown to outperform a classical approach [22] for compression history detection. The former model validates the Generalized Benford's Law model [27] from the perspective of quantized 2D block DCT distributions.

1.3 Thesis Structure

This thesis is structured as follows.

- **CHAPTER 1** presents the background to this thesis, such as JPEG compression, DCT and quantization.
- **CHAPTER 2** presents a detailed literature survey of probability density functions associated with 2D DCTs in JPEG.
- **CHAPTER 3** derives three distinct probability mass functions for de-quantized 2D block DCTs and compares them. The same process is carried out for quantized 2D block DCTs. The most suitable probability mass functions are presented and moments of those functions are derived.

- **CHAPTER 4** details applications of the probability mass functions derived in Chapter 3 and contrasts them against classical approaches.
- **CHAPTER 5** summarizes the results of the thesis and presents conclusions.

1.4 Background

JPEG compression has been the de-facto compression standard for image storage on different digital media, such as computers, cameras, cellphones and handheld multimedia players. JPEG is a lossy compression technique defined by ISO/IEC 10918-1 (1994) [9]. Owing to the relative simplicity of compression and decompression, JPEG images are susceptible to third-party tampering. The results of such tampering are often not visually evident, and research in the area of image forensics has sought to detect similar intrusions using JPEG image statistics.

1.4.1 JPEG Compression

The JPEG still image compression standard was ratified in 1993 by the ISO/IEC in the document ISO/IEC 10918-1. The standard specifies how a two-dimensional bitmap raster image may be compressed into a one-dimensional stream of data, with a lower bit allocation per pixel of the image, as compared to the original, uncompressed image. The process of JPEG compression is shown in the following figure.

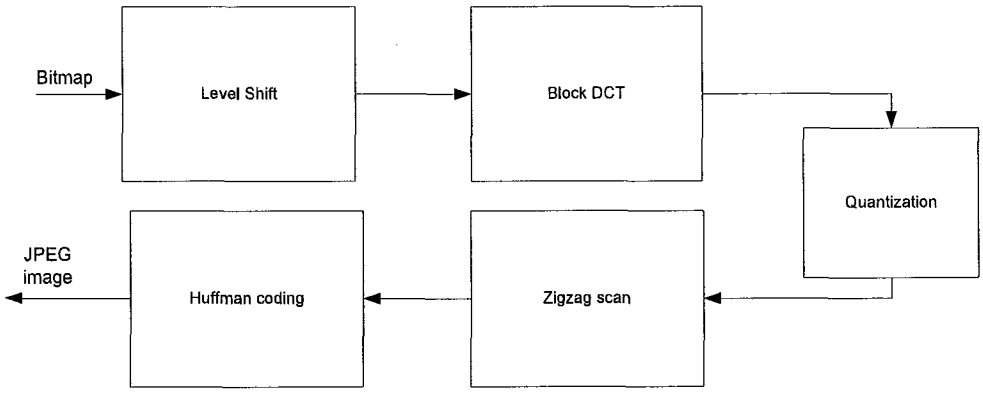

Figure 1.1 The JPEG Encoder Block Diagram.

Figure 1.1 shows the JPEG encoder block diagram. The input is a two-dimensional bitmap raster image to the Level Shift block.

The Level Shift removes the DC bias from the image pixels. It shifts the image pixels by $2^n - 1$, where n is the number of bits used to encode each pixel of the input bitmap.

The Block DCT performs type-II DCT, as detailed subsequently, on 8x8 sized non-overlapping sub-blocks of the image. The DCT is a unitary block transform that compacts the energy of the block into a limited number of nearly completely uncorrelated subbands [1] [2].

The Quantization block performs integer division on the 8x8 DCT block by a pre-calculated quantization matrix. This process involves integer rounding, which is irreversible and is the 'lossy' part of the compression process. To wit,

$$n = \left[\frac{x}{q}\right]. \tag{1.1}$$

Where n is the integer-rounded DCT value, x is the floating point DCT coefficient, q is the quantizer value and [...] is the process of rounding.

The Zigzag scan block converts the quantized 8x8 DCT block into a vector, by sorting it according to increasing frequency subbands. This process is needed to cluster the non-zero coefficients.

The Huffman coding block performs lossless entropy compression on the vector from the zigzag scan process.

The entire process outlined above is reversed on the decoder side. Huffman decoding is followed by a DCT de-quantization. The process of de-quantization involves multiplying the 2D block DCT coefficients by the same quantization matrix used during encoding. Therefore,

$$\tilde{x} = nq. \tag{1.2}$$

Where n is the integer-rounded DCT value, $\tilde{x}$ is an estimate of x, the floating point DCT coefficient and q is the quantizer value

Following the de-quantization, a 2D inverse DCT and a level shift is performed. The level-shifted value is rounded to the nearest integer to give the magnitude of the intensity of a pixel block.

JPEG compression leads to significant bit-per-pixel reduction. An uncompressed full color RGB image contains 24 bits to a pixel. After JPEG compression, depending on the image quality, the number of bits per pixel is reduced to a large extent, as shown in the following table. For reference, the uncompressed image has a size of 219726 bytes.

Table 1.1 Effect of JPEG compression on bits-per-pixel (bpp) of a color image

Quality Factor	**Compressed File Size** (Bytes)	**Bits Per Pixel**
100	83261	8.25
50	15138	5.5
10	4787	0.75
1	1523	0.13

Source: *JPEG* on Wikipedia. http://en.wikipedia.org/JPEG, retrieved March 16, 2010

1.4.2 Discrete Cosine Transform

The Discrete Cosine Transform (DCT) is a block transform[1] used in JPEG compression. The DCT was first proposed by Ahmed, Natarajan and Rao in [1]. It is a unitary transform that is closest in performance to the Karhunen-Loève Transform (KLT), in context of the following criteria:

- Energy compaction.
- Transform coefficient decorrelation.
- Rate distortion function.

The KLT [2] is an *optimal* block transform, in that the transform coefficients are completely decorrelated, and signal energy is compacted into the fewest subbands possible. This optimality is possible because the KLT basis vectors are input signal dependent. To elaborate, according to Mercer's theorem for finite dimensions [53], a square symmetric matrix can always be decomposed in the form,

$$S = UDU'.$$

Where S is the square symmetric matrix, U is orthogonal and its columns are the eigenvectors of S, U' is U's transpose and D, a diagonal matrix contains S's eigenvalues.

[1] A block transform is a finite length mapping from an $L^2(R)$ space to an $L^2(C)$ or $L^2(R)$ space. The mapping is bijective, and hence completely invertible. [2] has more information.

Using Mercer's theorem, Kari Karhunen and Michel Loève showed that the resulting transform coefficients are perfectly decorrelated for the case of centred stochastic processes, i.e., processes with zero mean.

When used as a transform, the matrix S is the autocorrelation matrix of the input signal and the matrix U is the KLT basis matrix. Consequently, the KLT is a signal dependent transform.

The DCT has the advantage over the KLT in that it is a signal independent transform [2]. As shall be seen subsequently, the DCT is an ideal transform for signals that may be modeled as Auto-Regressive (AR) random processes with a single historical coefficient, i.e., AR(1) random processes. Most natural images may be modeled as AR(1) processes [2].

The primary motivation for the DCT is that its basis vectors form a close approximation to the eigenvectors of the class of Toeplitz matrices shown below [2].

$$\psi = \begin{bmatrix} 1 & \rho & \dots & \rho^{M-1} \\ \rho & 1 & & \vdots \\ \vdots & & \ddots & \vdots \\ \rho^{M-1} & \dots & \dots & 1 \end{bmatrix}, \qquad 0 < \rho < 1. \tag{1.3}$$

This matrix is, in fact, the autocorrelation matrix of the AR(1) random process given as [2],

$$X[n] = \rho X[n-1] + W[n].$$

Where ρ is the correlation coefficient and $W[n]$ is a white noise process.

The eigenvectors of the autocorrelation matrix of a signal are the columns of the KLT forward transform block [2]. Thus, the forward DCT is a close approximation to the KLT of the class of signals modeled as AR(1) random processes.

To draw a parallel to the KLT in terms of matrix decomposition, the DCT is viewed as the eigenvectors of the following signal-independent tridiagonal matrix family [40].

$$B(\beta_1, \beta_2, \beta_3, \beta_4) = \frac{1}{2}\begin{bmatrix} \beta_1 & \beta_2 & & & & \\ 1 & 0 & 1 & & & \\ & 1 & 0 & 1 & & \\ & & & \ldots & & \\ & & & 1 & 0 & 1 \\ & & & & \beta_4 & \beta_4 \end{bmatrix}$$

The parameters β_1, β_2, β_3 and β_4 are determined from the boundary conditions imposed for the definition of the DCT. Püschel and Moura (2003) [40] explore DCT definitions in detail. In the context of this thesis, however, the second form of the DCT, known as type-II DCT, is of significance. For this specific case, the tridiagonal matrix is,

$$B(1,1,1,1) = \frac{1}{2}\begin{bmatrix} 1 & 1 & & & & \\ 1 & 0 & 1 & & & \\ & 1 & 0 & 1 & & \\ & & & \ldots & & \\ & & & 1 & 0 & 1 \\ & & & & 1 & 1 \end{bmatrix} \tag{1.4}$$

In signal processing literature, the tridiagonal form proposed by Strang (1999) [41] is preferred. Explicitly,

$$G = 2I - 2B(.)$$

Where I is the identity matrix.

Substituting from Equation (1.4),

$$G = \begin{bmatrix} 0 & -1 & & & \\ -1 & 1 & -1 & & \\ & -1 & 1 & -1 & \\ & & \cdots & & \\ & & -1 & 1 & -1 \\ & & & -1 & 0 \end{bmatrix} \tag{1.5}$$

The matrix G in Equation (1.5) is similar in magnitude to ψ in Equation (1.3), if the first and last diagonal terms are ignored, and if the value of ρ is close to 1. Therefore, the type-II DCT is comparable to the KLT in terms of matrix decomposition.

KLT basis corresponding to an AR(1) random process and DCT basis waveforms are shown in the following figure. The match between them is of note.

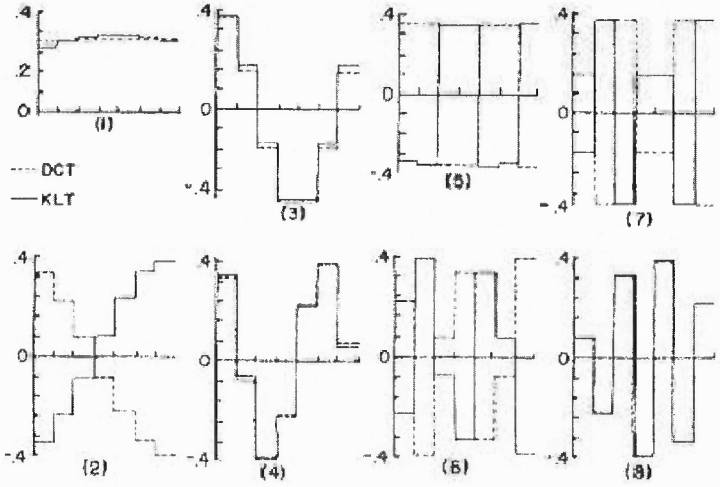

Figure 1.2 KLT basis vectors for the 8x8 Toeplitz matrix (with ρ = 0.9) and basis vectors of the DCT.

Source: N. Ahmed, T. Natarajan, and K. R. Rao, "Discrete Cosine Transform", IEEE Transactions on Computers, 90-93, Jan 1974.

The type-II DCT, which will henceforth be known simply as *DCT*, is analytically expressed for a real sequence of size M as,

$$G_x(0) = \frac{\sqrt{2}}{M}\sum_{m=0}^{M-1} X(m).$$

$$G_x(k) = \frac{2}{M}\sum_{m=0}^{M-1} X(m)cos\frac{(2m+1)k\pi}{2M}.$$

Where $X(m)$is the input data sequence, $G_x(k)$is the kth DCT coefficient.

The corresponding inverse transform is defined as,

$$X(m) = \frac{1}{\sqrt{2}}G_x(0) + \sum_{k=1}^{M-1} G_x(k)cos\frac{(2m+1)k\pi}{2M}.$$

By representing the forward and inverse DCTs in matrix form, it is seen that the inverse transform is the transpose of the forward transform, thus proving that the DCT is a real, unitary transform [2]. Therefore,

$$\Lambda^T\Lambda = \frac{M}{2}[I].$$

Where $[I]$ is an identity matrix, Λ is the forward transform matrix and Λ^T is its transpose.

Furthermore, [1], [3], [4], [5], [6] and [7] propose implementations of the DCT in $O(n\log_2 n)$ time complexity, with some of the implementations being based on the Cooley-Tukey FFT algorithm. Therefore, the DCT is a fast, practical alternative to the KLT for positively correlated signals.

The DCT definition is extended to two dimensions, and is defined in [8] as,

$$G_x(0,0) = \frac{1}{\sqrt{M}}\frac{1}{\sqrt{N}}\sum_{i=0}^{M-1}\sum_{j=0}^{N-1} X(i,j).$$

$$G_x(l,0) = \frac{\sqrt{2}}{\sqrt{M}}\frac{1}{\sqrt{N}}\sum_{i=0}^{M-1}\sum_{j=0}^{N-1} X(i,j)\cos\frac{(2i+1)l\pi}{2N}.$$

$$G_x(0,m) = \frac{1}{\sqrt{M}}\frac{\sqrt{2}}{\sqrt{N}}\sum_{i=0}^{M-1}\sum_{j=0}^{N-1} X(i,j)\cos\frac{(2j+1)m\pi}{2N}.$$

$$G_x(l,m) = \frac{\sqrt{2}}{\sqrt{M}}\frac{\sqrt{2}}{\sqrt{N}}\sum_{i=0}^{M-1}\sum_{j=0}^{N-1} X(i,j)\cos\frac{(2i+1)l\pi}{2N}\cos\frac{(2j+1)m\pi}{2N}.$$

Where the symbols have their usual meanings and (M, N) is the size of the 2D block.

The inverse 2D DCT is defined as,

$$X(i,j) = \frac{1}{\sqrt{M}}\frac{1}{\sqrt{N}}G_x(0,0) + \frac{\sqrt{2}}{\sqrt{M}}\frac{1}{\sqrt{N}}\sum_{m=1}^{N-1} G_x(l,0)\cos\frac{(2i+1)l\pi}{2N}$$

$$+ \frac{1}{\sqrt{M}}\frac{\sqrt{2}}{\sqrt{N}}\sum_{m=1}^{N-1} G_x(0,m)\cos\frac{(2j+1)m\pi}{2N}$$

$$+ \frac{\sqrt{2}}{\sqrt{M}}\frac{\sqrt{2}}{\sqrt{N}}\sum_{l=1}^{M-1}\sum_{m=1}^{N-1} G_x(l,m)\cos\frac{(2i+1)l\pi}{2N}\cos\frac{(2j+1)m\pi}{2N}.$$

As noted in Section 1.4.1, in JPEG compression, every 8x8 block in the image is transformed into an 8x8 transform block using the 2D DCT.

1.4.3 DCT Quantization

DCT coefficients in JPEG compression undergo a process of integer division called *quantization*. Quantization is an irreversible process where an 8x8 DCT sub-block is first divided coefficient-by-coefficient, by a fixed or adaptive matrix determined by an externally specified compression factor. The resultant matrix is then integer rounded. The externally specified compression factor generally ranges from 10 to 100, with 10 being the highest amount of compression and 100 being the lowest. This compression factor is typically denoted as *Q-factor*.

The choice of the quantization matrix set is determined by the designer of the JPEG encoder. The JPEG standard is only informative in this regard, but does provide example quantization tables. They are detailed in Annex K of [9] and may be used by an encoder. Those empirical matrix coefficients are based on psychovisual thresholding and luminance, chrominance and spatial image subsampling.

It is possible to derive quantization matrices using principles of rate distortion [10]. The process involves minimizing the distortion in the DCT coefficients, subject to a constrained data rate.

Quantization is a non-linear operation that modifies the probability distribution of the data being operated on. It is a lossy operation as well, and the error introduced due to this is a random variable with a statistical model that is generally approximated by a Uniform distribution [20] .

CHAPTER 2

LITERATURE SURVEY

This chapter focuses on detailing existing research on the various Probability Density Functions (PDFs) of DCT coefficients in JPEG compression. Different proposed models from existing literature for the PDFs of block DCT coefficients are explored in detail, while full-frame DCT and DCT quantization error probability distributions are explored briefly.

2.1 Block DCT PDF Models

In Section 1.4.1, it was stated that the process of JPEG compression divides an image into 8x8 non-overlapping sub-blocks. After Discrete Cosine transformation of each sub-block, an 8x8 block of coefficients is generated. Each of these 64 coefficients is treated as a distinct random variable, across multiple blocks of the image. The term *mode* is used to denote one of the 64 coefficients at a specific location in the block. For example, mode (1, 1) in an 8x8 DCT block is shown in the following figure.

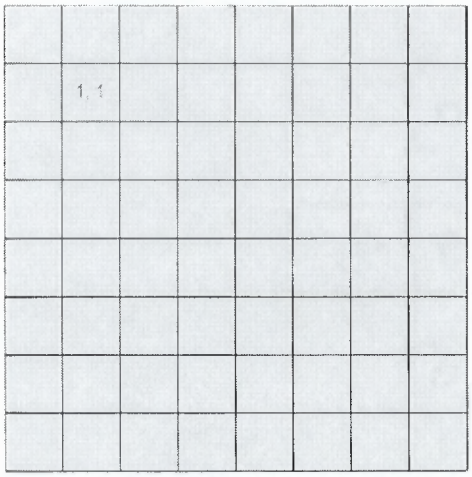

Figure 2.1 Mode (1, 1) in an 8x8 DCT coefficient block.

The mode (0, 0) will be known as the *DC* coefficient from this point onwards. This is because the DCT coefficient at (0, 0) is the average of the level shifted pixel values in the block. It has empirically been proven that the DC coefficient has a PDF that is different from the other modes of the DCT [12]. The *AC* coefficients, i.e., the coefficients at modes other than (0, 0) have been shown to have PDFs that are very similar to each other [12] [15] [17]. However, different papers have employed different PDFs to model AC block DCT coefficients. Following subsections detail three of the most commonly used PDF models for AC block DCT coefficients.

From this point on, *block DCT model* will denote the probability density model of a specific mode (generally AC) of the block DCT.

2.1.1 The Laplacian Model

The Laplacian model for AC DCT distributions is based on the Laplacian PDF. The Laplacian PDF [24] is given as,

$$f(x; b, \mu) = \frac{1}{2b} \exp\left\{-\left|\frac{x-\mu}{b}\right|\right\}. \tag{2.1}$$

Where μ is the mean of the distribution and b is the shape control parameter, related to the variance of the distribution.

This distribution is shown in the following plot.

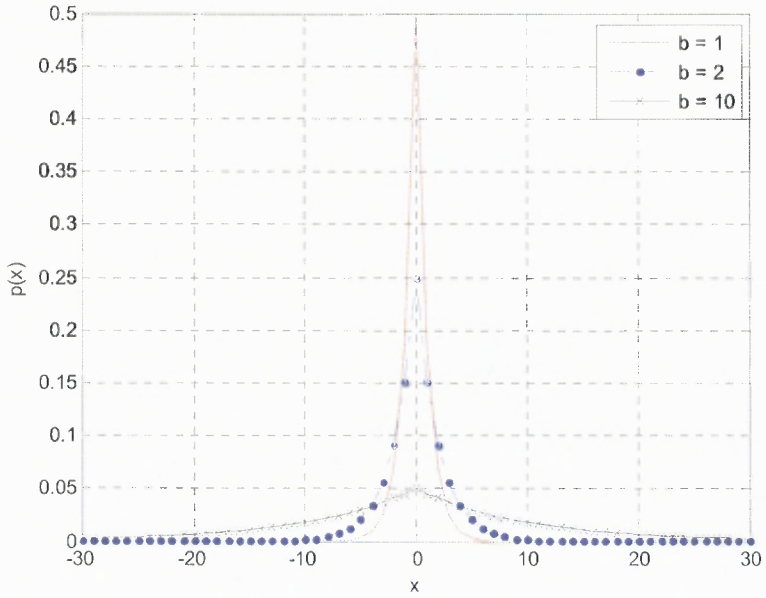

Figure 2.2 Laplace distributions for varying parameter *b*.

Early work on the distributions of 2D block DCT coefficients in images was carried out by Pratt (1978) [42], who conjectured that the DC coefficients should be Rayleigh distributed, since they are the sum of positive values (with the assumption of no level-shift), and that the AC coefficients, in general, must be Gaussian distributed as per the central limit theorem, with the assumption that each image pixel may be considered as being statistically independent from another. Tescher (1979) [43] and Murakami, Hatori and Yamamoto (1982) [44] indicated that the AC coefficients are best modeled as Laplacian, and the DC coefficients are best modeled as Gaussian. Reininger and Gibson (1983) summarized the findings in their seminal paper [12] and concluded that the DC coefficient is best modeled by a Gaussian PDF, while AC coefficients are best modeled by a Laplacian PDF. In concluding this, the paper evaluated Gaussian, Laplacian, Rayleigh and Gamma distributions for the DC coefficient and Gaussian, Laplacian and Gamma distributions for the AC coefficients.

Reininger and Gibson used the Kolmogorov-Smirnov (KS) test [14] on standard 256x256 8-bit PCM encoded grayscale images over multiple modes, to determine the goodness of fit of the different PMFs. The KS test detailed in Appendix A is summarized as follows.

The KS test is a distance measure between the sample distribution function and the given distribution function, with the distance given as follows.

$$t = \max_{i=1,2,\ldots M} |F_X(x_i) - F(x_i)|.$$

Where t is the KS test statistic. $F(x)$ is the input sample set with samples in $[1, M]$.

$$F_X(x) = \begin{cases} 0, & x < x_{(1)} \\ \dfrac{n}{M}, & x_{(n)} \leq x < x_{(n+1)}. \\ 1, & x \geq x_{(M)} \end{cases}$$

Where $x_{(n)}$ is the n^{th} order statistic of the data X.

The PDF with the lowest KS test statistic is the best fit distribution for the given data set.

The KS test results obtained in [12] are shown in the following figures for mode (0, 1) and (1, 0) AC coefficients.

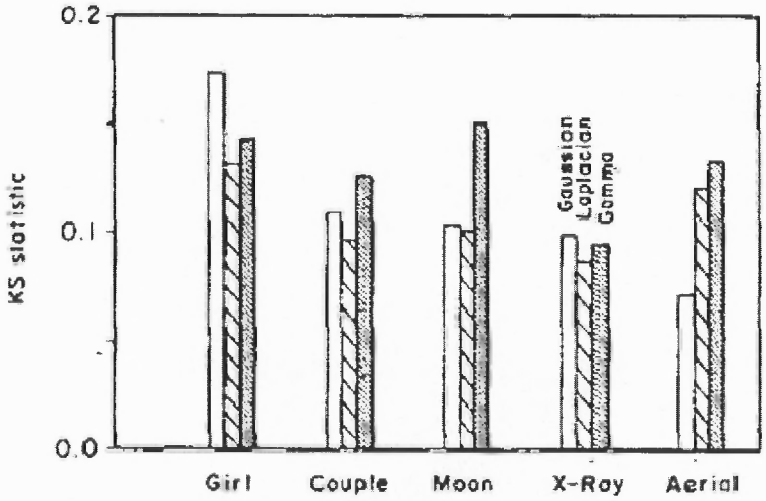

Figure 2.3 KS test statistics for mode (0,1) AC coefficients, for three different probability distributions, for five standard images.

Source: Reininger, R., and Gibson. J, 'Distribution of the two-dimensional DCT coefficients for images', IEEE Transactions on Communications, 1983, 31, (6)

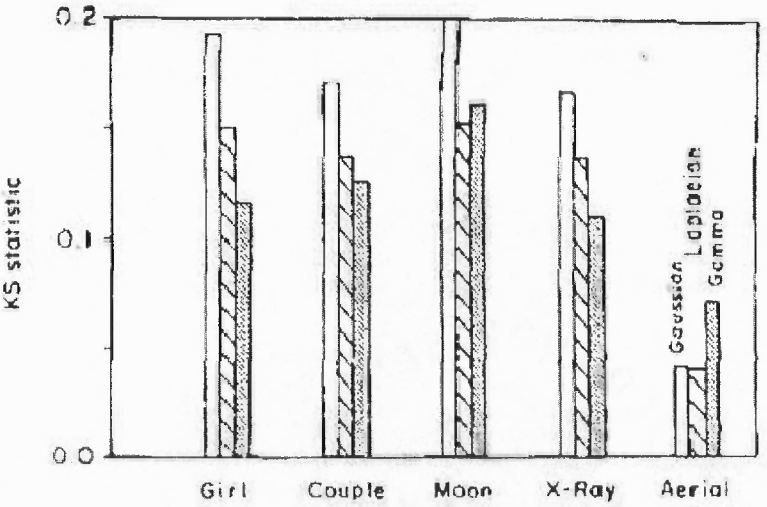

Figure 2.4 KS test statistics for mode (1,0) AC coefficients, for three different probability distributions, for five standard images.

Source: Reininger, R., and Gibson. J, 'Distribution of the two-dimensional DCT coefficients for images', IEEE Transactions on Communications, 1983, 31, (6)

From Figure 2.3 and Figure 2.4, it is seen that the Laplacian has the lowest KS test statistic for a majority of the images in both AC modes. Therefore, from these results

[12] concluded the Laplacian distribution was the most suitable PDF for AC block DCT coefficients.

2.1.2 The Generalized Normal Model

A second commonly employed model for AC block DCT PDF is the model based on the Generalized Normal distribution Nadarajah (2005) [15]. The Generalized Normal distribution specifies a family of PDFs with varying kurtosis [45]. The family therefore includes the entire range of well-known PDFs, from leptokurtic distributions such as the Laplacian to platykurtic distributions such as the Uniform distribution. [15] defines the Generalized Normal distribution as,

$$f(x;\sigma,\vartheta,\mu) = \frac{\vartheta\alpha(\vartheta)}{2\sigma\Gamma(1/\vartheta)}\exp\left\{-\left[\alpha(\vartheta)\left|\frac{x-\mu}{\sigma}\right|\right]^{\vartheta}\right\}. \quad (2.2)$$

Where μ is the mean of the distribution, σ is the standard deviation of the distribution, ϑ is the shape parameter of the distribution, related to its kurtosis, and, $\alpha(\vartheta) = \sqrt{\frac{\Gamma(3/\vartheta)}{\Gamma(1/\vartheta)}}$, where $\Gamma(...)$ is the complete Gamma function defined as,

$$\Gamma(z) = \int_0^{\infty} t^{z-1}e^{-t}dt$$

The Generalized Normal distribution for varying shape parameter ϑ is shown in the following plot. It is seen that for a high value of ϑ such as 100, the plot is nearly that of a Uniform distribution. Indeed, when ϑ is ∞, the Generalized Normal distribution defines a Uniform distribution. Similarly, when $\vartheta = 1$, it defines a Laplacian distribution and when $\vartheta = 2$, it defines a Normal distribution.

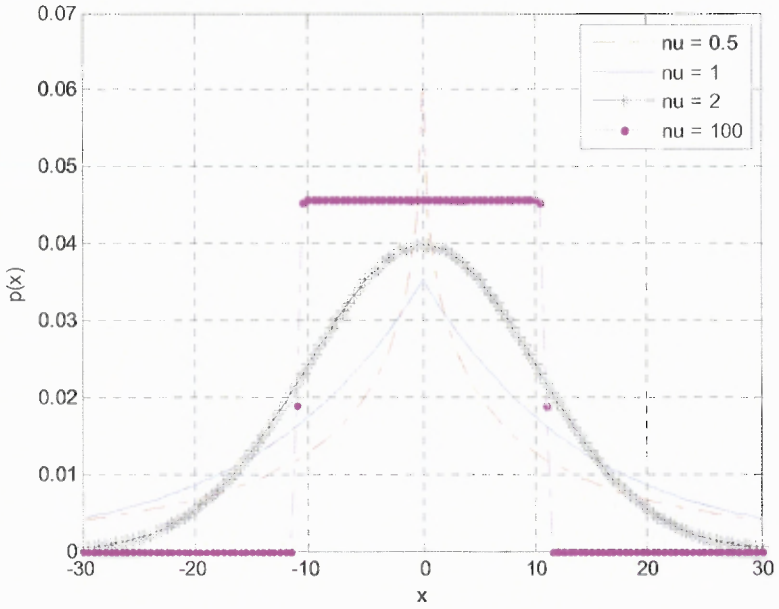

Figure 2.5 Generalized Normal distributions for varying parameter ϑ.

The parameters of this distribution are estimated from the random samples by maximizing the log-likelihood function with regard to each of the parameters. The estimation is briefly explored here.

The likelihood function for N Independent and Identically Distributed (IID) observations of the Generalized Normal is defined as,

$$L(x;\sigma,\vartheta,\mu) = \prod_{i=1}^{N} f(x_i;\sigma,\vartheta,\mu).$$

The log-likelihood function thereof is,

$$\log\big(L(x;\sigma,\vartheta,\mu)\big) = \sum_{i=1}^{N} \log\big(f(x_i;\sigma,\vartheta,\mu)\big).$$

Substituting from Equation (2.2) above,

$$\log\big(L(x;\sigma,\vartheta,\mu)\big) = \sum_{i=1}^{N} \log\left(\frac{\vartheta\alpha(\vartheta)}{2\sigma\Gamma(1/\vartheta)} \exp\left\{-\left[\alpha(\vartheta)\left|\frac{x_i-\mu}{\sigma}\right|\right]^{\vartheta}\right\}\right).$$

$$\log\big(L(x;\sigma,\vartheta,\mu)\big) = N\log\left(\frac{\vartheta\alpha(\vartheta)}{2\sigma\Gamma(1/\vartheta)}\right) + \sum_{i=1}^{N}\left\{-\left[\alpha(\vartheta)\left|\frac{x_i-\mu}{\sigma}\right|\right]^{\vartheta}\right\}.$$

Maximizing this log-likelihood function with respect to the parameters of the PDF implies,

$$\frac{\partial\log\big(L(x;\sigma,\vartheta,\mu)\big)}{\partial\vartheta} = 0. \tag{2.3}$$

$$\frac{\partial\log\big(L(x;\sigma,\vartheta,\mu)\big)}{\partial\sigma} = 0. \tag{2.4}$$

Du (1991) proposed the following equations as solutions to Equations (2.3) and (2.4).

For ϑ,

$$\frac{\psi\left(\frac{1}{\vartheta}+1\right)+\log(\vartheta)}{\vartheta^2} + \frac{1}{\vartheta^2}\log\left(\frac{1}{n}\sum_{i=1}^{n}|x_i|^{\vartheta}\right) - \frac{\sum_{i=1}^{n}|x_i|^{\vartheta}\log(|x_i|)}{\vartheta\sum_{i=1}^{n}|x_i|^{\vartheta}} = 0. \tag{2.5}$$

Where,

$$\psi(t) = -\gamma + \int_0^1 (1-t^{\tau-1})(1-t)^{-1}dt.$$

is the Digamma function ($\gamma = 0.577$ being the Euler constant). That is,

$$\psi(t) = \frac{d}{dt}\log\Gamma(t)$$

For σ,

$$\sigma^2 = \left[\frac{\tilde{\vartheta}\alpha(\tilde{\vartheta})^{\tilde{\vartheta}}\sum_{i=1}^{n}|x_i|^{\tilde{\vartheta}}}{n}\right]^{\frac{1}{\tilde{\vartheta}}}. \tag{2.6}$$

Where $\tilde{\vartheta}$ is the estimate of the shape factor, derived above.

Muller [15] showed that the Generalized Normal distribution model fits the PDF of AC block DCT coefficients better than the Laplacian distribution using the χ^2-Square test. This goodness-of-fit test, detailed in Appendix A is summarized as follows.

The empirical frequencies of the given data set X are compared with corresponding theoretical probabilities, to generate a test statistic χ^2 as follows.

$$\chi^2 = \sum_{i=1}^{k}\frac{(n_i - np_i)^2}{np_i}.$$

Where p_i is the probability of the i^{th} class of the standard distribution, m_i is the observed frequency in the i^{th} class of the input data set, k is the number of classes and N is the number of samples in the input set.

The PDF with the lower test statistic best matches the histogram of the given data set X.

The χ^2 test statistic for the Laplacian and Generalized Normal distributions as published in [15] is shown in the following table. Evidently, the Generalized Normal distribution is a better match for the AC block DCT histogram than the Laplacian distribution.

Table 2.1 $\chi 2$ test statistics for Laplacian (Laplace) and Generalized Normal (GN) distributions.

		Lena		Boats	
Mode		**k (class count)**	**$\chi 2$**	**k (class count)**	**$\chi 2$**
C10	GN	28	102	52	103
	Laplace		1524		2450
C01	GN	12	123	14	I52
	Laplace		1085		2143
C11	GN	12	70	10	25
	Laplace		2043		1169

Source: Muller, F.: Distribution Shape of Two-Dimensional DCT Coefficients of Natural Images,. Electronics Letters, 29, Oct. 1993, 1935–1936.

2.1.3 The Generalized Gamma Model

In 2005, Chang, Shin, Kim and Mitra proposed a model for block DCT coefficients based on the Generalized Gamma distribution (GΓF). The GΓF was developed for positive real values by E W Stacy (1962), and is given as,

$$f(x;\gamma,\beta,\eta) = \frac{\gamma\beta^{\eta-1}}{2\Gamma(\eta)} x^{\eta\gamma-1}\exp(-\beta x^{\gamma}), x \in R^{+}.$$

Where γ, β, η are model parameters.

Extending this to negative values [17],

$$f(x;\gamma,\beta,\eta,\mu) = \frac{\gamma\beta^{\eta}}{2\Gamma(\eta)} |x-\mu|^{\eta\gamma-1}\exp(-\beta|x-\mu|^{\gamma}), \forall\, x \in R. \quad (2.7)$$

A plot of the GΓF is shown in the following figure for varying parameters. It is of note that except in the case when the product of η and γ is 1, the distribution tends to 0 as x approaches 0.

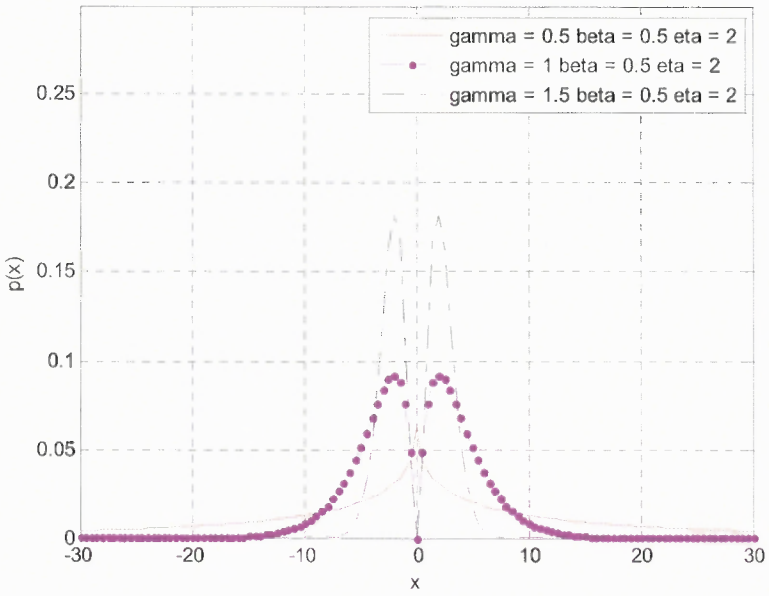

Figure 2.6 Generalized Gamma distributions for varying parameter γ.

The Generalized Normal (when $\eta\gamma = 1$), Gaussian (when $\gamma = 2$ and $\eta = 0.5$) and Laplacian (when $\gamma = 1$ and $\eta = 1$) PDFs are special cases of the GTF.

In the case of AC block DCT distributions, the mean of the distribution, μ is assumed zero. The remaining parameters are determined in a manner similar to the case of the Generalized Normal distribution, i.e., by minimizing the log-likelihood function of the PDF. From Equation (2.7),

$$L_f(x;\gamma,\beta,\eta) = \log\left[\prod_{i=1}^{n} \frac{\gamma\beta^{\eta}}{2\Gamma(\eta)} |x_i|^{\eta\gamma-1} \exp(-\beta|x_i|^{\gamma})\right].$$

Maximizing the log-likelihood for each of the parameters eventually leads to,

$$\beta = \frac{\eta}{\frac{1}{n}\sum_{i=1}^{n} |x_i|^{\gamma}}.$$

$$\psi(\eta) = \log\beta + \frac{1}{n}\sum_{i=1}^{n}\log|x_i|^{\gamma}.$$

$$\psi\left(\frac{\frac{1}{n}\sum_{i=1}^{n}|x_i|^{\gamma}}{\frac{1}{n^2}\sum_{i=1}^{n}\sum_{j=1}^{n}|x_i|^{\gamma}\log\frac{|x_i|^{\gamma}}{|x_j|^{\gamma}}}\right) + \log\left(\frac{1}{n^2}\sum_{i=1}^{n}\sum_{j=1}^{n}|x_i|^{\gamma}\log\frac{|x_i|^{\gamma}}{|x_j|^{\gamma}}\right) = \frac{1}{n}\sum_{i=1}^{n}\log|x_i|^{\gamma}.$$

$\psi(...)$being the digamma function.

Numerically solving these three equations in sequence gives the parameters of the model. [17] uses the χ^2-square goodness-of-fit test to evaluate the performance of the GΓF PMF across multiple modes using four standard 512x512 images. The results are summarized in the following table, where the term *image method* is used in lieu of the term *mode*.

Table 2.2 $\chi 2$ test statistics for Laplacian (Lap.), Generalized Normal (GGF) and Generalized Gamma (GΓF) distributions.

image	Lena			Boat			Barb			Baboon		
method	Lap.	GGF	GΓF	Lap.	GGF	GΓF	Lap.	GGF	GΓF	Lap.	GGF	GΓF
C_{10}	3096	890	831	3259	595	551	1041	257	256	253	226	196
C_{11}	4261	1296	892	3651	804	671	2234	405	400	264	260	215
C_{01}	2848	855	836	3730	735	706	1456	272	265	227	191	188
C_{20}	4258	1443	1257	5680	1301	1290	1947	360	352	414	360	272
C_{02}	4102	1215	1054	4036	835	701	2378	515	513	232	210	194
C_{12}	4680	1636	1278	5706	1762	1760	2925	629	607	298	269	218
C_{21}	5208	1845	1588	4450	950	837	2819	599	583	368	325	224
C_{03}	4164	1143	825	5001	1311	1296	2682	647	644	304	278	238
C_{30}	4259	1405	1292	7184	2054	2023	2357	490	470	373	285	207

Source: Chang, J.-H. Shin, J. W. Kim, N. S. Mitra, "Image Probability Distribution Based on Generalized Gamma Function", IEEE Signal Processing Letters, 2005.

The GΓF PDF is shown to outperform the Generalized Normal PDF by a small amount and the Laplacian PDF by a large amount. This is expected, since the GΓF PDF is more general than either of the distributions it is compared with.

2.1.4 Analytical Reasoning for 2D Block DCT PDFs

An analytical reasoning for the choice of the Laplacian and Generalized Normal distributions to model AC block DCT coefficients is briefly discussed in this subsection, with a summary of the paper by Lam and Goodman (2000) [16].

Recalling the 2D DCT $G_x(\ldots)$ on an 8x8 block $X(\ldots)$,

$$G_x(l,m) = \frac{c_l}{\sqrt{M}}\frac{c_m}{\sqrt{N}}\sum_{i=0}^{M-1}\sum_{j=0}^{N-1} X(i,j)\cos\frac{(2i+1)l\pi}{2N}\cos\frac{(2j+1)m\pi}{2N}.$$

$$c_l = \sqrt{2}\ for\ l \neq 0, and\ c_l = 1\ for\ l = 0.$$

$$c_m = \sqrt{2}\ for\ m \neq 0, and\ c_m = 1\ for\ m = 0.$$

The transform coefficient $G_x(l,m)$ is computed as a weighted sum of IID random variables, i.e., the weighted sum of the pixels of the block. Applying the Central Limit Theorem here, the transform coefficient can be approximated as a Gaussian random variable, assuming that the variance of each random variable, i.e., pixel, is known a priori. This is true even if the image pixels are slightly correlated, as noted in [16]. Therefore,

$$p(G_x(l,m)|\sigma^2) = \frac{1}{\sqrt{2\pi\sigma}}exp\left\{-\frac{{G_x}^2(l,m)}{2\sigma^2}\right\}.$$

Where σ^2 is the variance.

It follows that the probability distribution of DCT coefficients may be evaluated using conditional probability.

$$p\big(G_x(l,m)\big) = \int_0^\infty p(G_x(l,m)|\sigma^2)p(\sigma^2)d\sigma^2.$$

Where $p(\sigma^2)$ is the probability of the variance.

[16] showed empirically that the variance across blocks follows either an exponential distribution,

$$p(\sigma^2) = \lambda \exp(-\lambda\sigma^2), \sigma^2 > 0\,.$$

Where λ is a distribution variance control parameter.

or a half Gaussian distribution,

$$p(\sigma^2) = \frac{2}{\sqrt{2\pi}s}\lambda \exp\left(-\frac{\sigma^2}{2s^2}\right), \sigma^2 > 0.$$

Where s is a distribution variance control parameter.

With either distribution of the variance, the distribution of 2D block DCT coefficients is Laplacian. However, this is valid only for coefficients with fairly low values of kurtosis. When the kurtosis has a high value, the Generalized Normal is a better model for DCT distributions [16]. Since the Laplacian distribution is a special case of the Generalized Normal distribution, for a general kurtosis value, the Generalized Normal is the more appropriate distribution of the two.

There has been no literature on quantitative analysis of the Generalized Gamma distribution in the context of block DCT coefficients. This may perhaps be attributed to the fact that the paper by Chang et al. [17] is a relatively recent publication.

2.2 A Full-Frame DCT Model

The block DCT probability models explored in the previous section have been investigated in detail owing to their significance to image compression. Full-frame DCTs, on the other hand, have been investigated for their applications to image forensics as presented in Barni, Bartolini, Cappellini, Piva and Rigacci (1998) [18] and in Cox, Kilian, Leighton and Shamoon (1995) [47]. They will be briefly explored in this section.

In [18] a model for full-frame DCTs, based on previous models for block DCTs is proposed. Specific DCT coefficients are selected from a full-frame DCT block and their distributions are evaluated against Gaussian, Laplacian and Generalized Normal PDFs using $\chi 2$ test statistics, over multiple fixed sized images.

The DCT coefficients selected for this process from 170 256x256 images are taken from five equiangular sets of the full-frame DCT block. The distributions for the remaining coefficients are estimated via interpolation.

The coefficients are initially assumed to have a Generalized Normal distribution. This is acceptable, since both Gaussian and Laplacian distribution are special cases of the Generalized Normal distribution. The model parameters of the Generalized Normal distribution can be determined from the DCT coefficient data.

[18] reports that the shape defining parameter of the Generalized Normal PDF, ϑ, was found to be close to 1. This implies a leptokurtic distribution, such as a Laplacian PDF. It was therefore concluded that the distribution of full-frame DCT coefficients is Laplacian. The χ^2 test results from [18] are shown in the following figure.

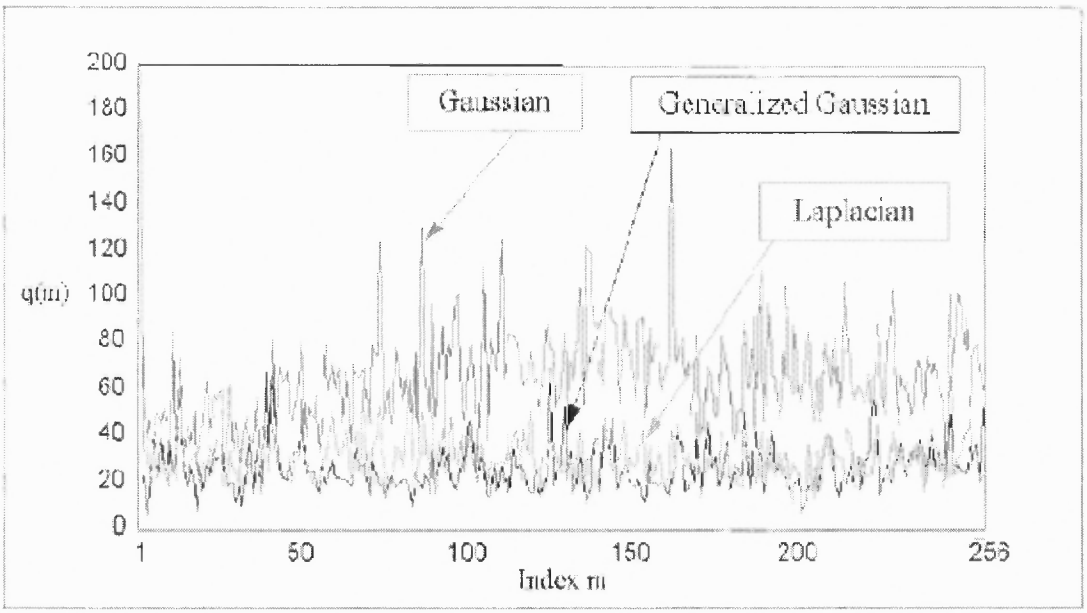

Figure 2.7 Results of χ^2 test under different PDF approximations.

Source: M. Barni, F. Bartolini, A. Piva, and F. Rigacci, "Statistical modeling of full frame DCT coefficients," in Proceedings of EUSIPCO'98, Rhodes, Greece, 1998

Thus, for full-frame DCTs the standard Laplacian PDF is found to have the lowest χ^2 test statistic amongst Laplacian, Gaussian and Generalized Normal distributions.

2.3 JPEG DCT Quantization Error Models

JPEG compression involves integer rounding of block DCT coefficients. Robertson and Stevenson (2001) [11] show that while the Uniform distribution is a convenient model for DCT quantization noise, it is not entirely accurate. This is due to the fact that in the case of DCT coefficients that are quantized to zero, such as high frequency coefficients in smooth areas of the image, the quantization error is better modeled with the Laplacian distribution. In the case of coefficients that are not quantized to zero, the Uniform distribution is the better model. This conclusion is of significance in Chapter 3.

CHAPTER 3

DISTRIBUTIONS OF QUANTIZED DCT COEFFICIENTS

In this chapter, the probability distributions of JPEG block DCT coefficients after quantization (known as *QPMF* henceforth) and the probability distributions of JPEG block DCT coefficients after de-quantization (known as *DQPMF* henceforth) are explored. The study of these coefficient distributions constitutes a large part of the original work in this thesis.

3.1 Introduction

The Probability Density Functions discussed in Section 2.1 characterized JPEG block DCT coefficients *before* the process of JPEG quantization. Those PDFs will be known as Pre-Quantized PDF (*PQPDF*) henceforth. Relevant parts the JPEG encoder and decoder in the following figure show where the QPMF, DQPMF and PQPDF fit in.

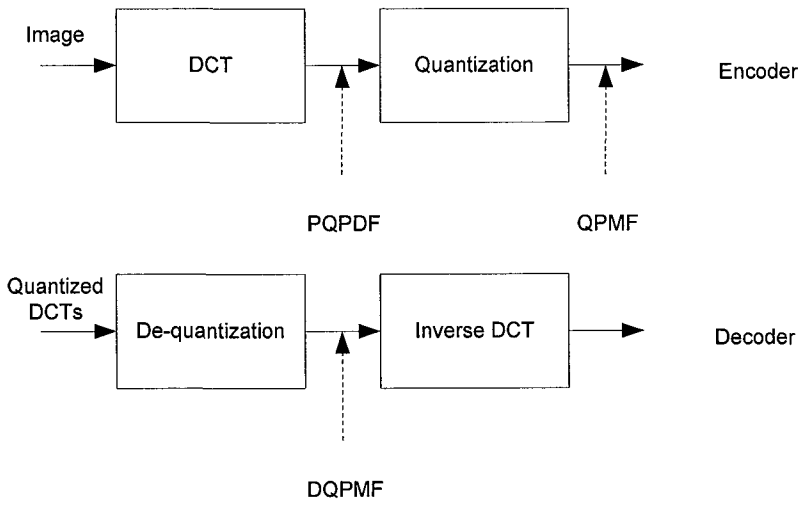

Figure 3.1 JPEG Encoder (a) and Decoder (b) sections showing the locations of the relevant PDFs and PMFs.

A lemma is now established, relating the QPMF and the DQPMF.

Lemma 3.1: The QPMF and DQPMF differ only by a deterministic, scalar multiplier. Intuitively, it may be concluded that while the QPMF exists, in theory, for all n (n being an integer), the DQPMF exists for all nq, with q being the scalar multiplier. Indeed, it may be concluded that the QPMF at a point k is relocated to the point kq in the DQPMF. The consequence thereof is that the QPMF and DQPMF are analytically identical, and differ in their abscissa only.

Expressions for QPMFs and DQPMFs are derived starting from the three PQPDFs detailed in Section 2.1. The derived PMFs take their names from the PQPDF on which they are based. Therefore, the following abbreviations are used.

- L-QPMF: The QPMF based on the Laplacian model for non-quantized block DCT.
- GN-QPMF: The QPMF based on the Generalized Normal model for non-quantized block DCT.
- GG-QPMF: The QPMF based on the Generalized Gamma model for non-quantized block DCT.
- L-DQPMF: The DQPMF based on the Laplacian model for non-quantized block DCT.
- GN-DQPMF: The DQPMF based on the Generalized Normal model for non-quantized block DCT.
- GG-DQPMF: The DQPMF based on the Generalized Gamma model for non-quantized block DCT.

The developed L-QPMF, GN-QPMF and GG-QPMF are compared against each other using goodness-of-fit tests. A similar comparison is made between the developed L-DQPMF, GN-DQPMF and GG-DQPMF. Expressions are then derived for the first four moments of the best fit QPMF and DQPMF, i.e., the PMFs with the lowest goodness-of-fit test statistics.

The approach used here to develop a DQPMF model differs from the approach used to model quantized JPEG DCT in Zou, Lu and Ling (2004) [28], in that the model developed in this study is formally derived from statistical properties of quantization. Furthermore, as shown in a subsequent section, the developed DQPMF and QPMF are based on the Generalized Normal, rather than the Generalized Laplacian used in the case of [28].

3.2 Analysis of the Statistics of Rounding and Quantization

A study of the effect of integer rounding and quantization on the statistics of a random variable is necessary for the derivation of the QPMF and DQPMF. Both rounding and quantization are non-linear operations, and have significant impact on the statistics of the operands, as will be seen subsequently.

The process of integer rounding is defined as follows.

$$n = [x] \mid \left(n - \frac{1}{2}\right) \leq x < \left(n + \frac{1}{2}\right) \qquad n \in Z \text{ and } x \in R.$$

$[\ldots]$ is the rounding operator.

Integer rounding is merely a special case of the broader concept of quantization, with the latter defined as,

$$n = Q(x) \mid \left(n - \frac{q}{2}\right) \leq x < \left(n + \frac{q}{2}\right).$$

$x \in R$. $q \in Z$ is the quantization parameter and $n \in Z$ is an integral multiple of q.

It must be mentioned at this point that the term *quantization* in the context of JPEG compression is defined differently from the same term in the broader context of signal processing. In the latter case, quantization is ultimately what is called *de-quantization* in the context of JPEG compression.

Titchmarsh (1986) [48] showed that the process of rounding and quantization may analytically be expressed as,

$$\text{Rounding: } n = [x] = x + \frac{1}{\pi}\sum_{k=1}^{\infty}\frac{\sin 2\pi kx}{k!}.$$

$$\text{Quantization: } n = Q(x) = x + \frac{q}{\pi}\sum_{k=1}^{\infty}\frac{\sin\left(2\pi k\frac{x}{q}\right)}{k!}.$$

Using the expressions above, it may be possible to determine the PDF of the quantized random variable. Random variable transformations as detailed in Kay (2005) [49] may be used to this effect. However, periodic, non-linear random variable transformations are often mathematically involved, and a sinusoidal transformation is no exception [19].

A significantly less mathematically involved, practical approach to deriving a PDF for the quantized random variable, involving operating on the analytical form of the PDF of the *non-quantized* random variable is presented in Widrow, Kollár and Liu (1996) [20] and is detailed in the following sub-section.

3.2.1 Deriving the PDF of Quantized Random Variables as per Widrow *et al.*

Linear systems principles were used in the approach presented by Widrow *et al.*, to develop an analytic form for the distribution of quantized random variables. The process, termed *area sampling* in [20], is detailed as follows.

1. The non-quantized random variable is considered as having a general bell-shaped probability distribution (PDF) as shown in Figure 3.2.

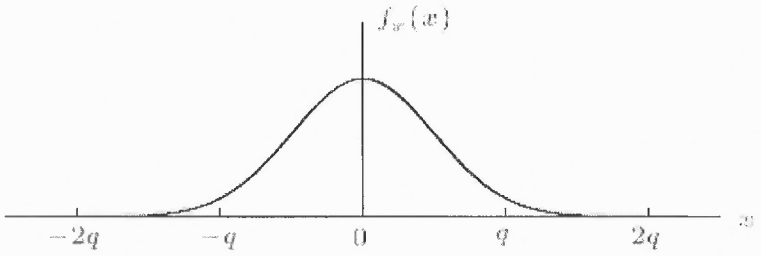

Figure 3.2 A General Bell-Shaped PDF.

Source: B. Widrow, I. Kollár, and M.C. Liu. Statistical theory of quantization. IEEE Transactions on Instrumentation and Measurement. 45(2):353-361, April 1996

2. This PDF is convolved with a Uniform distribution in the half-open interval, $(-q/2, q/2]$, where q is the quantization box size, as shown in Figure 3.4. The justification for performing this convolution is shown in the following systemic model, where the process of quantization is interpreted as adding Uniform distributed noise n to the non-quantized random variable x. [20] uses a Uniform noise PDF since it assumes a uniform quantizer.

   Indeed, as seen in Section 2.3, JPEG block DCT quantization error (or *noise*) is either Uniform distributed or Laplace distributed, depending on whether the magnitude of the error is close to a non-zero value or otherwise, respectively.

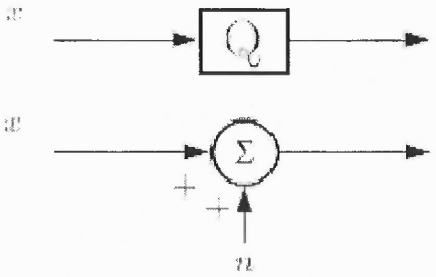

Figure 3.3 Systemic Model of Quantization.

Source: B. Widrow, I. Kollár, and M.C. Liu. Statistical theory of quantization. IEEE Transactions Instrumentation and Measurement.,45(2):353-361, April 1996

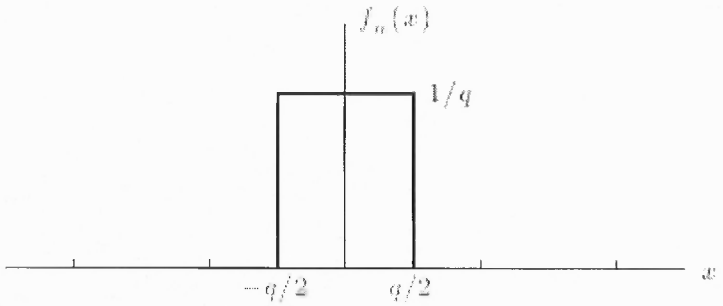

Figure 3.4 A Uniform Distribution in (*-q/2, q/2*].

Source: B. Widrow, I. Kollár, and M.C. Liu. Statistical theory of quantization. IEEE Transactions Instrumentation and Measurement.,45(2):353-361, April 1996

The result of the convolution operation is shown in the following figure, in the case of the interval $(-q/2, q/2]$ being significantly narrower than the width of the bell-shaped distribution. The procedure outlined here, however, imposes no such restriction on the size of the interval.

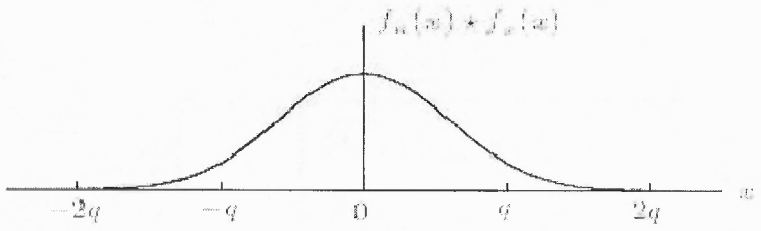

Figure 3.5 Result of Convolution.

Source: B. Widrow, I. Kollár, and M.C. Liu. Statistical theory of quantization. IEEE Transactions Instrumentation and Measurement.,45(2):353-361, April 1996

3. The result of the convolution is now sampled by an impulse train at multiples of q. This process, similar to sampling, results in a distribution function which exists only at integer multiples of q. The impulse train and the result of the sampling process are shown in the following figures.

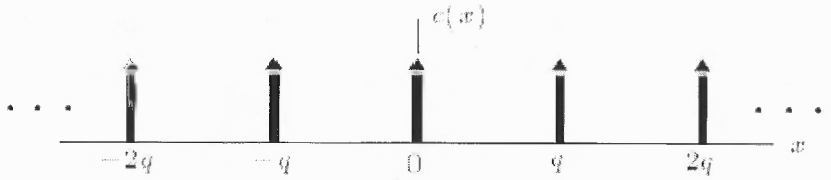

Figure 3.6 Impulse Train.

Source: B. Widrow, I. Kollár, and M.C. Liu. Statistical theory of quantization. IEEE Transactions Instrumentation and Measurement.,45(2):353-361, April 1996

The sampling leads to the following PDF.

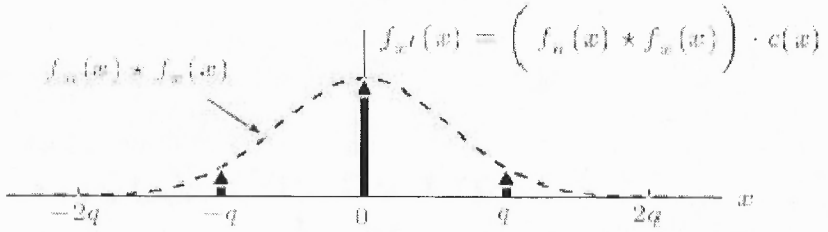

Figure 3.7 Result of Sampling.

Source: B. Widrow, I. Kollár, and M.C. Liu. Statistical theory of quantization. IEEE Transactions Instrumentation and Measurement.,45(2):353-361, April 1996

4. This sampled PDF can be converted to a discrete probability distribution function if unit impulse functions are used. The corresponding equation is as follows.

$$f_{x'}(x) = \big(f_n(x) * f_x(x)\big).\, c(x). \tag{3.1}$$

Where $f_{x'}(x)$ is the PDF of the quantized random variable, $f_n(x)$ is the Uniform PDF, $f_x(x)$ is the PDF of the non-quantized data and $c(x)$ is the impulse train.

In the context of JPEG block DCT distributions, $f_x(x)$ in Equation (3.1) is the PQPDF, and therefore could either be a Laplacian, a Generalized Normal or a Generalized Gamma distribution. The quantization *noise* is considered Uniform distributed, implying from Section 2.3 that the models will be better suited to coefficients that quantize to non-zero values. These basics will be used in the following section to develop expressions for the QPMFs corresponding to each PQPDF.

3.3 Quantized JPEG Block DCT PMFs

In this section, PMFs based on the Laplacian, Generalized Normal and Generalized Gamma distributions are developed. From each base distribution, the DQPMF is first derived, and the QPMF is deduced as per Lemma 3.1[2].

3.3.1 Quantized JPEG Block DCT PMFs Based on the Laplacian PDFs

The Laplacian PDF may be recalled from Equation (2.1) as,

$$p_X(x) = \frac{1}{2b}\exp\left(-\frac{|x-\mu|}{b}\right).$$

b is a parameter related to the variance of the PDF and μ is the mean of the PDF.

In the case of JPEG AC block DCTs, the mean may reasonably be assumed to be zero [16]. Therefore,

$$p_X(x) = \frac{1}{2b}\exp\left(-\frac{|x|}{b}\right). \tag{3.2}$$

To derive the expression for the Laplacian de-Quantized PMF (L-DQPMF), the procedure outlined in Section 3.2.1 is followed. Therefore, convolving Equation (3.2) with a Uniform PDF $f_n(x)$ in $(-q/2, q/2]$ as per Equation (3.1), the resulting PDF $f_R(t)$ is,

$$f_R(t) = p_X(x) * f_n(x).$$

$$f_R(t) = \frac{1}{2qb}\int_{t-\frac{q}{2}}^{t+\frac{q}{2}} \exp\left(-\frac{|x|}{b}\right) dx. \tag{3.3a}$$

Solutions to this integral are considered in the following cases.

---

[2] The Lemma states, "The DQPMF and QPMF are analytically identical, and differ only in their abscissa."

a. $\left[t-\frac{q}{2}<t<\ t+\frac{q}{2}\right]<0$:

In this case, $|x|=\ -x$. Therefore, Equation (3.3a) reduces to,

$$f_R(t)=\frac{1}{2qb}\int_{t-\frac{q}{2}}^{t+\frac{q}{2}}\exp\left(\frac{x}{b}\right)dx.$$

Evaluating,

$$f_R(t)=\frac{b}{2qb}\left[\exp\left(\frac{t+q/2}{b}\right)-\exp\left(\frac{t-q/2}{b}\right)\right].$$

Or,

$$f_R(t)=\frac{1}{2q}\left[\exp\left(\frac{t+q/2}{b}\right)-\exp\left(\frac{t-q/2}{b}\right)\right].$$

Expressed more concisely,

$$f_R(t)=\frac{1}{2q}\exp\left(\frac{t}{b}\right)\left[\exp\left(\frac{q}{2b}\right)-\exp\left(-\frac{q}{2b}\right)\right].$$

Since the term is the square braces is a hyperbolic sine,

$$f_R(t)=\frac{1}{q}\exp\left(\frac{t}{b}\right)\sinh\left(\frac{q}{2b}\right). \tag{3.3b}$$

b. $0<\left[t-\frac{q}{2}<t<\ t+\frac{q}{2}\right]$:

In this case, $|x|=\ x$. Equation (3.3a) reduces to,

$$f_R(t)=\frac{1}{2qb}\int_{t-\frac{q}{2}}^{t+\frac{q}{2}}\exp\left(-\frac{x}{b}\right)dx.$$

Evaluating the integral in a manner similar to the previous case,

$$f_R(t)=\frac{1}{q}\exp\left(-\frac{t}{b}\right)\sinh\left(\frac{q}{2b}\right). \tag{3.3c}$$

c. $t-\frac{q}{2}<0<t+\frac{q}{2}$:

The integral on either side of this interval centered at zero is split into two parts. Therefore from Equation (3.3a),

$$f_R(t)=\frac{1}{2qb}\left[\int_{t-\frac{q}{2}}^{0^-}\exp\left(\frac{x}{b}\right)dx+\int_{0^+}^{t+\frac{q}{2}}\exp\left(-\frac{x}{b}\right)dx\right].$$

Evaluating,

$$f_R(t)=\frac{b}{2qb}\left[1-\exp\left(\frac{t-q/2}{b}\right)+1-\exp\left(-\frac{t+q/2}{b}\right)\right].$$

And,

$$f_R(t)=\frac{1}{2q}\left[2-\exp\left(-\frac{t+q/2}{b}\right)+\exp\left(\frac{t-q/2}{b}\right)\right].$$

$$f_R(t)=\frac{1}{2q}\left[2-\exp\left(-\frac{q}{2b}\right)\left\{\exp\left(-\frac{t}{b}\right)+\exp\left(\frac{t}{b}\right)\right\}\right].$$

The term inside the braces is identified a hyperbolic cosine. Therefore,

$$f_R(t)=\frac{1}{q}\left[1-\exp\left(-\frac{q}{2b}\right)\cosh\left(\frac{t}{b}\right)\right]. \tag{3.3d}$$

Summarizing these results,

$$f_R(t)=\begin{cases}\frac{1}{q}\exp\left(\frac{t}{b}\right)\sinh\left(\frac{q}{2b}\right), & \left[t-\frac{q}{2}<t<t+\frac{q}{2}\right]<0.\\ \frac{1}{q}\left[1-\exp\left(-\frac{q}{2b}\right)\cosh\left(\frac{t}{b}\right)\right], & \left[t-\frac{q}{2}<0<t+\frac{q}{2}\right].\\ \frac{1}{q}\exp\left(-\frac{t}{b}\right)\sinh\left(\frac{q}{2b}\right), & \left[t-\frac{q}{2}<t<t+\frac{q}{2}\right]>0.\end{cases}$$

Or,

$$f_R(t)=\begin{cases}\frac{1}{q}\left[1-\exp\left(-\frac{q}{2b}\right)\cosh\left(\frac{t}{b}\right)\right], & \left[t-\frac{q}{2}<0<t+\frac{q}{2}\right].\\ \frac{1}{q}\exp\left(-\frac{|t|}{b}\right)\sinh\left(\frac{q}{2b}\right), & \text{otherwise.}\end{cases} \tag{3.4}$$

Finally, Equation (3.4) is multiplied by an impulse train at nq, as per Equation (3.1). Thus,

$$p_R(t) = \begin{cases} \frac{1}{q}\left[1 - \exp\left(-\frac{q}{2b}\right)\cosh\left(\frac{t}{b}\right)\right] q\delta(t) & t - \frac{q}{2} < 0 < t + \frac{q}{2}. \\ \frac{1}{q}\left[\exp\left(-\frac{|t|}{b}\right)\sinh\left(\frac{q}{2b}\right)\right] q\delta(t - lq) & \text{otherwise}, -\infty < l < \infty, l \neq 0. \end{cases}$$

The continuous abscissa impulse function, $\delta(t)$ in the equation above may be replaced with impulse function for a discrete axis, $\delta[n]$. Then,

$$p_R(n) = \begin{cases} \frac{1}{q}\left[1 - \exp\left(-\frac{q}{2b}\right)\cosh\left(\frac{n}{b}\right)\right] q\delta[n] & n = 0. \\ \frac{1}{q}\left[\exp\left(-\frac{|n|}{b}\right)\sinh\left(\frac{q}{2b}\right)\right] q\delta[n - lq] & n \neq 0, -\infty < l < \infty, l \neq 0, l \in Z. \end{cases}$$

More compactly,

$$p_R(nq) = \begin{cases} 1 - \exp\left(-\frac{q}{2b}\right) & n = 0. \\ \exp\left(-\frac{|nq|}{b}\right)\sinh\left(\frac{q}{2b}\right) & n \neq 0, n \in Z. \end{cases} \tag{3.5}$$

The result in Equation (3.5) is visually verified below. Laplacian random variables are generated with a fixed shaping factor b = 3. The random variables are quantized with the quantization steps, q = 1, 2 and 3. The following graphs plot the normalized histogram of these quantized random variables and the corresponding L-DQPMF.

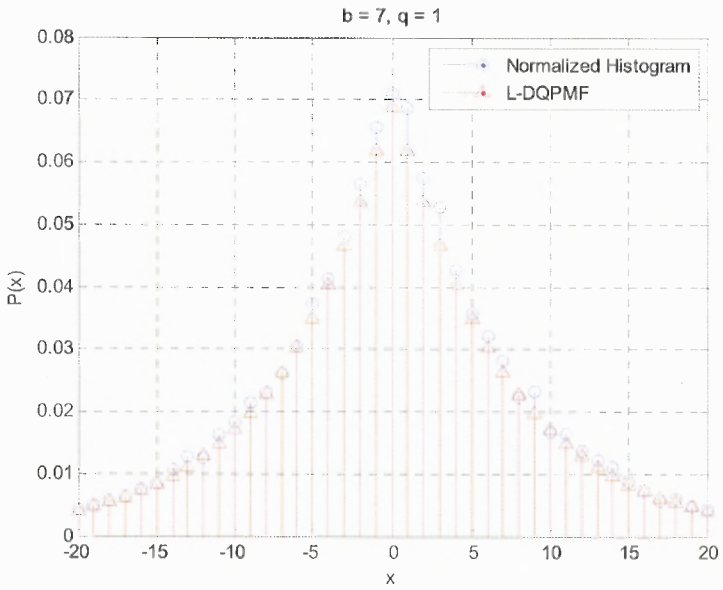

Figure 3.8 Normalized histogram and L-DQPMF with $b = 7$ and $q = 1$.

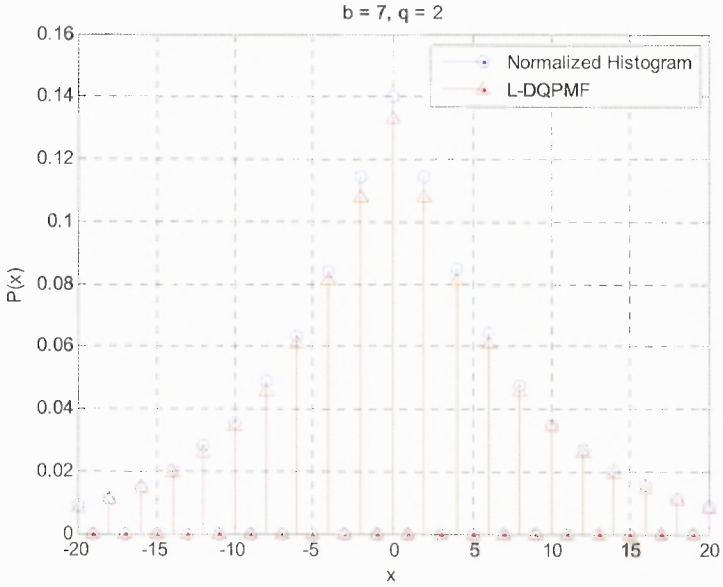

Figure 3.9 Normalized histogram and L-DQPMF with $b = 7$ and $q = 2$.

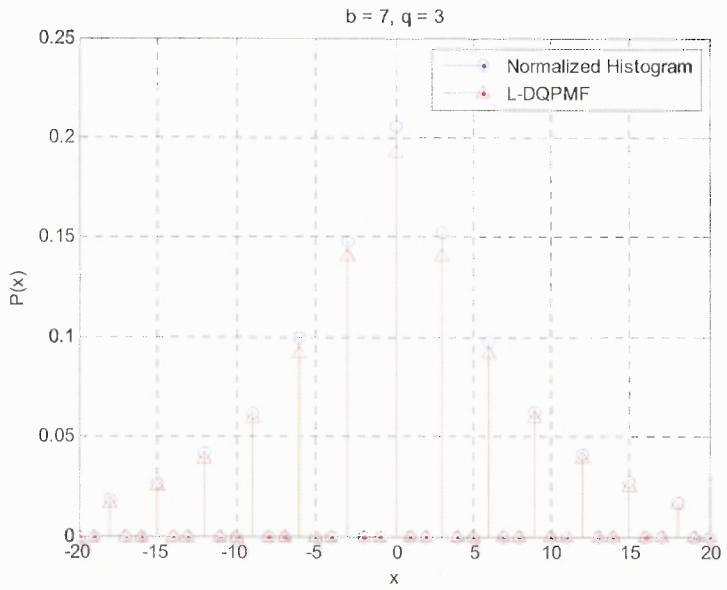

Figure 3.10 Normalized histogram and L-DQPMF with $b = 7$ and $q = 3$.

Visual evidence suggests that the L-DQPMF fits the empirical histogram well. This goodness of fit may be quantified with the KS and the χ^2 test statistic[3], as shown in a subsequent section.

An expression for the Laplacian Quantized PMF (L-QPMF) may be derived using Lemma 3.1 and Equation (3.5). Retaining the analytic form of Equation (3.5) for all integral n, the following relation describes the L-QPMF.

$$p_R(n) = \begin{cases} 1 - \exp\left(-\dfrac{k}{2b}\right) & n = 0. \\ \exp\left(-\dfrac{|kn|}{b}\right)\sinh\left(\dfrac{k}{2b}\right) & n \neq 0, n \in Z. \end{cases} \tag{3.6}$$

Equation (3.6) is visually verified below. Laplacian random variables are generated with a fixed shaping factor $b = 3$. The random variables are integer-divided by $k = 1$, 2 and 3. Normalized histograms of integer divided random variables and the corresponding L-QPMFs are plotted in the following graphs.

[3] Refer to Appendix A.

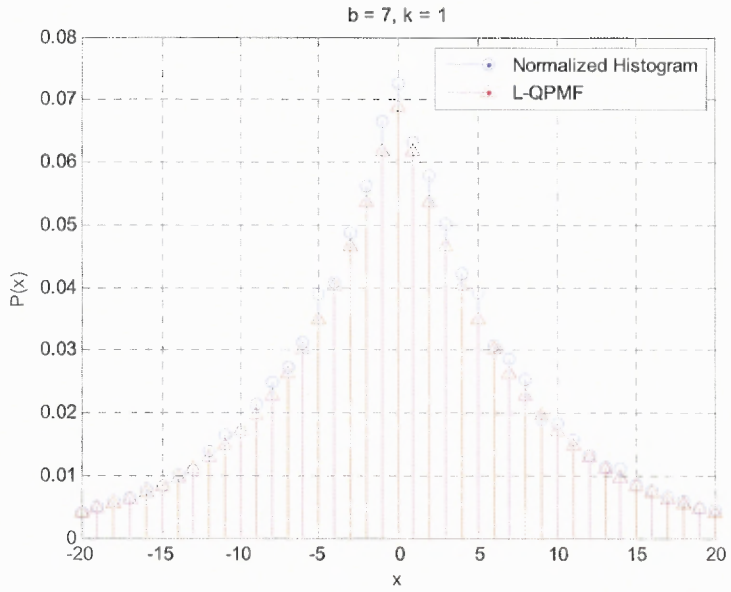

Figure 3.11 Normalized histogram and L-QPMF with $b = 7$ and $k = 1$.

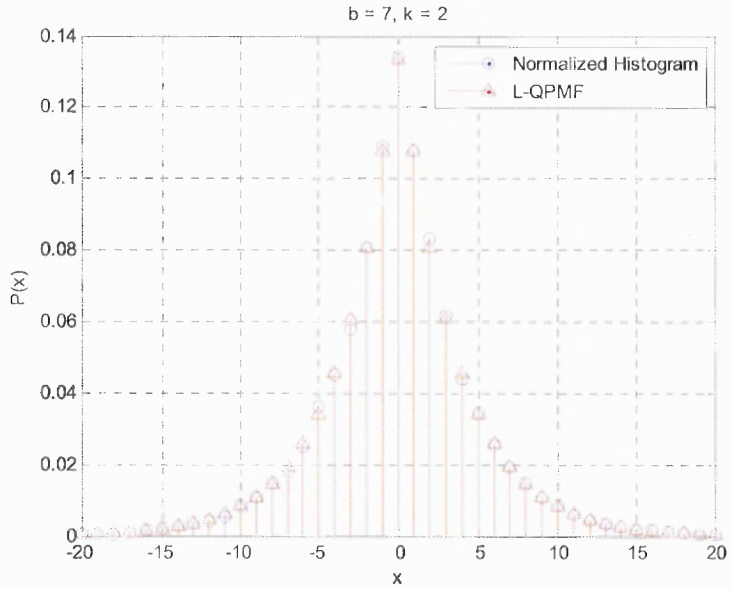

Figure 3.12 Normalized histogram and L-QPMF with $b = 7$ and $k = 2$.

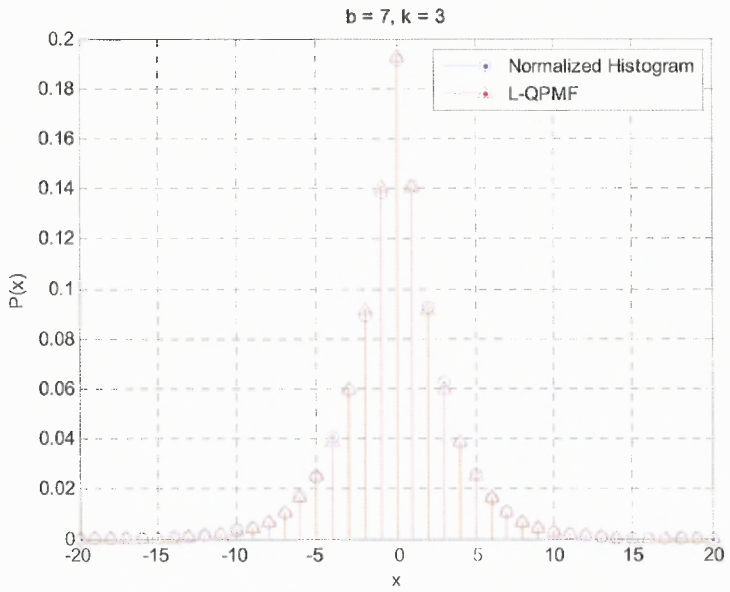

Figure 3.13 Normalized histogram and L-QPMF with $b = 7$ and $k = 3$.

Visual confirmation of the above fit is quantified with the KS and the χ^2 test statistics in a subsequent section.

3.3.2 Quantized JPEG Block DCT PMFs Based on the Generalized Normal PDFs

Models for GN-DQPMF and GN-QPMF may be derived starting from the Generalized Normal distribution, in a manner similar to the one outlined in the previous section.

The Generalized Normal distribution is recalled from Equation (2.2) as follows.

$$f(x;\sigma,\vartheta,\mu) = \frac{\vartheta\alpha(\vartheta)}{2\sigma\Gamma(1/\vartheta)}\exp\left\{-\left[\alpha(\vartheta)\left|\frac{x-\mu}{\sigma}\right|\right]^{\vartheta}\right\}.$$

Where μ is the mean of the distribution, σ is the standard deviation of the distribution, ϑ is the shape parameter of the distribution, related to its kurtosis, and, $\alpha(\vartheta) = \sqrt{\frac{\Gamma(3/\vartheta)}{\Gamma(1/\vartheta)}}$, where $\Gamma(\ldots)$ is the complete Gamma function defined as,

$$\Gamma(z) = \int_0^{\infty} t^{z-1}e^{-t}dt.$$

As in the previous section, the mean of the data may reasonably be assumed to be zero. Therefore, the PDF $p_X(x)$,

$$p_X(x) = \frac{\vartheta\alpha(\vartheta)}{2\sigma\Gamma(1/\vartheta)} \exp\left\{-\left[\alpha(\vartheta)\left|\frac{x}{\sigma}\right|\right]^{\vartheta}\right\}. \tag{3.7}$$

Now, the Gaussian Normal de-Quantized PMF (GN-DQPMF) and Gaussian Normal Quantized QPMF (GN-QPMF) are derived in a manner similar to the L-DQPMF and L-QPMF.

For the GN-DQPMF, Section 3.2.1 is recalled. Convolving Equation (3.7) with a Uniform PDF in $\left(-\frac{q}{2}, \frac{q}{2}\right]$, $f_n(x)$, as per Equation (3.1), the following PDF $f_R(t)$ is obtained.

$$f_R(t) = p_X(x) * f_n(x) = \int_{t-\frac{q}{2}}^{t+\frac{q}{2}} \frac{1}{q} \frac{\vartheta\alpha(\vartheta)}{2\sigma\Gamma(1/\vartheta)} \exp\left\{-\left[\alpha(\vartheta)\left|\frac{x}{\sigma}\right|\right]^{\vartheta}\right\} dx.$$

$$f_R(t) = \frac{1}{q} \frac{\vartheta\alpha(\vartheta)}{2\sigma\Gamma(1/\vartheta)} \int_{t-\frac{q}{2}}^{t+\frac{q}{2}} \exp\left\{-\left[\alpha(\vartheta)\left|\frac{x}{\sigma}\right|\right]^{\vartheta}\right\} dx. \tag{3.8}$$

This is a generic exponential-power integral, which cannot easily be evaluated in closed-form. For practical purposes, a numerical solution to this integral may be found using the Simpson's 1/3 rule for *small* and *smooth* intervals [21], stated here as follows. A general function, $f(x)$ is considered to be integrated in the interval $[x_0, x_2]$.

$$g = \int_{x_0}^{x_2} f(x)\, dx.$$

According to the Simpson's 1/3 rule, the integral is approximated as,

$$g = \int_{x_0}^{x_2} f(x)\, dx \cong \frac{h}{3}[f(x_0) + 4f(x_1) + f(x_2)].$$

Where $h = \frac{x_2 - x_0}{2}$ and $x_1 = x_0 + h = x_0 + \frac{x_2 - x_0}{2} = \frac{x_2 + x_0}{2}$. Therefore,

$$g = \int_{x_0}^{x_2} f(x)\,dx \cong \left(\frac{x_2 - x_0}{6}\right)\left[f(x_0) + 4f\left(\frac{x_2 + x_0}{2}\right) + f(x_2)\right]. \tag{3.9}$$

Applying Equation (3.9) to the integral in Equation (3.8),

$$f_R(t) = \frac{1}{q}\frac{\vartheta\alpha(\vartheta)}{2\sigma\Gamma(1/\vartheta)}\frac{q}{6}\left[\exp\left\{-\left[\alpha(\vartheta)\left|\frac{t + q/2}{\sigma}\right|\right]^{\vartheta}\right\} + 4\exp\left\{-\left[\alpha(\vartheta)\left|\frac{t}{\sigma}\right|\right]^{\vartheta}\right\} + \exp\left\{-\left[\alpha(\vartheta)\left|\frac{t - q/2}{\sigma}\right|\right]^{\vartheta}\right\}\right].$$

And,

$$f_R(t) = \frac{\vartheta\alpha(\vartheta)}{12\sigma\Gamma(1/\vartheta)}\left[\exp\left\{-\left[\alpha(\vartheta)\left|\frac{t + q/2}{\sigma}\right|\right]^{\vartheta}\right\} + 4\exp\left\{-\left[\alpha(\vartheta)\left|\frac{t}{\sigma}\right|\right]^{\vartheta}\right\} + \exp\left\{-\left[\alpha(\vartheta)\left|\frac{t - q/2}{\sigma}\right|\right]^{\vartheta}\right\}\right]. \tag{3.10}$$

The analytic form of Equation (3.10) is evaluated for the following cases.

a. $0 < \left[t - \frac{q}{2} < t < t + \frac{q}{2}\right]$:

In this case, $\left|\frac{t \pm q/2}{\sigma}\right| = -\left(\frac{t \pm q/2}{\sigma}\right)$. Therefore,

$$f_R(t) = \frac{\vartheta\alpha(\vartheta)}{12\sigma\Gamma(1/\vartheta)}\left[\exp\left\{-\left[-\alpha(\vartheta)\left(\frac{t + q/2}{\sigma}\right)\right]^{\vartheta}\right\} + 4\exp\left\{-\left[-\alpha(\vartheta)\left(\frac{t}{\sigma}\right)\right]^{\vartheta}\right\} + \exp\left\{-\left[-\alpha(\vartheta)\left(\frac{t - q/2}{\sigma}\right)\right]^{\vartheta}\right\}\right].$$

b. $0 < \left[t - \frac{q}{2} < t < t + \frac{q}{2}\right]$:

In this case, $\left|\frac{t \pm q/2}{\sigma}\right| = \left(\frac{t \pm q/2}{\sigma}\right)$. Therefore,

$$f_R(t) = \frac{\vartheta\alpha(\vartheta)}{12\sigma\Gamma(1/\vartheta)}\left[\exp\left\{-\left[\alpha(\vartheta)\left(\frac{t+q/2}{\sigma}\right)\right]^{\vartheta}\right\} + 4\exp\left\{-\left[\alpha(\vartheta)\left(\frac{t}{\sigma}\right)\right]^{\vartheta}\right\} + \exp\left\{-\left[\alpha(\vartheta)\left(\frac{t-q/2}{\sigma}\right)\right]^{\vartheta}\right\}\right].$$

c. $t - \frac{q}{2} < 0 < t + \frac{q}{2}$:

In this case, the general form derived in Equation (3.10) cannot be used, because the interval$\left(t - \frac{q}{2}, t + \frac{q}{2}\right]$ is not infinitely differentiable [50]. Indeed, since the Simpson's 1/3 rule is derived from the midpoint and trapezoidal integral approximations [21], the area in the integration interval must at the very least be trapezoidal in nature. In this scenario, there are two trapeziums, i.e., one before zero and one after zero, as shown in the figure on the following page. The areas of the trapeziums are approximations to the integrals.

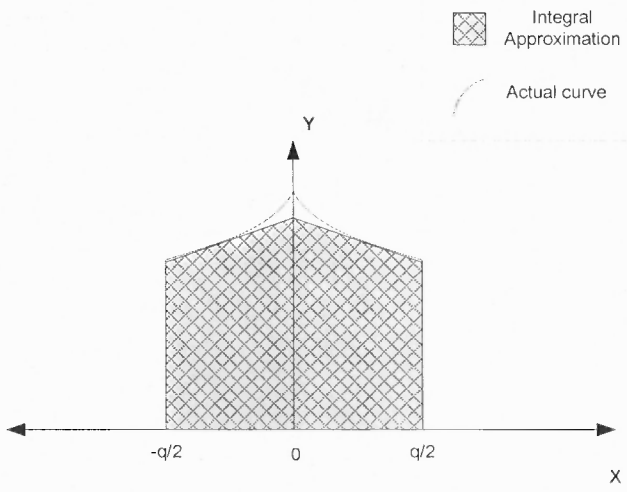

Figure 3.14 Trapezoidal approximation to the integral.

The integral for this interval may therefore be derived by dividing it into two half intervals. To wit,

$$f_R{}^{\pm}(t) = \frac{\vartheta\alpha(\vartheta)}{12q\sigma\Gamma(1/\vartheta)}\left(\frac{q}{2} + |t|\right)\left[\exp\left\{-\left[\alpha(\vartheta)\left|\frac{t - q/2}{\sigma}\right|\right]^{\vartheta}\right\}\right.$$

$$\left. + 4\exp\left\{-\left[\alpha(\vartheta)\left|\frac{t - q/2}{\sigma}\right|\right]^{\vartheta}\right\} + 1\right].$$

In $\left[t - \frac{q}{2}, 0^{-}\right]$, all values of the independent variable t are less than 0. Therefore,

$$f_R{}^{-}(t) = \frac{\vartheta\alpha(\vartheta)}{12q\sigma\Gamma(1/\vartheta)}\left(\frac{q}{2} - t\right)\left[\exp\left\{-\left[-\alpha(\vartheta)\left(\frac{t - q/2}{\sigma}\right)\right]^{\vartheta}\right\}\right.$$

$$\left. + 4\exp\left\{-\left[-\alpha(\vartheta)\left(\frac{t - q/2}{2\sigma}\right)\right]^{\vartheta}\right\} + 1\right].$$

In a similar fashion, in$\left[0^{+}, t + \frac{q}{2}\right]$, all values of the independent variable t are greater than or equal to 0. Therefore,

$$f_R{}^{+}(t) = \frac{\vartheta\alpha(\vartheta)}{12q\sigma\Gamma(1/\vartheta)}\left(t + \frac{q}{2}\right)\left[\exp\left\{-\left[\alpha(\vartheta)\left(\frac{t + q/2}{\sigma}\right)\right]^{\vartheta}\right\}\right.$$

$$\left. + 4\exp\left\{-\left[\alpha(\vartheta)\left(\frac{t + q/2}{2\sigma}\right)\right]^{\vartheta}\right\} + 1\right].$$

On careful examination, it becomes evident that $f_R{}^{-}(t)$ and $f_R{}^{+}(t)$ are of equal magnitude. Therefore, in the interval $\left[t - \frac{q}{2}, t + \frac{q}{2}\right]$,

$$f_R(t) = \frac{\vartheta\alpha(\vartheta)}{12q\sigma\Gamma(1/\vartheta)}\left(|t| + \frac{q}{2}\right)\left[\exp\left\{-\left[\alpha(\vartheta)\left(\frac{|t| + q/2}{\sigma}\right)\right]^{\vartheta}\right\}\right.$$

$$\left. + 4\exp\left\{-\left[\alpha(\vartheta)\left(\frac{|t| + q/2}{2\sigma}\right)\right]^{\vartheta}\right\} + 1\right]. \qquad (3.11)$$

Finally, Equations (3.10) and (3.11) are sampled by an impulse train. Thus the resultant distribution $p_R(nq)$ is,

$$p_R(nq) = \begin{cases} \frac{q\vartheta\alpha(\vartheta)}{12\sigma\Gamma(1/\vartheta)}\left[\exp\left\{-\left[\alpha(\vartheta)\left(\frac{q}{2\sigma}\right)\right]^{\vartheta}\right\} + 4\exp\left\{-\left[\alpha(\vartheta)\left(\frac{q}{4\sigma}\right)\right]^{\vartheta}\right\} + 1\right] & n = 0. \\ \frac{q\vartheta\alpha(\vartheta)}{12\sigma\Gamma(1/\vartheta)}\left[\exp\left\{-\left[\alpha(\vartheta)\left|\frac{nq+q/2}{\sigma}\right|\right]^{\vartheta}\right\} + 4\exp\left\{-\left[\alpha(\vartheta)\left|\frac{nq}{\sigma}\right|\right]^{\vartheta}\right\} + \exp\left\{-\left[\alpha(\vartheta)\left|\frac{nq-q/2}{\sigma}\right|\right]^{\vartheta}\right\}\right] & n \neq 0, n \in Z. \end{cases} \quad (3.12)$$

Equation (3.12) is visually verified as follows. Generalized Normal random variables are generated with a fixed standard deviation $\sigma = 10$ and shape factors $\vartheta = 0.5, 1$ and 2. It must be noted that the latter two shape factors correspond to Laplacian and Normal random variables, whose generation process is well-known [49] i.e., hard-thresholding logarithms of Uniform random variables generates Laplacian random variables, and the Box-Muller Transformation of Uniform random variables generates Normal random variables. The process to generate $\vartheta = 0.5$ random variables is not as well known, and involves using Lambert W functions [38] and Uniform random variables in a method developed in [31] and outlined in Appendix C. The random variables thus generated are quantized by q = 1, 2 and 3 respectively. The normalized histogram of the quantized random variables and the corresponding GN-DQPMFs are shown graphically in the following plots.

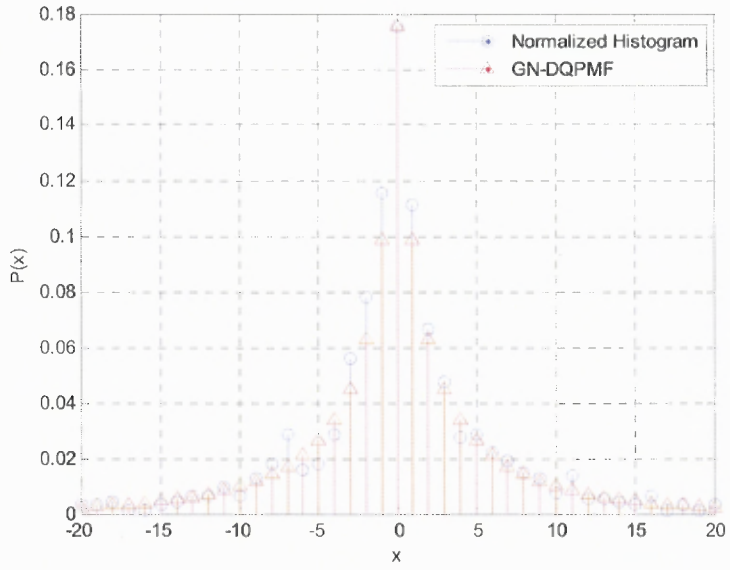

Figure 3.15 Normalized histogram and GN-DQPMF with $\vartheta = 0.5$ and $q = 1$.

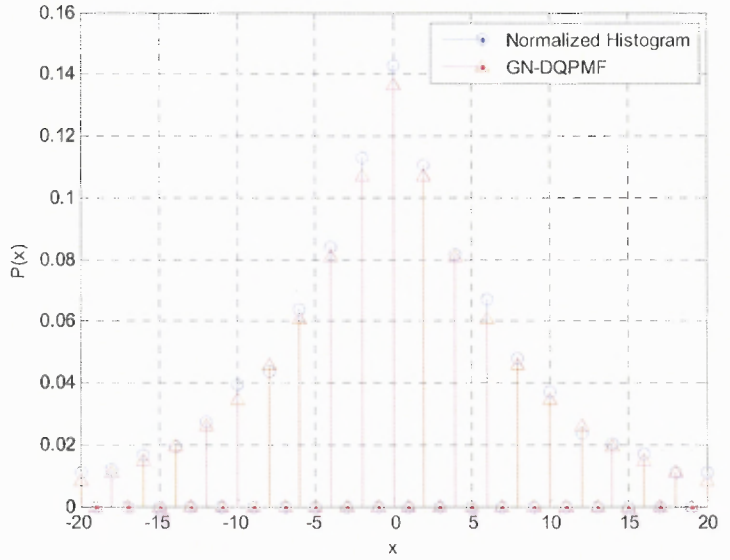

Figure 3.16 Normalized histogram and GN-DQPMF with $\vartheta = 1$ and $q = 2$.

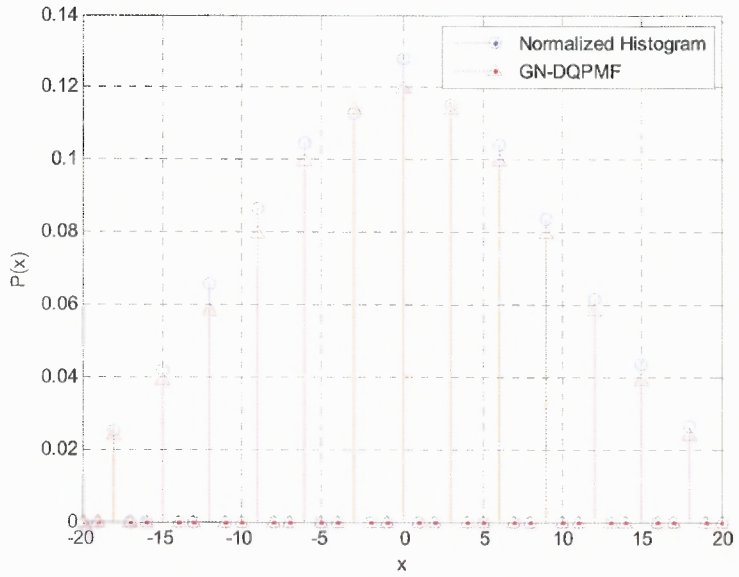

Figure 3.17 Normalized histogram and GN-DQPMF with $\vartheta = 2$ and $q = 3$.

An expression for the Generalized Normal Quantized PMF (GN-QPMF) may be derived by recalling Lemma 3.1. From Equation (3.12),

$$p_R(n) = \begin{cases} \dfrac{k\vartheta\alpha(\vartheta)}{12\sigma\Gamma(1/\vartheta)}\left[\exp\left\{-\left[\alpha(\vartheta)\left(\dfrac{k}{2\sigma}\right)\right]^{\vartheta}\right\} + \right. \\ \qquad \left. 4\exp\left\{-\left[\alpha(\vartheta)\left(\dfrac{k}{4\sigma}\right)\right]^{\vartheta}\right\} + 1\right] & n = 0. \\ \dfrac{k\vartheta\alpha(\vartheta)}{12\sigma\Gamma(1/\vartheta)}\left[\exp\left\{-\left[k\alpha(\vartheta)\left|\dfrac{n+1/2}{\sigma}\right|\right]^{\vartheta}\right\} + \right. & \\ \qquad 4\exp\left\{-\left[k\alpha(\vartheta)\left|\dfrac{n}{\sigma}\right|\right]^{\vartheta}\right\} + & \\ \qquad \left. \exp\left\{-\left[k\alpha(\vartheta)\left|\dfrac{n-1/2}{\sigma}\right|\right]^{\vartheta}\right\}\right] & n \neq 0, n \in Z. \end{cases} \tag{3.13}$$

Equation (3.13) is visually verified as follows. Generalized Normal random variables are generated with a fixed standard deviation $\sigma = 5\sqrt{2}$ and shape factors $\vartheta = 0.5$, 1 and 2. The random variables thus generated are integer divided by $k = 1$, 2 and 3

respectively. The histogram and the corresponding GN-QPMF are plotted in the following graphs.

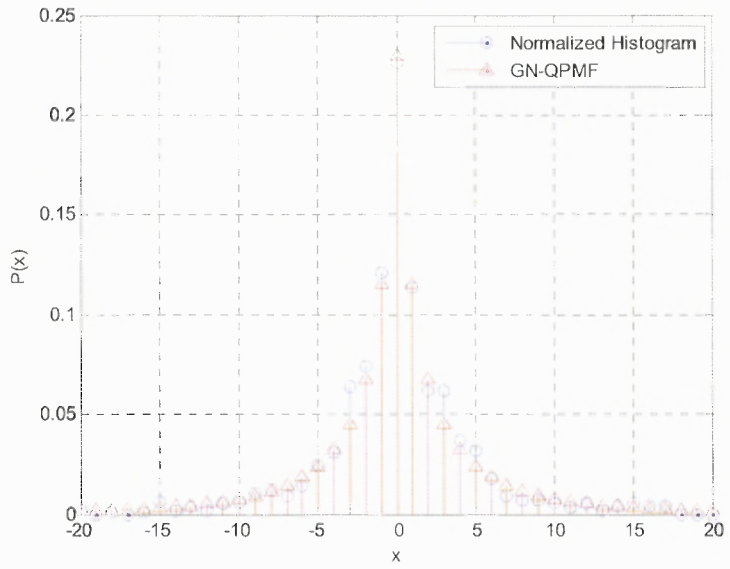

Figure 3.18 Normalized histogram and GN-QPMF with $\vartheta = 0.5$ and $k = 1$.

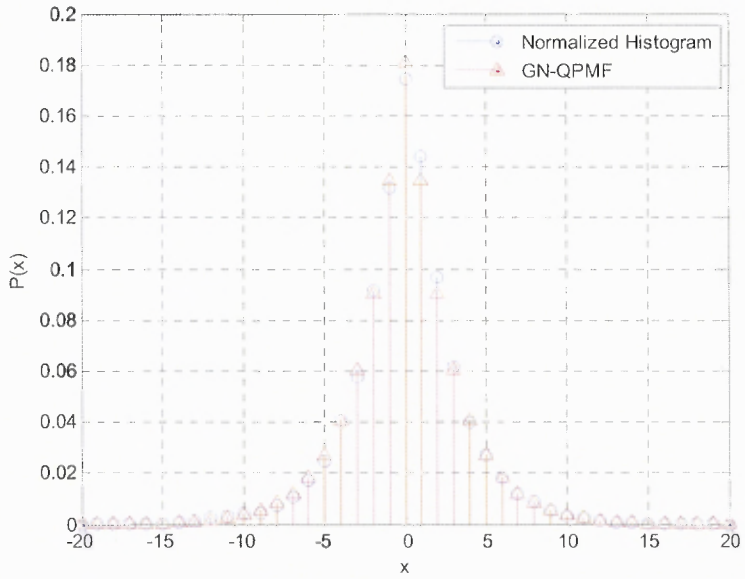

Figure 3.19 Normalized histogram and GN-QPMF with $\vartheta = 1$ and $k = 2$.

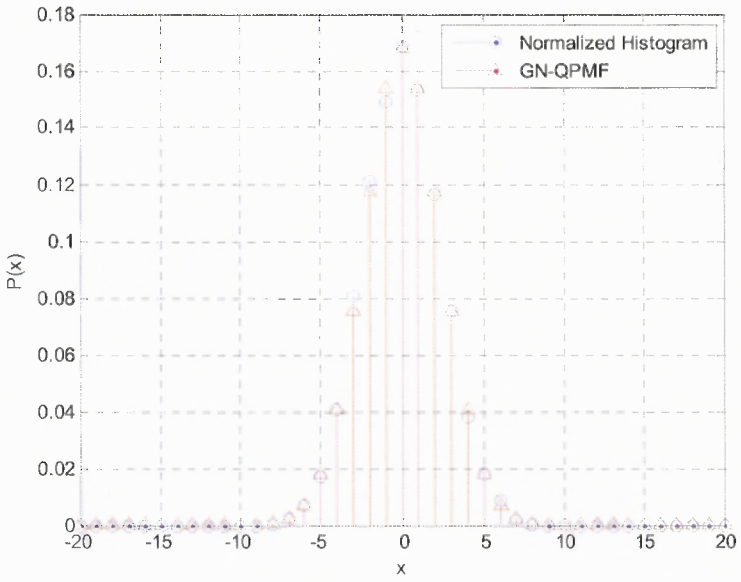

Figure 3.20 Normalized histogram and GN-QPMF with $\vartheta = 2$ and $k = 3$.

Visual confirmation of the above fits is quantified with the KS and the χ^2 test statistics in a subsequent section.

3.3.3 Quantized JPEG Block DCT PMFs Based on the Generalized Gamma PDFs

The Generalized Gamma PDF, $f(x; \gamma, \beta, \eta, \mu)$, is recalled from Equation (2.6) to be,

$$f(x; \gamma, \beta, \eta, \mu) = \frac{\gamma \beta^{\eta}}{2\Gamma(\eta)} |x - \mu|^{\eta\gamma - 1} \exp(-\beta |x - \mu|^{\gamma}), \forall\, x \in R.$$

As with earlier models, a zero mean is assumed for the current context. Therefore,

$$p_X(x) = \frac{\gamma \beta^{\eta}}{2\Gamma(\eta)} |x|^{\eta\gamma - 1} \exp(-\beta |x|^{\gamma}), \forall\, x \in R. \tag{3.14}$$

The Generalized Gamma Quantized and de-Quantized PMFs (GG-QPMF and GG-DQPMF respectively) are derived in a manner similar to corresponding derivations in previous sections.

Following the approach detailed in Section 3.2.1, convolving Equation (3.14) with a Uniform PDF in $\left(-\frac{q}{2},\frac{q}{2}\right]$ as per Equation (3.1), the PDF of the quantized data, $f_R(t)$ is obtained as follows.

$$f_R(t) = p_X(x) * f_n(x) = \int_{t-\frac{q}{2}}^{t+\frac{q}{2}} \frac{1}{q}\frac{\gamma\beta^{\eta}}{2\Gamma(\eta)}|x|^{\eta\gamma-1}\exp(-\beta|x|^{\gamma})\,dx.$$

$$f_R(t) = p_X(x) * f_n(x) = \frac{1}{q}\frac{\gamma\beta^{\eta}}{2\Gamma(\eta)}\int_{t-\frac{q}{2}}^{t+\frac{q}{2}} |x|^{\eta\gamma-1}\exp(-\beta|x|^{\gamma})\,dx. \qquad (3.15)$$

As in the previous section, this integral is best evaluated using the Simpson's 1/3 rule, recalled here from Equation (3.9).

$$\int_{x_0}^{x_2} f(x)\,dx \cong \left(\frac{x_2 - x_0}{6}\right)\left[f(x_0) + 4f\left(\frac{x_2 + x_0}{2}\right) + f(x_2)\right].$$

Therefore,

$$f_R(t) = \frac{1}{q}\frac{\gamma\beta^{\eta}}{2\Gamma(\eta)}\frac{q}{6}\left[\left|t+\frac{q}{2}\right|^{\eta\gamma-1}\exp\left(-\beta\left|t+\frac{q}{2}\right|^{\gamma}\right) + 4|t|^{\eta\gamma-1}\exp(-\beta|t|^{\gamma}) + \left|t-\frac{q}{2}\right|^{\eta\gamma-1}\exp\left(-\beta\left|t-\frac{q}{2}\right|^{\gamma}\right)\right].$$

And,

$$f_R(t) = \frac{\gamma\beta^{\eta}}{12\Gamma(\eta)}\left[\left|t+\frac{q}{2}\right|^{\eta\gamma-1}\exp\left(-\beta\left|t+\frac{q}{2}\right|^{\gamma}\right) + 4|t|^{\eta\gamma-1}\exp(-\beta|t|^{\gamma}) + \left|t-\frac{q}{2}\right|^{\eta\gamma-1}\exp\left(-\beta\left|t-\frac{q}{2}\right|^{\gamma}\right)\right].$$

This expression is evaluated for three cases as follows.

a. $\left[t-\frac{q}{2} < t < t+\frac{q}{2}\right] < 0$:

In this case, $\left|t+\frac{q}{2}\right| = -t-\frac{q}{2}$. Therefore,

$$f_R(t) = \frac{\gamma\beta^{\eta}}{12\Gamma(\eta)}\left[\left(-t-\frac{q}{2}\right)^{\eta\gamma-1}\exp\left(-\beta\left(-t-\frac{q}{2}\right)^{\gamma}\right) + 4(-t)^{\eta\gamma-1}\exp(-\beta(-t)^{\gamma})\right.$$

$$\left. + \left(-t+\frac{q}{2}\right)^{\eta\gamma-1}\exp\left(-\beta\left(-t+\frac{q}{2}\right)^{\gamma}\right)\right]. \qquad (3.16)$$

b. $0 < \left[t-\frac{q}{2} < t < t+\frac{q}{2}\right]$:

In this case, $\left|t+\frac{q}{2}\right| = t+\frac{q}{2}$. Therefore,

$$f_R(t) = \frac{\gamma\beta^{\eta}}{12\Gamma(\eta)}\left[\left(t+\frac{q}{2}\right)^{\eta\gamma-1}\exp\left(-\beta\left(t+\frac{q}{2}\right)^{\gamma}\right) + 4(t)^{\eta\gamma-1}\exp(-\beta(t)^{\gamma})\right.$$

$$\left. + \left(t-\frac{q}{2}\right)^{\eta\gamma-1}\exp\left(-\beta\left(t-\frac{q}{2}\right)^{\gamma}\right)\right]. \qquad (3.17)$$

On combining Equations (3.16) and (3.17),

$$f_R(t) = \frac{\gamma\beta^{\eta}}{12\Gamma(\eta)}\left[\left(|t|+\frac{q}{2}\right)^{\eta\gamma-1}\exp\left(-\beta\left(|t|+\frac{q}{2}\right)^{\gamma}\right) + 4(|t|)^{\eta\gamma-1}\exp(-\beta(|t|)^{\gamma})\right.$$

$$\left. + \left(|t|-\frac{q}{2}\right)^{\eta\gamma-1}\exp\left(-\beta\left(|t|-\frac{q}{2}\right)^{\gamma}\right)\right]. \qquad (3.18)$$

c. $t-\frac{q}{2} < 0 < t+\frac{q}{2}$:

This case is identical to the corresponding case in the previous section. The two half-intervals on either side of zero may be approximated by trapeziums. Therefore,

$$f_R{}^{\pm}(t) = \frac{1}{q}\frac{\gamma\beta^{\eta}}{6\Gamma(\eta)}\left(\frac{q}{2}+|t|\right)\left[1 + 2\left(\left|t\pm\frac{q}{2}\right|\right)^{\eta\gamma-1}\exp\left(-\frac{\beta}{2}\left(\left|t\pm\frac{q}{2}\right|\right)^{\gamma}\right)\right.$$

$$\left. + \left(\left|t\pm\frac{q}{2}\right|\right)^{\eta\gamma-1}\exp\left(-\frac{\beta}{2}\left(\left|t\pm\frac{q}{2}\right|\right)^{\gamma}\right)\right]. \qquad (3.19)$$

In the interval $\left[t-\frac{q}{2}, 0^{-}\right]$,

$$f_R{}^{-}(t) = \frac{1}{q}\frac{\gamma\beta^{\eta}}{6\Gamma(\eta)}\left(\frac{q}{2}-t\right)\left[1+2\left(-t+\frac{q}{2}\right)^{\eta\gamma-1}\exp\left(-\frac{\beta}{2}\left(-t+\frac{q}{2}\right)^{\gamma}\right)\right.$$
$$\left.+\left(-t+\frac{q}{2}\right)^{\eta\gamma-1}\exp\left(-\frac{\beta}{2}\left(-t+\frac{q}{2}\right)^{\gamma}\right)\right].$$

And in the interval $\left[0^{+}, t+\frac{q}{2}\right]$,

$$f_R{}^{+}(t) = \frac{1}{q}\frac{\gamma\beta^{\eta}}{6\Gamma(\eta)}\left(\frac{q}{2}+t\right)\left[1+2\left(t+\frac{q}{2}\right)^{\eta\gamma-1}\exp\left(-\frac{\beta}{2}\left(t+\frac{q}{2}\right)^{\gamma}\right)\right.$$
$$\left.+\left(t+\frac{q}{2}\right)^{\eta\gamma-1}\exp\left(-\frac{\beta}{2}\left(t+\frac{q}{2}\right)^{\gamma}\right)\right].$$

On combining, in the interval $\left(t-\frac{q}{2}, 0, t+\frac{q}{2}\right]$,

$$f_R(t) = \frac{1}{q}\frac{\gamma\beta^{\eta}}{6\Gamma(\eta)}\left(\frac{q}{2}+|t|\right)\left[1+2\left(|t|+\frac{q}{2}\right)^{\eta\gamma-1}\exp\left(-\frac{\beta}{2}\left(|t|+\frac{q}{2}\right)^{\gamma}\right)\right.$$
$$\left.+\left(|t|+\frac{q}{2}\right)^{\eta\gamma-1}\exp\left(-\beta\left(|t|+\frac{q}{2}\right)^{\gamma}\right)\right]. \qquad (3.20)$$

Finally, Equations (3.18) and (3.20) are sampled by a train of unit impulse functions. Thus,

$$p_R(nq) = \begin{cases} \frac{q\gamma\beta^{\eta}}{12\Gamma(\eta)}\left[1+2\left(\frac{q}{2}\right)^{\eta\gamma-1}\exp\left(-\frac{\beta}{2}\left(\frac{q}{2}\right)^{\gamma}\right)\right. & + \\ \left.\left(\frac{q}{2}\right)^{\eta\gamma-1}\exp\left(-\beta\left(\frac{q}{2}\right)^{\gamma}\right)\right] & n=0. \\ \frac{q\gamma\beta^{\eta}}{12\Gamma(\eta)}\left[\left(nq+\frac{q}{2}\right)^{\eta\gamma-1}\exp\left(-\beta\left(nq+\frac{q}{2}\right)^{\gamma}\right)\right. & + \\ 4(nq)^{\eta\gamma-1}\exp(-\beta(nq)^{\gamma}) & + \\ \left.\left(nq-\frac{q}{2}\right)^{\eta\gamma-1}\exp\left(-\beta\left(nq-\frac{q}{2}\right)^{\gamma}\right)\right] & n\neq 0, n\in Z. \end{cases} \qquad (3.21)$$

The analytic form in Equation (3.21) cannot be verified by using Generalized Gamma random variables with arbitrary model parameters, since very little literature

exists regarding the generation of such random variables. It may instead be visually verified using Laplacian, Gaussian and Generalized Normal random variables, since their PDFs are special cases of the Generalized Gamma distribution.

Thus, Laplacian, Gaussian and Generalized Normal ($\vartheta = 0.5$) random variables are generated with a standard deviation of 10. They are quantized with $q = 1$, 2 and 3 respectively. The normalized histogram of the quantized random variables and the corresponding GG-DQPMF are shown in the plots on the following pages.

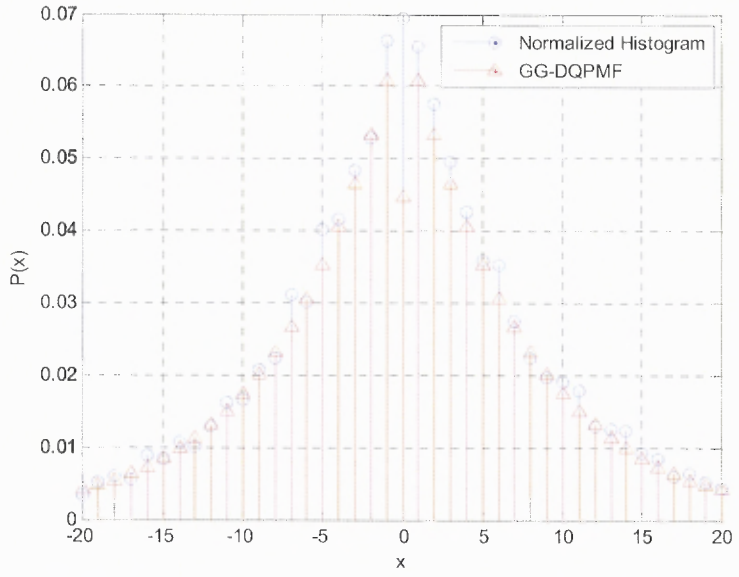

Figure 3.21 Normalized histogram and GG-DQPMF for Laplacian random variables quantized with $q = 1$.

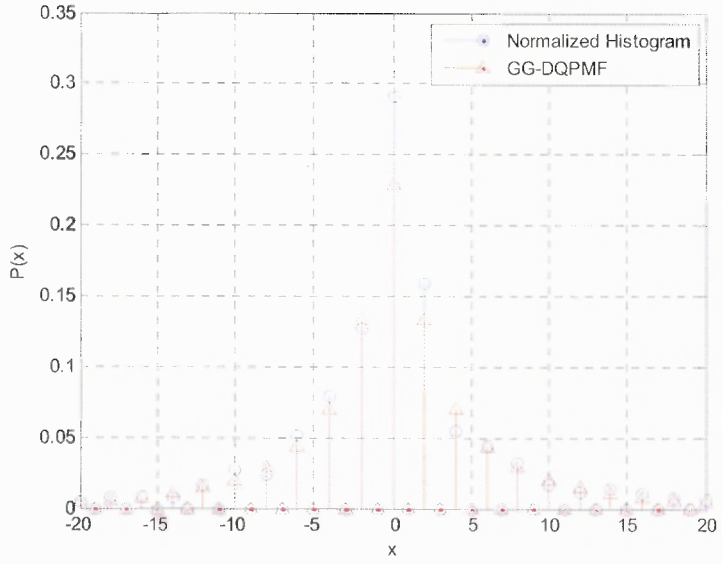

Figure 3.22 Normalized histogram and GG-DQPMF for Generalized Normal random variables with $\vartheta = 0.5$ and quantized with $q = 2$.

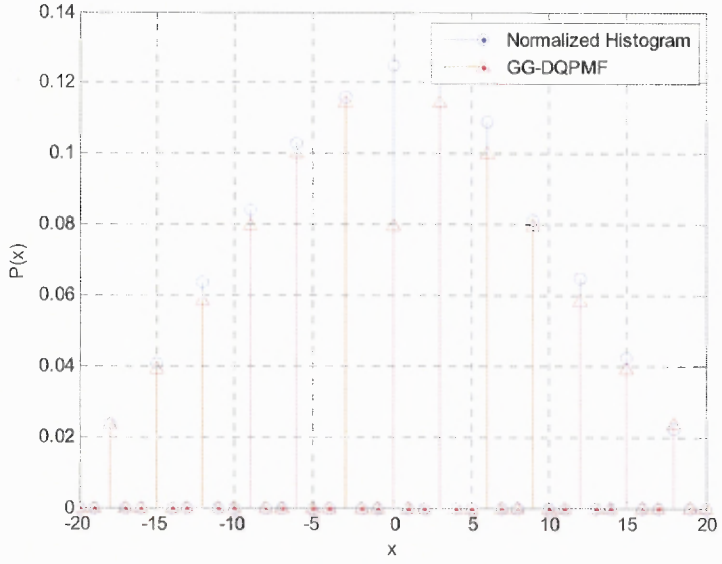

Figure 3.23 Normalized histogram and GG-DQPMF for Gaussian random variables quantized with $q = 3$.

Using Lemma 3.1 in conjunction with Equation (3.21), the following expression for the Generalized Gamma QPMF (GG-QPMF) is obtained.

$$p_R(n) = \begin{cases} \frac{\gamma k \beta^{\eta}}{12\Gamma(\eta)}\left[1 + 2\left(\frac{k}{2}\right)^{\eta\gamma-1}\exp\left(-\frac{\beta}{2}\left(\frac{k}{2}\right)^{\gamma}\right) + \left(\frac{k}{2}\right)^{\eta\gamma-1}\exp\left(-\beta\left(\frac{k}{2}\right)^{\gamma}\right)\right] & n = 0. \\ \frac{\gamma k \beta^{\eta}}{12\Gamma(\eta)}\left[\left(nk + \frac{k}{2}\right)^{\eta\gamma-1}\exp\left(-\beta\left(nk + \frac{k}{2}\right)^{\gamma}\right) + 4(nk)^{\eta\gamma-1}\exp(-\beta(nk)^{\gamma}) + \left(nk - \frac{k}{2}\right)^{\eta\gamma-1}\exp\left(-\beta\left(nk - \frac{k}{2}\right)^{\gamma}\right)\right] & n \neq 0, n \in Z. \end{cases} \quad (3.22)$$

As in the case of Equation (3.21), the analytic form in Equation (3.22) is visually verified using Laplacian, Gaussian and Generalized Normal random variables.

Laplacian, Gaussian and Generalized Normal (ϑ = 0.5) random variables are generated with a standard deviation of 10. They are integer-divided with k = 1, 2 and 3 respectively. The normalized histogram of the rounded random variables and the corresponding GG-QPMFs are shown in the following plots.

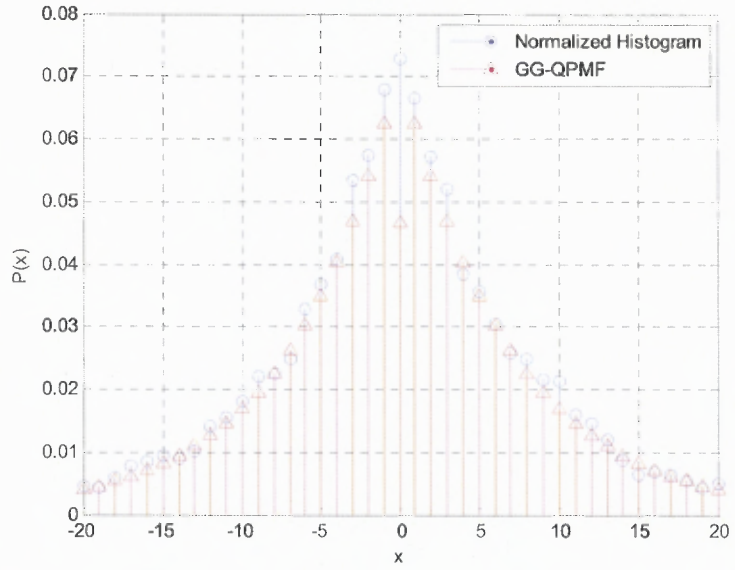

Figure 3.24 Normalized histogram and GG-QPMF for Laplacian random variables with integer division factor k = 1.

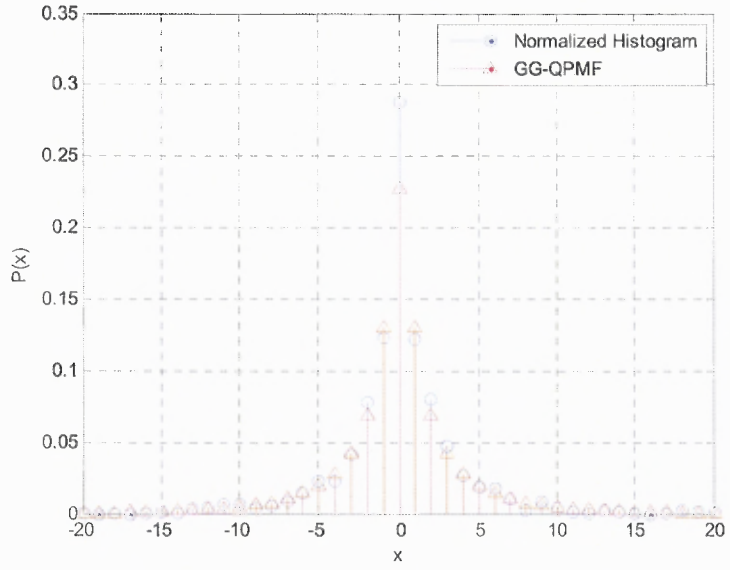

Figure 3.25 Normalized histogram and GG-QPMF for Generalized Normal random variables with $\vartheta = 0.5$ and integer division factor $k = 2$.

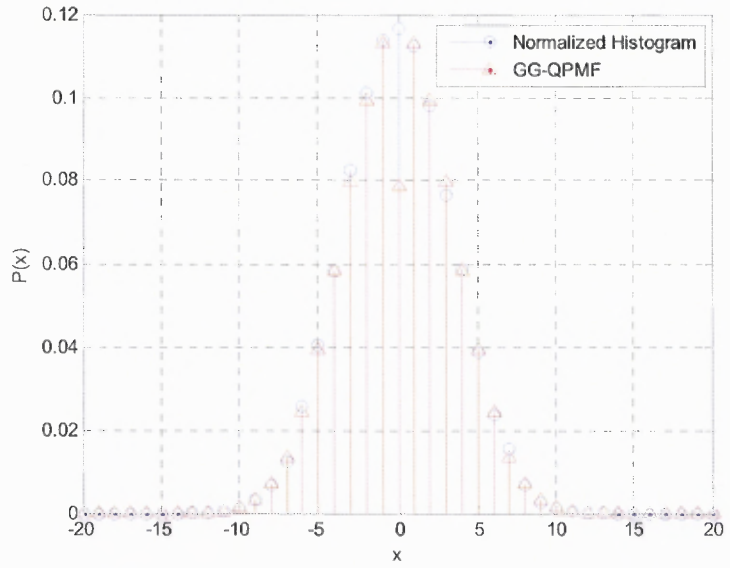

Figure 3.26 Normalized histogram and GG-QPMF for Gaussian random variables with integer division factor $k = 3$.

It is of note that in all cases, the GG-DQPMFs and the GG-QPMFs have a value at zero that is significantly lower than that of the normalized histogram of the random variable. This is attributed to the Generalized Gamma distribution tending to zero at

abscissa values close to zero, as shown graphically in Section 2.1.3. This is in contrast to the cases of the Laplacian and Generalized Normal distributions, whose values tend to a maximum at abscissa values close to zero.

3.3.4 Results

The results of running KS and χ^2 goodness-of-fit tests for the (1, 1), (1, 0) and (0, 1) modes of image block DCTs are shown in the following tables, for the following PMFs.

1. Laplacian Quantized PMF (L-QPMF), Generalized Normal Quantized PMF (GN-QPMF) and Generalized Gamma Quantized PMF (GG-QPMF).
2. Laplacian de-Quantized PMF (L-DQPMF), Generalized Normal de-Quantized PMF (GN-DQPMF) and Generalized Gamma de-Quantized PMF (GG-DQPMF).

The tests have been carried out for JPEG Q-factors ranging from 10 to 100. Four typical images chosen from the USC-SIPI database [29] for testing are shown below.

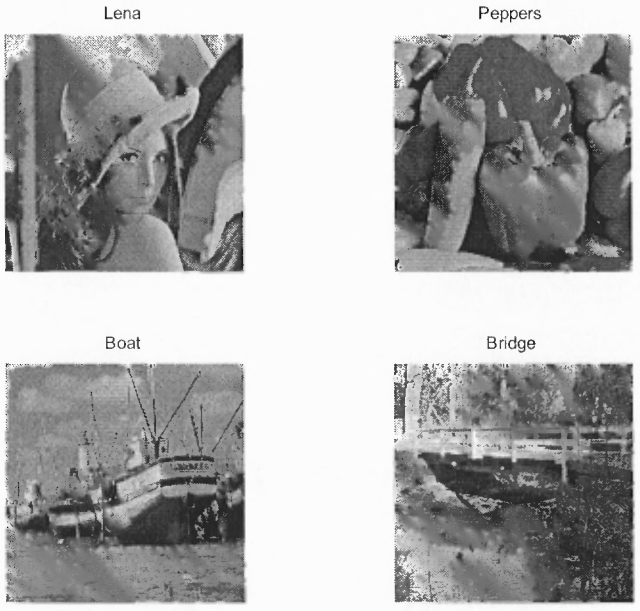

Figure 3.27 Standard Images For KS and χ^2-Squared Test .

Source: USC SIPI Image Database. http://sipi.usc.edu/database/database.cgi?volume=misc, retrieved March 30, 2010

Table 3.1 KS Test Results for QPMFs of Lena

	KS Tests								
	Generalized Normal QPMF			**Laplacian QPMF**			**Generalized Gamma QPMF**		
	Mode			**Mode**			**Mode**		
Q-factor	**(0, 1)**	**(1, 0)**	**(1, 1)**	**(0, 1)**	**(1,0)**	**(1, 1)**	**(0, 1)**	**(1,0)**	**(1, 1)**
100	0.287129	0.198020	0.188119	0.435644	0.376238	0.386139	0.188119	0.108911	0.079208
90	0.168317	0.148515	0.099010	0.267327	0.247525	0.148515	0.099010	0.108911	0.118812
80	0.128713	0.099010	0.148515	0.188119	0.148515	0.227723	0.099010	0.138614	0.148515
70	0.099010	0.207921	0.425743	0.148515	0.227723	0.425743	0.108911	0.207921	0.425743
60	0.118812	0.306931	0.524752	0.138614	0.306931	0.524752	0.118812	0.306931	0.524752
50	0.188119	0.405941	0.603960	0.188119	0.405941	0.603960	0.188119	0.405941	0.603960
40	0.336634	0.504950	0.663366	0.336634	0.504950	0.663366	0.336634	0.504950	0.663366
30	0.465347	0.613861	0.742574	0.465347	0.613861	0.742574	0.465347	0.613861	0.742574
20	0.623762	0.702970	0.811881	0.623762	0.702970	0.811881	0.623762	0.702970	0.811881
10	0.792079	0.841584	0.900990	0.792079	0.841584	0.900990	0.792079	0.841584	0.900990

Table 3.2 χ^2 Test Results for QPMFs of Lena

	χ^2 Tests								
	Generalized Normal QPMF			**Laplacian QPMF**			**Generalized Gamma QPMF**		
	Mode			**Mode**			**Mode**		
Q-factor	**(0, 1)**	**(1, 0)**	**(1, 1)**	**(0, 1)**	**(1,0)**	**(1, 1)**	**(0, 1)**	**(1,0)**	**(1, 1)**
100	507	380	572	1268	1593	2255	235	171	176
90	649	422	554	1542	1828	2315	317	175	226
80	632	434	452	1540	1879	2261	318	238	191
70	632	350	348	1570	1809	2266	323	204	148
60	633	290	287	1551	1757	2219	336	178	124
50	591	251	259	1518	1717	2147	329	153	116
40	533	203	250	1486	1720	1989	308	130	122
30	507	196	324	1496	1684	1785	303	109	206
20	390	276	600	1442	1503	1272	246	95	455
10	421	1065	992	1160	974	546	153	283	1713

Table 3.3 KS Test Results for DQPMFs of Lena

	KS Tests								
	Generalized Normal DQPMF			**Laplacian DQPMF**			**Generalized Gamma DQPMF**		
	Mode			**Mode**			**Mode**		
Q-factor	**(0, 1)**	**(1, 0)**	**(1, 1)**	**(0, 1)**	**(1,0)**	**(1, 1)**	**(0, 1)**	**(1,0)**	**(1, 1)**
100	0.178218	0.128713	0.059406	0.435644	0.376238	0.386139	0.188119	0.108911	0.079208
90	0.069307	0.039604	0.029703	0.148515	0.128713	0.118812	0.069307	0.029703	0.039604
80	0.039604	0.029703	0.019802	0.089109	0.089109	0.089109	0.049505	0.029703	0.019802
70	0.029703	0.019802	0.019802	0.059406	0.049505	0.049505	0.029703	0.019802	0.019802
60	0.029703	0.019802	0.019802	0.059406	0.039604	0.039604	0.029703	0.019802	0.019802
50	0.029703	0.019802	0.019802	0.039604	0.039604	0.039604	0.029703	0.019802	0.019802
40	0.019802	0.019802	0.019802	0.039604	0.029703	0.039604	0.019802	0.019802	0.019802
30	0.019802	0.019802	0.019802	0.029703	0.019802	0.019802	0.019802	0.019802	0.019802
20	0.019802	0.019802	0.019802	0.019802	0.019802	0.019802	0.019802	0.009901	0.019802
10	0.009901	0.009901	0.009901	0.009901	0.009901	0.009901	0.009901	0.009901	0.009901

Table 3.4 χ^2 Test Results for DQPMFs of Lena

	χ^2 Tests								
	Generalized Normal DQPMF			**Laplacian DQPMF**			**Generalized Gamma DQPMF**		
	Mode			**Mode**			**Mode**		
Q-factor	**(0, 1)**	**(1, 0)**	**(1, 1)**	**(0, 1)**	**(1,0)**	**(1, 1)**	**(0, 1)**	**(1,0)**	**(1, 1)**
100	232	207	202	1,268	1,593	2,255	235	171	176
90	189	192	257	1,155	1,527	2,156	148	105	124
80	230	248	206	1,160	1,510	2,091	150	113	102
70	262	314	103	1,149	1,461	2,077	140	98	64
60	315	261	58	1,093	1,440	2,050	138	86	44
50	371	222	52	1,058	1,392	1,979	133	72	46
40	460	151	51	1,044	1,362	1,817	136	45	66
30	588	123	65	1,012	1,354	1,594	126	42	154
20	623	137	73	930	1,086	1,046	91	29	418
10	748	289	169	631	372	134	0	213	1,686

Table 3.5 KS Test Results for QPMFs of Peppers

	KS Tests								
	Generalized Normal QPMF			**Laplacian QPMF**			**Generalized Gamma QPMF**		
	Mode			**Mode**			**Mode**		
Q-factor	**(0, 1)**	**(1, 0)**	**(1, 1)**	**(0, 1)**	**(1,0)**	**(1, 1)**	**(0, 1)**	**(1,0)**	**(1, 1)**
100	0.277228	0.217822	0.217822	0.465347	0.346535	0.39604	0.19802	0.138614	0.128713
90	0.188119	0.188119	0.108911	0.306931	0.277228	0.168317	0.089109	0.069307	0.168317
80	0.118812	0.128713	0.227723	0.188119	0.188119	0.227723	0.108911	0.108911	0.227723
70	0.108911	0.099010	0.465347	0.148515	0.158416	0.465347	0.108911	0.118812	0.465347
60	0.128713	0.207921	0.554455	0.158416	0.207921	0.554455	0.128713	0.207921	0.554455
50	0.158416	0.297030	0.623762	0.198020	0.297030	0.623762	0.158416	0.297030	0.623762
40	0.306931	0.415842	0.683168	0.306931	0.415842	0.683168	0.306931	0.415842	0.683168
30	0.455446	0.544554	0.752475	0.455446	0.544554	0.752475	0.455446	0.544554	0.752475
20	0.623762	0.673267	0.821782	0.623762	0.673267	0.821782	0.623762	0.673267	0.821782
10	0.782178	0.811881	0.900990	0.782178	0.811881	0.900990	0.782178	0.811881	0.900990

Table 3.6 χ^2 Test Results for QPMFs of Peppers

	χ^2 Tests								
	Generalized Normal QPMF			**Laplacian QPMF**			**Generalized Gamma QPMF**		
	Mode			**Mode**			**Mode**		
Q-factor	**(0, 1)**	**(1, 0)**	**(1, 1)**	**(0, 1)**	**(1,0)**	**(1, 1)**	**(0, 1)**	**(1,0)**	**(1, 1)**
100	497	515	469	1221	1340	1746	261	176	225
90	643	641	501	1555	1653	1870	290	180	315
80	670	644	421	1600	1652	1871	337	234	277
70	666	625	331	1595	1659	1778	359	257	232
60	718	573	299	1708	1632	1787	397	256	217
50	656	569	268	1608	1637	1658	381	246	182
40	613	490	258	1614	1610	1661	357	202	146
30	581	449	362	1570	1630	1549	338	189	149
20	462	347	777	1537	1543	1315	273	155	249
10	287	300	2723	1247	1156	592	146	123	949

Table 3.7 KS Test Results for DQPMFs of Peppers

	KS Tests								
	Generalized Normal DQPMF			Laplacian DQPMF			Generalized Gamma DQPMF		
	Mode			Mode			Mode		
Q-factor	(0, 1)	(1, 0)	(1, 1)	(0, 1)	(1,0)	(1, 1)	(0, 1)	(1,0)	(1, 1)
100	0.198020	0.138614	0.148515	0.465347	0.346535	0.39604	0.19802	0.138614	0.128713
90	0.069307	0.059406	0.049505	0.148515	0.108911	0.138614	0.069307	0.059406	0.049505
80	0.049505	0.029703	0.039604	0.089109	0.079208	0.089109	0.049505	0.029703	0.039604
70	0.039604	0.019802	0.019802	0.069307	0.049505	0.049505	0.039604	0.029703	0.019802
60	0.029703	0.019802	0.029703	0.049505	0.039604	0.049505	0.029703	0.019802	0.019802
50	0.029703	0.019802	0.019802	0.039604	0.029703	0.039604	0.029703	0.019802	0.019802
40	0.029703	0.019802	0.019802	0.039604	0.029703	0.039604	0.029703	0.019802	0.019802
30	0.019802	0.019802	0.019802	0.029703	0.019802	0.019802	0.019802	0.019802	0.019802
20	0.019802	0.019802	0.019802	0.019802	0.009901	0.019802	0.019802	0.019802	0.019802
10	0.009901	0.009901	0.009901	0.009901	0.009901	0.009901	0.009901	0.009901	0.009901

Table 3.8 χ^2 Test Results for DQPMFs of Peppers

	χ^2 Tests								
	Generalized Normal DQPMF			**Laplacian DQPMF**			**Generalized Gamma DQPMF**		
	Mode			**Mode**			**Mode**		
Q-factor	**(0, 1)**	**(1, 0)**	**(1, 1)**	**(0, 1)**	**(1,0)**	**(1, 1)**	**(0, 1)**	**(1,0)**	**(1, 1)**
100	276	199	282	1,222	1,340	1,747	261	176	225
90	224	163	295	1,137	1,263	1,654	185	100	165
80	261	188	257	1,149	1,230	1,674	188	90	144
70	298	238	178	1,093	1,198	1,571	179	95	116
60	323	251	119	1,105	1,184	1,598	179	87	97
50	376	300	95	1,050	1,197	1,466	171	93	71
40	449	398	68	1,036	1,159	1,473	172	85	60
30	572	333	66	989	1,158	1,345	159	82	71
20	683	350	93	920	950	1,066	119	44	179
10	774	515	124	615	529	115	0	23	889

Table 3.9 χ^2 Test Results for QPMFs of Boat

	KS Tests								
	Generalized Normal QPMF			**Laplacian QPMF**			**Generalized Gamma QPMF**		
	Mode			**Mode**			**Mode**		
Q-factor	**(0, 1)**	**(1, 0)**	**(1, 1)**	**(0, 1)**	**(1,0)**	**(1, 1)**	**(0, 1)**	**(1,0)**	**(1, 1)**
100	0.217822	0.227723	0.099010	0.366337	0.405941	0.217822	0.158416	0.267327	0.089109
90	0.188119	0.158416	0.108911	0.267327	0.257426	0.128713	0.09901	0.079208	0.138614
80	0.118812	0.089109	0.217822	0.178218	0.148515	0.217822	0.148515	0.079208	0.217822
70	0.118812	0.108911	0.465347	0.138614	0.128713	0.465347	0.158416	0.09901	0.465347
60	0.138614	0.148515	0.554455	0.19802	0.188119	0.554455	0.118812	0.148515	0.554455
50	0.217822	0.277228	0.643564	0.217822	0.277228	0.643564	0.217822	0.277228	0.643564
40	0.356436	0.396040	0.702970	0.356436	0.396040	0.702970	0.356436	0.396040	0.702970
30	0.475248	0.544554	0.772277	0.475248	0.544554	0.772277	0.475248	0.544554	0.772277
20	0.633663	0.673267	0.841584	0.633663	0.673267	0.841584	0.633663	0.673267	0.841584
10	0.792079	0.811881	0.910891	0.792079	0.811881	0.910891	0.792079	0.811881	0.910891

Table 3.10 χ^2 Test Results for QPMFs of Boat

	χ^2 Tests								
	Generalized Normal QPMF			**Laplacian QPMF**			**Generalized Gamma QPMF**		
	Mode			**Mode**			**Mode**		
Q-factor	**(0, 1)**	**(1, 0)**	**(1, 1)**	**(0, 1)**	**(1,0)**	**(1, 1)**	**(0, 1)**	**(1,0)**	**(1, 1)**
100	467	203	286	1317	723	942	104	100	111
90	595	255	350	1632	914	1089	127	117	200
80	571	251	299	1610	917	1086	163	143	213
70	591	286	246	1718	1009	1056	193	205	216
60	561	254	194	1688	952	997	195	195	182
50	521	247	182	1657	974	985	171	201	180
40	482	213	152	1603	949	940	159	181	149
30	415	185	143	1533	911	799	135	168	97
20	329	134	195	1448	801	669	105	116	52
10	254	178	434	1116	651	348	116	53	147

Table 3.11 KS Test Results for DQPMFs of Boat

	KS Tests								
	Generalized Normal DQPMF			Laplacian DQPMF			Generalized Gamma DQPMF		
	Mode			Mode			Mode		
Q-factor	(0, 1)	(1, 0)	(1, 1)	(0, 1)	(1,0)	(1, 1)	(0, 1)	(1,0)	(1, 1)
100	0.158416	0.267327	0.108911	0.366337	0.405941	0.217822	0.158416	0.267327	0.089109
90	0.049505	0.09901	0.059406	0.118812	0.138614	0.089109	0.049505	0.09901	0.049505
80	0.039604	0.079208	0.039604	0.069307	0.089109	0.049505	0.039604	0.079208	0.039604
70	0.019802	0.039604	0.029703	0.049505	0.049505	0.029703	0.019802	0.039604	0.029703
60	0.019802	0.039604	0.019802	0.049505	0.039604	0.029703	0.019802	0.039604	0.019802
50	0.019802	0.039604	0.019802	0.029703	0.039604	0.019802	0.019802	0.039604	0.019802
40	0.019802	0.019802	0.019802	0.029703	0.029703	0.019802	0.019802	0.019802	0.019802
30	0.019802	0.019802	0.019802	0.029703	0.029703	0.019802	0.019802	0.019802	0.019802
20	0.019802	0.019802	0.019802	0.019802	0.019802	0.019802	0.019802	0.019802	0.019802
10	0.009901	0.009901	0.009901	0.009901	0.009901	0.009901	0.009901	0.009901	0.009901

Table 3.12 χ^2 Test Results for DQPMFs of Boat

	χ^2 Tests								
	Generalized Normal DQPMF			**Laplacian DQPMF**			**Generalized Gamma DQPMF**		
	Mode			**Mode**			**Mode**		
Q-factor	**(0, 1)**	**(1, 0)**	**(1, 1)**	**(0, 1)**	**(1,0)**	**(1, 1)**	**(0, 1)**	**(1,0)**	**(1, 1)**
100	126	91	124	1,317	723	942	104	100	111
90	90	47	99	1,235	660	879	40	47	87
80	116	59	103	1,201	635	856	35	62	97
70	147	73	105	1,218	627	822	40	82	108
60	206	97	75	1,191	623	813	41	88	101
50	302	135	71	1,156	624	793	40	99	102
40	436	205	68	1,118	599	765	35	94	90
30	459	363	76	1,029	551	610	22	86	42
20	418	612	97	925	447	436	5	52	5
10	607	834	244	585	286	71	37	7	116

Table 3.13 KS Test Results for QPMFs of Bridge

	KS Tests								
	Generalized Normal QPMF			Laplacian QPMF			Generalized Gamma QPMF		
	Mode			Mode			Mode		
Q-factor	(0, 1)	(1, 0)	(1, 1)	(0, 1)	(1,0)	(1, 1)	(0, 1)	(1,0)	(1, 1)
100	0.405941	0.643564	0.188119	0.485149	0.821782	0.188119	0.415842	0.752475	0.188119
90	0.079208	0.148515	0.069307	0.089109	0.128713	0.069307	0.069307	0.108911	0.069307
80	0.089109	0.099010	0.188119	0.089109	0.118812	0.188119	0.089109	0.079208	0.188119
70	0.099010	0.108911	0.445545	0.099010	0.089109	0.445545	0.099010	0.108911	0.445545
60	0.168317	0.128713	0.534653	0.168317	0.128713	0.534653	0.168317	0.128713	0.534653
50	0.306931	0.217822	0.613861	0.306931	0.217822	0.613861	0.306931	0.217822	0.613861
40	0.415842	0.366337	0.683168	0.415842	0.366337	0.683168	0.415842	0.366337	0.683168
30	0.534653	0.495050	0.762376	0.534653	0.49505	0.762376	0.534653	0.49505	0.762376
20	0.663366	0.643564	0.821782	0.663366	0.643564	0.821782	0.663366	0.643564	0.821782
10	0.801980	0.811881	0.900990	0.80198	0.811881	0.900990	0.80198	0.811881	0.900990

Table 3.14 χ^2 Test Results for QPMFs of Bridge

	χ^2 Tests								
	Generalized Normal QPMF			**Laplacian QPMF**			**Generalized Gamma QPMF**		
	Mode			**Mode**			**Mode**		
Q-factor	**(0, 1)**	**(1, 0)**	**(1, 1)**	**(0, 1)**	**(1,0)**	**(1, 1)**	**(0, 1)**	**(1,0)**	**(1, 1)**
100	103	129	125	117	115	125	101	102	123
90	128	155	89	131	134	89	123	108	113
80	104	147	70	115	139	69	123	109	118
70	135	175	52	143	179	51	149	170	119
60	100	168	48	117	172	46	132	158	122
50	99	160	35	107	155	32	135	158	133
40	81	128	28	108	149	24	151	160	168
30	86	141	27	102	119	21	165	148	205
20	70	111	29	69	142	13	195	195	241
10	121	113	70	64	154	13	279	318	390

Table 3.15 KS Test Results for DQPMFs of Bridge

	KS Tests								
	Generalized Normal DQPMF			**Laplacian DQPMF**			**Generalized Gamma DQPMF**		
	Mode			**Mode**			**Mode**		
Q-factor	**(0, 1)**	**(1, 0)**	**(1, 1)**	**(0, 1)**	**(1,0)**	**(1, 1)**	**(0, 1)**	**(1,0)**	**(1, 1)**
100	0.425743	0.702970	0.188119	0.485149	0.821782	0.188119	0.415842	0.752475	0.188119
90	0.138614	0.247525	0.089109	0.168317	0.277228	0.089109	0.148515	0.277228	0.079208
80	0.089109	0.148515	0.049505	0.099010	0.168317	0.049505	0.099010	0.158416	0.059406
70	0.059406	0.099010	0.029703	0.069307	0.108911	0.029703	0.069307	0.099010	0.039604
60	0.059406	0.079208	0.029703	0.059406	0.079208	0.029703	0.059406	0.089109	0.029703
50	0.049505	0.059406	0.019802	0.049505	0.069307	0.019802	0.049505	0.069307	0.029703
40	0.039604	0.059406	0.019802	0.039604	0.059406	0.019802	0.049505	0.069307	0.029703
30	0.039604	0.039604	0.019802	0.039604	0.049505	0.019802	0.049505	0.049505	0.029703
20	0.019802	0.029703	0.019802	0.029703	0.029703	0.019802	0.029703	0.029703	0.029703
10	0.009901	0.009901	0.009901	0.009901	0.009901	0.009901	0.009901	0.009901	0.009901

Table 3.16 χ^2 Test Results for DQPMFs of Bridge

	χ^2 Tests								
	Generalized Normal DQPMF			**Laplacian DQPMF**			**Generalized Gamma DQPMF**		
	Mode			**Mode**			**Mode**		
Q-factor	**(0, 1)**	**(1, 0)**	**(1, 1)**	**(0, 1)**	**(1,0)**	**(1, 1)**	**(0, 1)**	**(1,0)**	**(1, 1)**
100	97	111	122	118	115	125	101	102	123
90	37	64	23	56	65	25	49	47	47
80	19	42	15	39	41	17	52	31	63
70	21	36	19	35	33	19	44	40	83
60	15	36	19	31	32	17	62	35	90
50	16	35	15	28	28	10	68	44	106
40	15	32	14	26	23	8	91	54	148
30	22	35	23	23	18	5	106	69	183
20	37	49	65	17	18	4	164	101	230
10	172	107	323	17	7	0	256	208	381

It is may be noted that on average, the GN-QPMF and the GG-QPMF have lower test statistics than the L-QPMF. This is intuitive, since the former two specify distribution families of which the Laplacian distribution is a special case. It is also seen that while the GG-QPMF generally outperforms the GN-QPMF, the performance difference is not significantly high.

In the case of DQPMFs, the KS test statistics indicate that on average, the GG-DQPMF is the best fit distribution with the GN-DQPMF being a close second. This is evident from the χ^2 test results as well, for moderately high (> 40) Q-factors. As in the case of QPMFs, the trend is that the GG-DQPMF outperforms the GN-DQPMF by a small amount, while both of them outperform the L-DQPMF by a significant amount, for most Q-factors.

Before proceeding further, it must be mentioned that the KS test statistic is preferred over the χ^2 test statistic, for the purposes of goodness-of-fit comparisons here. This is because the KS test statistic, unlike the χ^2 test statistic, is more robust because it is not affected by the size of the test sample set. With that being said, the following graphs plot the average KS test statistic against JPEG Q-factors ranging from 10 to 100, for the first 8 modes of the quantized and de-quantized block DCT. The quantized and de-quantized block DCT histograms are compared against GN-, GG- and L- QPMFs and DQPMFs respectively, and the KS test statistics are generated. The averaging is performed across 44 test images from the miscellaneous image set of the USC SIPI database [29].

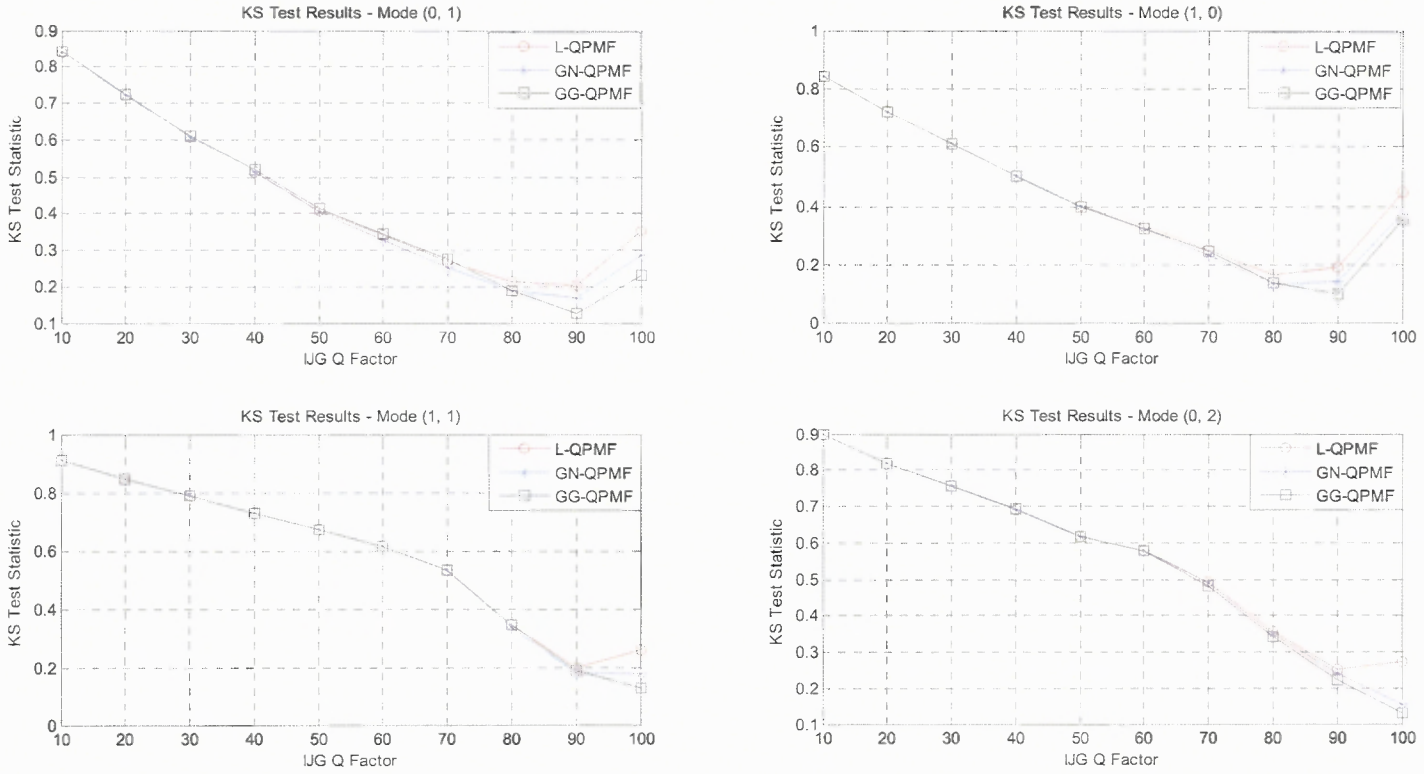

Figure 3.28 Average KS Test Statistic versus Q-factor for Modes (0, 1) (1, 0) (1, 1) and (0, 2), for QPMF.

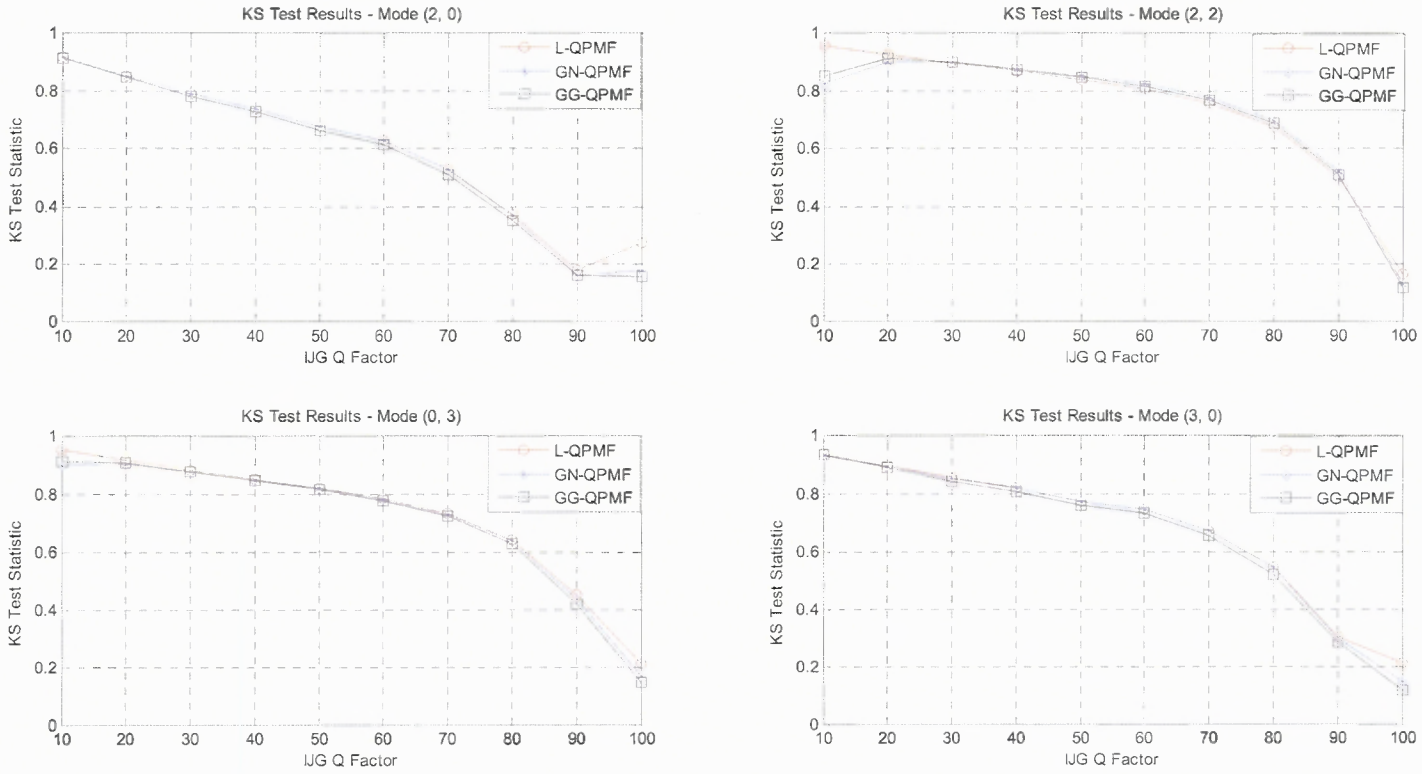

Figure 3.29 Average KS Test Statistic versus Q-factor for Modes (2, 0) (2, 2) (0, 3) and (3, 0), for QPMF.

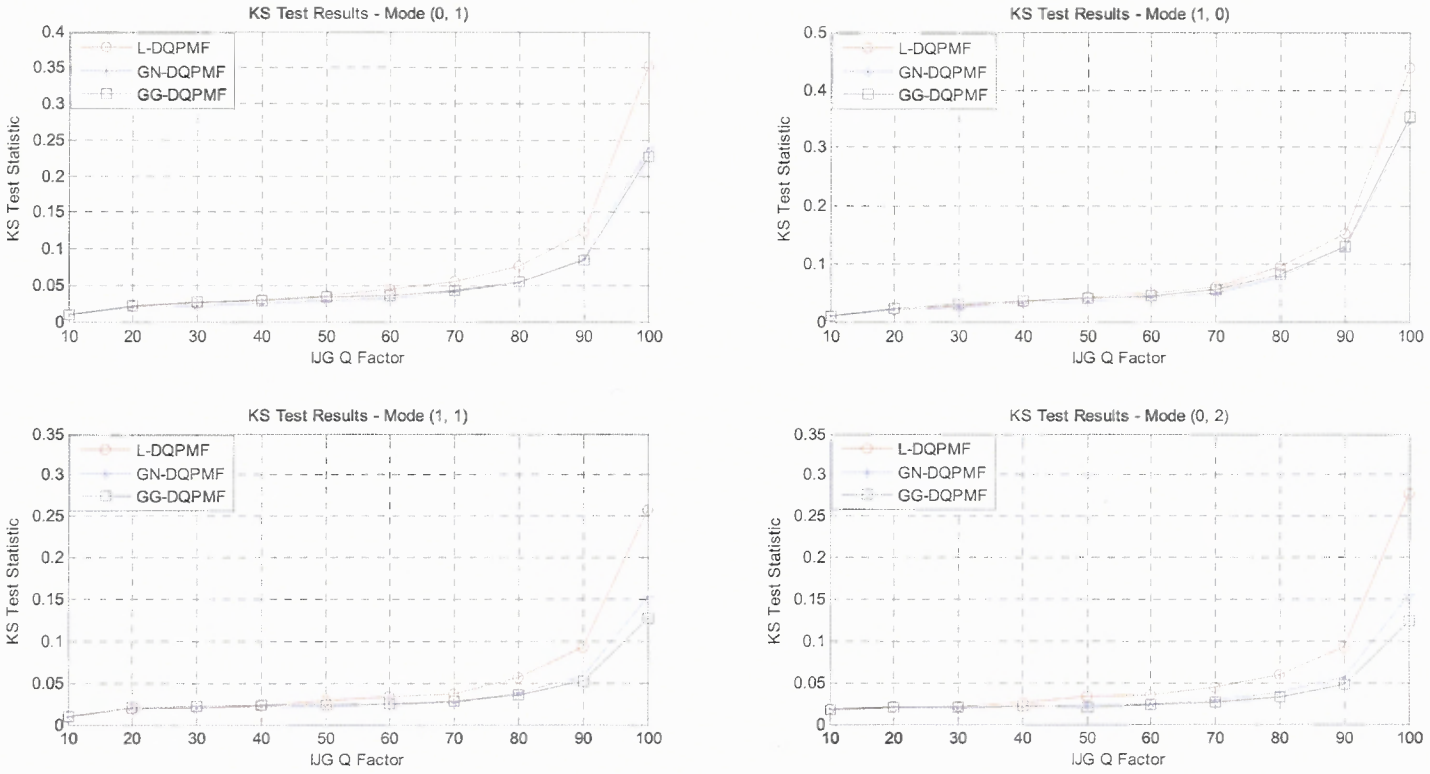

Figure 3.30 Average KS Test Statistic versus Q-factor for Modes (0, 1) (1, 0), (0, 2) and (2, 0), for DQPMF.

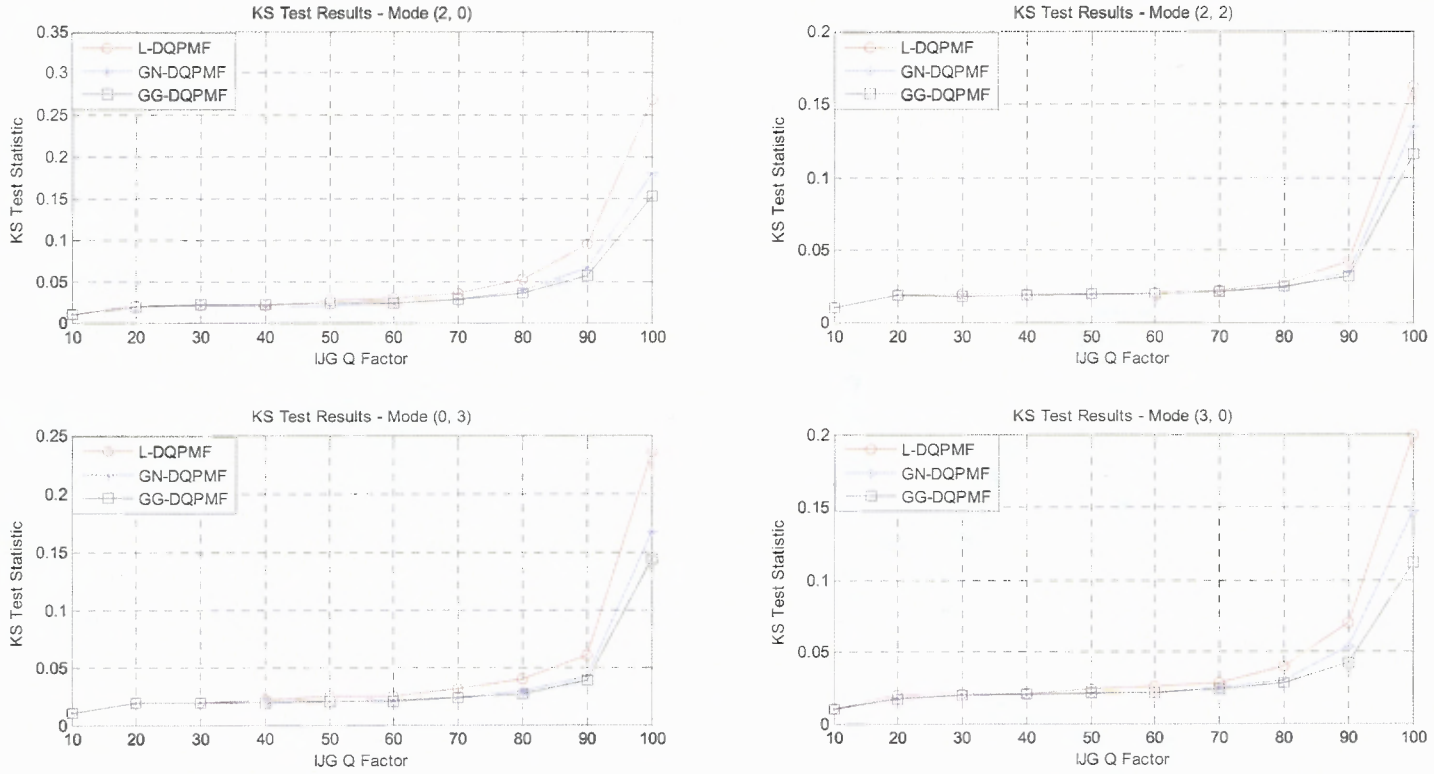

Figure 3.31 Average KS Test Statistic versus Q-factor for Modes (2, 0), (2, 2), (0, 3) and (3, 0), for DQPMF.

From the plots in Figures (3.28) and (3.29) the following observations are made.

- For low values of the IJG[4] Q-factor ($Q < 60$), the KS test statistic is nearly equal for all three QPMFs. This may be attributed to the large number of values clustered at and around zero in the PMFs. For high values of the Q-factor ($Q \geq 60$), the L-QPMF has a higher value of test statistic than the other two. In general, the test statistic is nearly equal for the GN-QPMF and the GG-QPMF, except for the (1, 0) and (1, 1) modes, when the test statistic for the latter is lower. This implies that the preferred PMF could be either Generalized Gamma based (GG-QPMF) or Generalized Normal based (GN-QPMF).
- Despite the GG-QPMF fitting the empirical histogram better than the GN-QPMF, the difference is not significant across Q-factors and block DCT modes. Since the GN-QPMF has only two parameters (assuming zero mean) and the GG-QPMF has three (similarly, assuming zero mean), the former is the preferred distribution.

Similarly from the Figures (3.30) and (3.31), the following observations are made.

- It is seen that for low values of the IJG Q-factor ($Q < 50$), the KS test statistic is nearly equal for all three DQPMFs. As in the case of QPMFs, this may be attributed to the high percentage of values clustered around zero in the PMFs. For high values of the Q-factor ($Q \geq 50$), the L-DQPMF has a higher value of test statistic than the other two. In general, the test statistic for the GN-DQPMF is nearly equal to that for the GG-DQPMF, with the GG-DQPMF outperforming the GN-DQPMF slightly. This implies that the preferred PMF could be either Generalized Gamma based (GG-DQPMF) or Generalized Normal based (GN-DQPMF).
- Despite the GG-DQPMF fitting the empirical histogram better than the GN-DQPMF, the difference is not significant across Q-factors and block DCT modes. Since the GN-DQPMF has only two parameters (assuming zero mean) and the GG-DQPMF has three (similarly, assuming zero mean), the former is the preferred distribution, in a manner similar to the GN-QPMF.

It is thus concluded that the GN-QPMF is the preferred distribution for quantized block DCT data on the JPEG encoder end, while the GN-DQPMF is the preferred distribution for de-quantized block DCT data on the JPEG decoder end.

[4] IJG – Independent JPEG Group. The IJG Q-factor specifies a standard set of quality factors in JPEG compression, with values ranging from 10 (lowest quality) to 100 (highest quality).

In light of these conclusions, the problem of deriving the model parameters of the GN-DQPMF from de-quantized JPEG block DCT coefficients will have to be tackled.

Recalling the process of JPEG decoding, it is to be noted that the de-quantized block DCT coefficients are modeled well by the GN-DQPMF. However, the parameters of the GN-DQPMF, i.e., ϑ and σ are not known, and must be determined from the corresponding mode of the de-quantized block DCT coefficients. In lieu of the commonly employed method of maximizing the log-likelihood function of the distribution, analytic expressions for the first few moments of the GN-DQPMF shall be derived and used to determine these model parameters.

The moments of the GN-DQPMF can be derived using Sheppard's corrections [20]. Explicitly, if q is the quantization parameter and x' is the quantized version of x, the first four moments of x' are related to the first four moments of x as follows.

$$E\{x\} = E\{x'\} - 0.$$

$$E\{x^2\} = E\{x'^2\} - \left(\frac{1}{12}q^2\right).$$

$$E\{x^3\} = E\{x'^3\} - \left(\frac{1}{4}E\{x'\}q^2\right).$$

$$E\{x^4\} = E\{x'^4\} - \left(\frac{1}{2}q^2E\{x'^2\} - \frac{7}{240}q^4\right).$$

Where $E\{...\}$ is the expectation operator.

Using these relations to obtain the moments of the GN-DQPMF,

$$E\{x'\} = E\{x\} = 0. \tag{3.23}$$

$$E\{x'^2\} = \sigma^2 + \left(\frac{1}{12}q^2\right). \tag{3.24}$$

$$E\{x'^3\} = E\{x^3\} = 0. \tag{3.25}$$

$$E\{x'^4\} = E\{x^4\} + \left(\frac{1}{2}q^2 E\{x'^2\} - \frac{7}{240}q^4\right)$$

$$= E\{x^4\} + \left[\frac{1}{2}q^2\left\{\sigma^2 + \left(\frac{1}{12}q^2\right)\right\} - \frac{7}{240}q^4\right]$$

$$E\{x'^4\} = E\{x^4\} + \left[\frac{q^2}{2}\sigma^2 + \left(\frac{1}{80}q^4\right)\right]. \quad (3.26)$$

From Equations (3.23) to (3.26) it is possible to deduce the following.

- The 'power' in the quantized random variable, is greater than the power in the non-quantized random variable by a factor of $\left(\frac{q^2}{12}\right)$. This is clearly because of the Uniform distributed quantization noise being added to the random variable, as stated in Section 3.2.
- The skewness, defined as the ratio of the third moment to the cube of the standard deviation [49], of the quantized random variable is equal to zero, since the third moments of x and x' are the same, and the skewness of x is 0 as per Nadarajah [45]. This is intuitive, since the skewness is a measure of the symmetry of the distribution, and the symmetry of the distribution remains unchanged after quantization.
- The kurtosis κ' of x' is derived as follows.

$$\kappa' = \frac{E\{x'^4\}}{\left[E\{x'^2\}\right]^2} = \frac{E\{x^4\} + \left[\frac{q^2}{2}E\{x^2\} + \left(\frac{1}{80}q^4\right)\right]}{\left[E\{x^2\} + \frac{q^2}{12}\right]^2}.$$

Expanding the denominator,

$$\kappa' = \frac{E\{x^4\} + \left[\frac{q^2}{2}E\{x^2\} + \left(\frac{1}{80}q^4\right)\right]}{[E\{x^2\}]^2 + \frac{q^4}{144} + E\{x^2\}\frac{q^2}{6}}.$$

Dividing the right hand side of this equation by $[E\{x^2\}]^2$,

$$\kappa' = \frac{\kappa + \left[\frac{q^2}{2E\{x^2\}} + \left(\frac{q^4}{80[E\{x^2\}]^2}\right)\right]}{1 + \left[\frac{q^4}{144[E\{x^2\}]^2} + \frac{q^2}{6E\{x^2\}}\right]}.$$

Using Equation (3.24),

$$\kappa' = \frac{\kappa + \left[\frac{q^2}{2\sigma^2} + \frac{q^4}{80\sigma^4}\right]}{1 + \left[\frac{q^4}{144\sigma^4} + \frac{q^2}{6\sigma^2}\right]}. \tag{3.27}$$

Using Equations (3.27) and (3.24), it is now possible to derive the Kurtosis of x', given the Kurtosis of x, the quantization step q and the second moment of x'.

The Kurtosis of x is used to determine the shape factor ϑ as per [45]. Equation (3.27) in conjunction with,

$$\kappa = \frac{\Gamma(1/\vartheta)\Gamma(5/\vartheta)}{\Gamma^2(3/\vartheta)}. \tag{3.28}$$

may numerically be solved to estimate the value ϑ.

The second parameter σ may be estimated from Equation (3.24).

The moments of the GN-QPMF may similarly be derived from Sheppard's corrections [20]. For the GN-QPMF, q is invariably equal to 1 (since it is rounded), but there exists a division factor, k. It can empirically be verified that this division factor divides the second moment by a factor k^2 and the fourth moment by a factor k^4. Therefore the moments of the GN-QPMF from Equations (3.23) to (3.26) are,

$$E\{x'\} = E\{x\} = 0. \tag{3.29}$$

$$E\{x'^2\} = \left(\frac{\sigma}{k}\right)^2 + \left(\frac{1}{12}\right). \tag{3.30}$$

$$E\{x'^3\} = E\{x^3\} = 0. \tag{3.31}$$

$$E\{x'^4\} = \frac{E\{x^4\}}{k^4} + \left[\frac{1}{2}\frac{\sigma^2}{k^2} + \left(\frac{1}{80}\right)\right]. \tag{3.32}$$

3.3.5 Summary

The Generalized Normal De-quantized PMF (GN-DQPMF) is the preferred distribution for the PMF of de-quantized block DCT coefficients on the JPEG decoder end. It is given as,

$$p_R(nq) = \begin{cases} \frac{q\vartheta\alpha(\vartheta)}{12\sigma\Gamma(1/\vartheta)}\left[\exp\left\{-\left[\alpha(\vartheta)\left(\frac{q}{2\sigma}\right)\right]^{\vartheta}\right\} + 4\exp\left\{-\left[\alpha(\vartheta)\left(\frac{q}{4\sigma}\right)\right]^{\vartheta}\right\} + 1\right] & n = 0. \\ \frac{q\vartheta\alpha(\vartheta)}{12\sigma\Gamma(1/\vartheta)}\left[\exp\left\{-\left[\alpha(\vartheta)\left|\frac{2nq+q}{2\sigma}\right|\right]^{\vartheta}\right\} + 4\exp\left\{-\left[\alpha(\vartheta)\left|\frac{nq}{\sigma}\right|\right]^{\vartheta}\right\} + \exp\left\{-\left[\alpha(\vartheta)\left|\frac{2nq-q}{2\sigma}\right|\right]^{\vartheta}\right\}\right] & n \neq 0, n \in Z. \end{cases} \quad (3.33)$$

Where σ is the square root of the variance of the distribution, ϑ is the shape parameter of the distribution, related to its kurtosis, q is the quantization step, and $\alpha(\vartheta) = \sqrt{\frac{\Gamma(3/\vartheta)}{\Gamma(1/\vartheta)}}$, where $\Gamma(\ldots)$ is the complete Gamma function, defined as,

$$\Gamma(z) = \int_0^{\infty} t^{z-1}e^{-t}dt.$$

The moments of the GN-DQPMF are related to the moments of the Generalized Normal pre-quantization PDF (GN-PQPDF), i.e., the PDF of the non-quantized AC block DCT coefficients as follows.

$$E\{x'\} = E\{x\} = 0. \quad (3.34)$$

$$E\{x'^2\} = \sigma^2 + \left(\frac{1}{12}q^2\right). \quad (3.35)$$

$$E\{x'^3\} = E\{x^3\} = 0. \tag{3.36}$$

$$E\{x'^4\} = E\{x^4\} + \left[\frac{q^2}{2}\sigma^2 + \left(\frac{q^4}{80}\right)\right]. \tag{3.37}$$

The Generalized Normal Quantized PMF (GN-QPMF) is the preferred distribution for the PMF of quantized block DCT coefficients on the JPEG encoder end. It is given as,

$$p_R(n) = \begin{cases} \frac{k\vartheta\alpha(\vartheta)}{12\sigma\Gamma(1/\vartheta)}\left[\exp\left\{-\left[\alpha(\vartheta)\left(\frac{k}{2\sigma}\right)\right]^{\vartheta}\right\} + 4\exp\left\{-\left[\alpha(\vartheta)\left(\frac{k}{4\sigma}\right)\right]^{\vartheta}\right\} + 1\right] & n = 0. \\ \frac{k\vartheta\alpha(\vartheta)}{12\sigma\Gamma(1/\vartheta)}\left[\exp\left\{-\left[k\alpha(\vartheta)\left|\frac{2n+1}{2\sigma}\right|\right]^{\vartheta}\right\} + 4\exp\left\{-\left[k\alpha(\vartheta)\left|\frac{n}{\sigma}\right|\right]^{\vartheta}\right\} + \exp\left\{-\left[k\alpha(\vartheta)\left|\frac{2n-1}{2\sigma}\right|\right]^{\vartheta}\right\}\right] & n \neq 0, n \in Z. \end{cases} \tag{3.38}$$

Where σ is the square root of the variance of the distribution, ϑ is the shape parameter of the distribution, related to its kurtosis, k is the quantization divisor for encoding, and $\alpha(\vartheta) = \sqrt{\frac{\Gamma(3/\vartheta)}{\Gamma(1/\vartheta)}}$, where $\Gamma(...)$ is the complete Gamma function, defined as,

$$\Gamma(z) = \int_0^{\infty} t^{z-1}e^{-t}dt.$$

The moments of the Generalized Normal Quantized PMF (GN-QPMF) in relation to the moments of the Generalized Normal pre-quantized PDF (GN-PQPDF) are summarized as follows.

$$E\{x'\} = E\{x\} = 0. \tag{3.39}$$

$$E\{x'^2\} = \left(\frac{\sigma}{k}\right)^2 + \left(\frac{1}{12}\right). \tag{3.40}$$

$$E\{x'^3\} = E\{x^3\} = 0. \tag{3.41}$$

$$E\{x'^4\} = \frac{E\{x^4\}}{k^4} + \left[\frac{1}{2}\left(\frac{\sigma}{k}\right)^2 + \left(\frac{1}{80}\right)\right]. \tag{3.42}$$

CHAPTER 4

APPLICATIONS OF THE QUANTIZED AND DE-QUANTIZED BLOCK DCT MODELS

This chapter details potential applications of the models developed in Chapter 3. The applications proposed in this chapter constitute the remaining part of the original body of work in this thesis.

4.1 Introduction

In Chapter 3, it was concluded that the Generalized Normal Quantized PMF (GN-QPMF) and the Generalized Normal de-Quantized PMF (GN-DQPMF) summarized in Equations (3.33) and (3.38) respectively, are the preferred PMFs for quantized and de-quantized AC block DCT coefficients, owing to a combination of sound goodness-of-fit and low model parameter estimation complexity.

In this chapter, the GN-QPMF and GN-DQPMF are used in the following image forensic applications.

- Detection of compression history in bitmap images - It is shown that the GN-DQPMF may be used to detect if a bitmap image was ever JPEG compressed in the past.
- Detection of quality factor of historical JPEG compression in bitmap images - It is shown that the GN-DQPMF may be used to detect the value of the IJG Q-factor[5] in a bitmap image that contains compression history.
- Validating the Generalized Benford's Law [27] for leading digit distributions of quantized block DCTs – A detailed study of Benford's Law and leading digit distributions in the context of image processing is first performed. It is then shown that the GN-QPMF may be used to derive a model for all quantized AC block DCT coefficients, which is used to validate the Generalized Benford's Law.

[5] Refer to Section 1.4.3 for the definition of Q-factor.

Each of these applications is detailed in subsequent sections. Existing research in the area is first explored, and the results obtained from the proposed approach are compared with the results of one of the existing approaches.

4.2 Detection of Compression History in Bitmap Images

4.2.1 Introduction

A bitmap image may defined as a two-dimensional image, with each pixel represented in no more or no less than n bits per pixel, where n is the resolution of the image intensity. Typically, n has a value of 8 for grayscale images, leading to 256 grayscale intensity levels. Bitmap images are uncompressed in the sense that, their pixels do not have to undergo any form of source decoding for the purposes of rendering. That, however, does not obviate the likelihood of the image having been compressed and then decompressed in a lossy fashion in the past. Thus, one image forensic application would be to determine the presence of any *compression history* in the image. Approaches to determine compression history have ranged from using statistical properties of transform coefficients of the image as proposed in Fan and Queiroz (2003) [22], Neelamani, Queiroz, Fan and Baraniuk (2003) [34], Fu, Shi and Su (2007) [27] to image texture analysis proposed in He, Lin, Wang and Tang (2009) [33]. Since the approach to be proposed subsequently deals with statistical properties of the transform coefficients, previous research employing related approaches will be explored.

4.2.2 The Approach Proposed by Fan and Queiroz

An early paper on detecting compression history in bitmaps was by Fan and Queiroz (2003) [22]. This seminal paper presents an approach to detect the presence and extent of JPEG compression history in bitmaps using block boundaries and DCT coefficient statistics of the bitmap, respectively.

The process of compression history detection in this context involves estimating and thresholding discontinuities across block boundaries. The following image is used as reference.

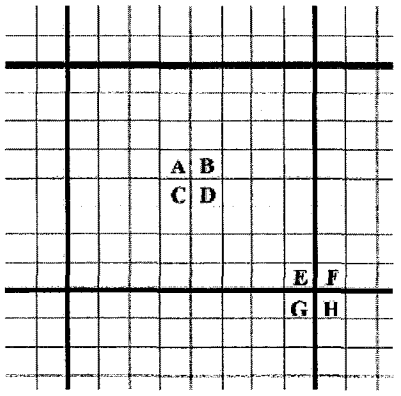

Figure 4.1 For each block two numbers are computed, i.e., involving same pixel pattern but spanning, or not, multiple blocks.

Source: Z. Fan and R. de Queiroz, "Identification of bitmap compression history: JPEG detection and quantizer estimation," IEEE Transactions on Image Processing, vol. 12, pp. 230–235, Feb. 2003.

The grid in Figure 4.1 represents a bitmap image block of size 8x8 pixels. The following absolute differences are computed from this block.

$$Z' = |A - B - C + D|.$$

$$Z'' = |E - F - G + H|.$$

This process is repeated for all blocks in the image.

The histograms of $Z'$and Z'', i.e., H_I and H_{II} are computed. The sum of absolute differences between the histograms is then computed.

$$K = \sum |H_I - H_{II}|.$$

By thresholding K, it is possible to determine if a bitmap was historically compressed. This approach cannot detect bitmaps historically compressed with a Q-factor greater than 90 [22].

4.2.3 The Proposed Approach

In the proposed approach to detecting the presence of compression history, the histogram of a specific AC mode of the block DCT of the bitmap is compared with the GN-DQPMF, generated with model parameters determined from the mode, using the approach detailed in Section 3.3.4, for an IJG Q-factor of 100 (i.e., $q = 1$). The goodness-of-fit test statistic obtained hence is hard-thresholded against an empirically determined threshold value and the decision is made thereof.

It must be noted that the GN-DQPMF generated is not an exact match to the normalized histogram of the mode, even in the case of a near-uncompressed bitmap (Q-factor of 100). This is because the block DCT of a bitmap is an approximation to the de-quantized DCT coefficients, the latter being an intermediate result of JPEG decompression.

Before the algorithm for compression history detection is explored in depth however, a few key approximations are investigated.

4.2.3.1 Practical Estimations of the Parameters of the GN-DQPMF

Estimating the parameters of the GN-DQPMF, (ϑ, σ) specified in Equation (3.33) and recalled here, is carried out on a specific AC mode of the block DCT.

$$p_R(nq) = \begin{cases} \dfrac{q\vartheta\alpha(\vartheta)}{12\sigma\Gamma(1/\vartheta)}\left[\exp\left\{-\left[\alpha(\vartheta)\left(\dfrac{q}{2\sigma}\right)\right]^{\vartheta}\right\} + 4\exp\left\{-\left[\alpha(\vartheta)\left(\dfrac{q}{4\sigma}\right)\right]^{\vartheta}\right\} + 1\right] & n = 0. \\ \dfrac{q\vartheta\alpha(\vartheta)}{12\sigma\Gamma(1/\vartheta)}\left[\exp\left\{-\left[\alpha(\vartheta)\left|\dfrac{2nq+q}{2\sigma}\right|\right]^{\vartheta}\right\} + 4\exp\left\{-\left[\alpha(\vartheta)\left|\dfrac{nq}{\sigma}\right|\right]^{\vartheta}\right\} + \exp\left\{-\left[\alpha(\vartheta)\left|\dfrac{2nq-q}{2\sigma}\right|\right]^{\vartheta}\right\}\right] & n \neq 0, n \in Z. \end{cases} \tag{4.1}$$

The relation in Equation (3.35) is recalled as follows.

$$E\{x'^2\} = \sigma^2 + \left(\frac{1}{12}q^2\right).$$

Alternately,

$$\sigma = \sqrt{E\{x'^2\} - \left(\frac{1}{12}q^2\right)}.$$

In this application, x' is a specific block DCT mode. Indeed, here q is unknown, since the bitmap image has no quantization table. However, it may not be necessary, since the effect q has on the value of σ is diminished by the large value of $E\{x'^2\}$.

To confirm the veracity of this assertion, a set of four typical images were JPEG compressed with Q-factors ranging from 100 to 10. The $E\{x'^2\}$ of the (1, 1) mode was found in each case, and compared against the value of $\left(\frac{q^2}{12}\right)$. The results are tabulated as follows.

Table 4.1 Second Moment versus $q^2/12$

Q-factor		Images			
		Lena	Boat	Peppers	Boat
	$\frac{q^2}{12}$	$E\{x'^2\}$	$E\{x'^2\}$	$E\{x'^2\}$	$E\{x'^2\}$
100	0	1367	1121	2002	1374
90	1	1368	1121	2003	1374
80	2	1368	1125	2002	1377
70	5	1370	1123	2008	1383
60	8	1373	1126	2016	1379
50	12	1374	1130	2014	1390
40	19	1377	1134	2007	1383
30	33	1378	1143	2041	1401
20	70	1388	1124	2074	1427
10	252	1407	1160	2198	1502

All numerical values are rounded to the nearest integer.

Except perhaps in the case of a Q-factor of 10, the value of $\frac{q^2}{12}$ is significantly lower than the value of $E\{x'^2\}$. The following approximation may therefore be made.

$$\sigma \cong \sqrt{E\{x'^2\}}. \tag{4.2}$$

To estimate ϑ, Equations (3.27) and (3.28) recalled here, are used.

$$\kappa' = \frac{\kappa + \left[\frac{q^2}{2\sigma^2} + \frac{q^4}{80\sigma^4}\right]}{1 + \left[\frac{q^4}{144\sigma^4} + \frac{q^2}{6\sigma^2}\right]}.$$

And,

$$\kappa = \frac{\Gamma(\frac{1}{\vartheta})\Gamma(\frac{5}{\vartheta})}{\Gamma^2(\frac{3}{\vartheta})}. \tag{4.3}$$

If the following substitutions are considered,

$$\kappa' = \frac{\kappa + \left[\frac{q^2}{2\sigma^2} + \frac{q^4}{80\sigma^4}\right]}{1 + \left[\frac{q^4}{144\sigma^4} + \frac{q^2}{6\sigma^2}\right]} = \frac{\kappa + [A + B]}{1 + [C + D]}.$$

then it may empirically be shown that the powers of σ have a diminishing effect on the values of *A, B, C* and *D*. Their values have been tabulated as follows for the (1, 1) mode of the image Lena, for Q-factors ranging from 100 to 10.

Table 4.2 *A, B, C* and *D* for varying Q-factors - Lena

Q-factor	**Lena**			
	A	***B***	***C***	***D***
100	0.0004	0.0000	0.0000	0.0001
90	0.0033	0.0000	0.0000	0.0011
80	0.0091	0.0000	0.0000	0.0030
70	0.0234	0.0000	0.0000	0.0078
60	0.0364	0.0001	0.0000	0.0121
50	0.0524	0.0001	0.0001	0.0175
40	0.0817	0.0003	0.0002	0.0272
30	0.1451	0.0011	0.0006	0.0484
20	0.3029	0.0046	0.0025	0.1010
10	1.0755	0.0578	0.0321	0.3585

Indeed, even at a Q-factor of 10, while the expected kurtosis κ is 14.162, the value of κ' is 13.265, which is a fair approximation.

Therefore, the following approximation is valid for most Q-factors.

$$\kappa \cong \kappa'. \tag{4.4}$$

The pattern of diminished values of *A, B, C* and *D* is seen in other images as well, as shown in the following tables.

Table 4.3 *A, B, C* and *D* for varying Q-factors - Peppers

Q-factor	Peppers			
	A	***B***	***C***	***D***
100	0.0004	0.0000	0.0000	0.0001
90	0.0040	0.0000	0.0000	0.0013
80	0.0111	0.0000	0.0000	0.0037
70	0.0285	0.0000	0.0000	0.0095
60	0.0444	0.0001	0.0001	0.0148
50	0.0637	0.0002	0.0001	0.0212
40	0.0992	0.0005	0.0003	0.0331
30	0.1750	0.0015	0.0009	0.0583
20	0.3743	0.0070	0.0039	0.1248
10	1.3033	0.0849	0.0472	0.4344

Table 4.4 *A, B, C* and *D* for varying Q-factors - Boat

Q-factor	Boat			
	A	***B***	***C***	***D***
100	0.0004	0.0000	0.0000	0.0001
90	0.0033	0.0000	0.0000	0.0011
80	0.0091	0.0000	0.0000	0.0030
70	0.0231	0.0000	0.0000	0.0077
60	0.0362	0.0001	0.0000	0.0121
50	0.0518	0.0001	0.0001	0.0173
40	0.0813	0.0003	0.0002	0.0271
30	0.1429	0.0010	0.0006	0.0476
20	0.2946	0.0043	0.0024	0.0982
10	1.0067	0.0507	0.0282	0.3356

Finally, to summarize from Equations (4.2), (4.3) and (4.4), the parameters of the GN-DQPMF are estimated as,

$$\sigma \cong \sqrt{E\{x'^2\}}. \tag{4.5}$$

$$\kappa' - \frac{\Gamma(1/\vartheta)\Gamma(5/\vartheta)}{\Gamma^2(3/\vartheta)} = 0. \tag{4.6}$$

4.2.3.2 Algorithm and Results

With the approximations from the previous section considered, the algorithm for the proposed approach to detecting compression history is shown in the following figure.

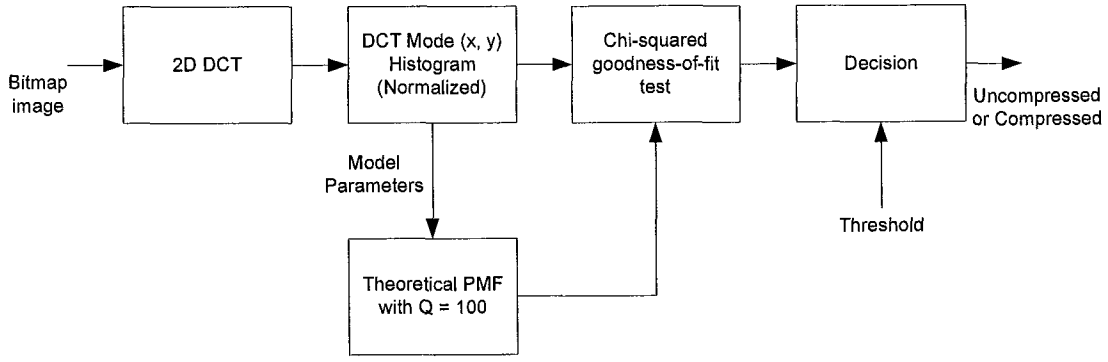

Figure 4.2 Proposed algorithm for compression history detection.

The steps of this algorithm are as follows.

1. The 2D block DCT of the bitmap image is performed, and the (1, 1) mode is extracted. Alternately, the DCT may be performed such that only the (1, 1) mode is generated. This would allow for significant computational savings.
2. The normalized histogram of the (1, 1) mode is computed and the parameters of the GN-DQPMF for this mode are estimated using Equations (4.5) and (4.6). Setting q to 1, samples of the PMF are generated.
3. A χ^2 goodness-of-fit test is performed between the normalized histogram and the generated PMF samples.
4. The statistic from step 3 is compared against an empirical threshold (explained subsequently) to determine if the image has been compressed or not.
5. Optionally, the decision may be confirmed by performing steps 1 to 5 for modes (0, 1) and (1, 0), at the cost of increased computation.

5. Optionally, the decision may be confirmed by performing steps 1 to 5 for modes (0, 1) and (1, 0), at the cost of increased computation.

To validate this algorithm, a general empirical threshold for the decision process must be determined first. For this purpose, a few standard bitmap files (for instance from [29]) are chosen and subjected to a 2D block DCT operation with a Q-factor of 100. The (1, 1) mode is extracted from this DCT and the GN-DQPMF parameters are derived from it, as detailed above. The (1, 1) mode is then quantized for Q-factors ranging from 100 to 10 and the χ^2 test statistic between the normalized histogram of the (1, 1) mode and samples of the GN-DQPMF (with $q = 1$) is calculated. Clearly, the test statistic for a Q-factor of 100 will be the lowest (since for a Q-factor of 100, q will equal 1) and a general threshold may be calculated from the magnitude of this particular statistic across different images.

To illustrate this point, a few results are tabulated as follows.

Table 4.5 Q-factors and χ^2 test statistics for compression detection

Q-factor	**χ2 test statistic (Sample set size = 1000)**			
	Lena	**Baboon**	**Peppers**	**Bridge**
100	777	342	667	317
90	7117	6590	7265	6398
80	14167	13042	13755	12756
70	23217	23806	22791	22633
60	28604	30352	27663	28645
50	33522	36973	32100	35268
40	39685	47081	37726	45825
30	50083	64744	47592	60605
20	64122	93703	58135	87097
10	97868	170263	74466	149044

From these results, it is seen that the χ^2 test statistic is lowest at a Q-factor of 100, as expected. Of note is the fact that the χ^2 test statistic for a Q-factor of 100 has a numerical value of less than 1000, while the test statistics for lower Q-factors are significantly higher than 1000. Thus, factoring in a potential error of 500, 1500 may be considered as a general, empirical threshold for detection of compression. Therefore, if the normalized (1, 1) mode histogram of a bitmap's DCT leads to a χ^2 test statistic of value greater than 1500 when compared against a generated GN-DQPMF, it may with some degree of certainty, be concluded that the image had undergone compression in the past. With this as reference, the following experiments have been carried out.

Table 4.6 χ^2 test statistics for compression detection with arbitrary Q-factors

Image	**Q-factor**	**χ2 test statistic**	**Decision (Statistical threshold = 1500)**
Splash	95	6996	Compressed
Tiffany	100	340	Uncompressed
F-16	70	21359	Compressed
Aerial	20	90434	Compressed
Stream and Bridge	100	570	Uncompressed
Boat	100	574	Uncompressed
Elaine	50	32376	Compressed
House	40	45459	Compressed

JPEG compression history detection tests were run across 44 images from [29], and the results are tabulated in the following page. The χ2 test statistic threshold used is 1500, as noted above, for 1000 samples of the normalized mode histogram.

Table 4.7 Q-factors and Detection Success Rate for compression history detection

Compression Q-factor	Detection Success Rate
95	98%
90	100%
85	100%
80	100%
75	100%
70	100%
65	100%
60	100%
55	100%
50	100%
45	100%
40	100%
35	100%
30	100%
25	100%
20	100%
15	100%
10	100%

Compared against the Fan and Queiroz approach, the proposed technique has the advantage that a compression factor of 95 is estimated with 98 % confidence. As per Fan and Queiroz's results shown in the following table, their approach detailed in Section 4.2.2 can detect compression up to a Q-factor of 90, with reasonable confidence bounds.

Table 4.8 Thresholds for the Fan and Queiroz approach, across images and Q-factors

VALUES OF λ FOR SEVERAL IMAGES AND QUALITY FACTORS USING THE PROPOSED ALGORITHM. BY THRESHOLDING THE VALUES TO 0.25 ONE CAN DETECT JPEG COMPRESSED IMAGES WITH SOME CONFIDENCE. VALUES OF $\lambda > 0.25$ ARE HIGHLIGHTED. NOTE THAT WITH THIS THRESHOLD, DETECTION IS POSSIBLE WITH QUALITY FACTORS AS HIGH AS 90

Image	Orig	Q100	Q90	Q70	Q50	Q30	Q10
Baby	0.0779	0.0889	*0.3998*	*0.7072*	*0.7982*	*0.9058*	*1.1212*
Barbara	0.1106	0.1131	*0.4732*	*0.6795*	*0.7581*	*0.8597*	*1.1073*
Chapel	0.0484	0.0468	*0.5243*	*0.6330*	*0.7351*	*0.7863*	*0.8758*
Cameraman	0.2279	0.2258	*0.6171*	*0.6878*	*0.8085*	*0.7555*	*0.7971*
Kids	0.0266	0.0315	*0.5943*	*0.9024*	*1.0789*	*1.2194*	*1.2409*
Lake	0.0506	0.0496	0.1855	*0.4167*	*0.5106*	*0.5868*	*0.8100*
Lena	0.0844	0.0678	*0.6359*	*0.9514*	*1.0343*	*1.1013*	*1.1232*
Mixed	0.0967	0.1071	*0.3341*	*0.5213*	*0.7133*	*0.7921*	*0.8967*
Shaver	0.0355	0.0897	*0.6339*	*0.6844*	*0.5876*	*0.5434*	*0.5790*
Wine	0.1169	0.0978	0.1794	*0.3527*	*0.4689*	*0.5820*	*0.8743*

Source: Z. Fan and R. de Queiroz, "Identification of bitmap compression history: JPEG detection and quantizer estimation," IEEE Transactions on Image Processing, vol. 12, pp. 230–235, Feb. 2003.

The proposed approach, as in the Fan and Queiroz approach, suffers from the drawback that a bitmap image previously compressed with a Q-factor of 100 would be reported as having no compression history.

4.3 Detection of Historical JPEG Q-factor in a Bitmap Image

JPEG Q-factor detection is an important image forensics application. Often, uncompressed images received from unknown media may have undergone JPEG compression in the past, and it is instructive to know the extent of that compression.

4.3.1 The Approach Proposed by Fan and Queiroz

Fan and Queiroz (2003) [22] proposed a method to detect the extent of historical JPEG compression in a bitmap image, i.e., the JPEG Q-factor, using 2D block DCT statistics. In this approach, a likelihood function to determine the quantization step is derived and is used to estimate the Q-factor.

The approach first develops an analytic expression for the histogram of a single AC mode of the block DCT of the bitmap by convolving an impulse train located at a-priori estimates of the quantization step q, with a bounded Gaussian pulse. This effectively describes the *bumps*[6] shown in the following figure (ignoring the envelope).

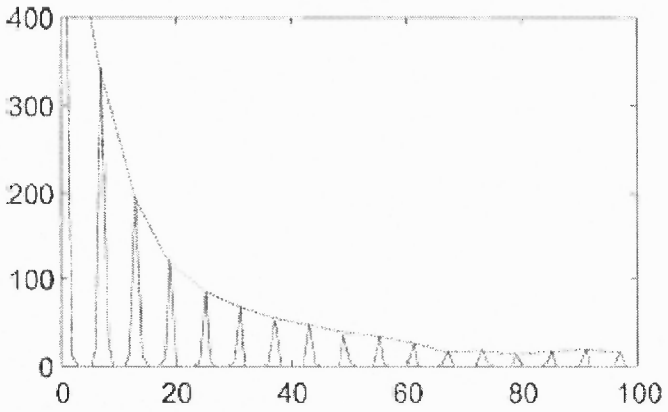

Figure 4.3 Histogram of the (0, 1) mode of a decompressed bitmap (Lena) DCT.

Source: Z. Fan and R. de Queiroz, "Identification of bitmap compression history: JPEG detection and quantizer estimation," IEEE Transactions on Image Processing, vol. 12, pp. 230–235, Feb. 2003.

Then, the approach attempts to locate the true locations of the peaks of the bumps using a Maximum Likelihood Estimator (MLE), shown below.

$$q(m,n) = \arg\max\left\{\sum_{s}\log\left\{\int_{Ys'-0.5}^{Ys'+0.5}\sum_{k}[\mathrm{G}(Y-rq-kq)]\,dY\right\} + N\log q\right\}. \qquad (4.7)$$

Here, $q(m,n)$ is the estimated quantization step for mode (m,n), Ys' is the block DCT coefficient corresponding to the mode (m,n) for block s, $G(...)$ is the bounded Gaussian pulse describing each bump, r and k are integral indices into the image, N is a count of the blocks in the image, q is an a-priori estimate of the quantization step.

[6] Each 'bump' is an impulse-like pulse in the figure.

The a-priori estimate of q is the location of the first peak following the peak at zero. The final estimate of q is mapped back to obtain the JPEG Q-factor.

This approach was refined by Neelamani *et al* (2003) [34] to cater to color images. The refinement is in the modeling of DCT coefficients by a Laplacian PDF and the addition of explicit normalization.

4.3.2 Proposed Approach

The proposed approach employs the GN-DQPMF in a manner that is very similar to the compression history detection approach proposed in Section 4.2.3.

4.3.2.1 Algorithm

GN-DQPMFs are generated for Q-factors ranging from 10 to 100 in uniform steps with model parameters determined from the (1, 1) mode of the bitmap's block DCT using Equations (4.5) and (4.6). The χ^2 test statistic is then used as a distance measure between the PMFs and the normalized histogram of the (1, 1) mode. The Q-factor corresponding to the PMF with the lowest χ^2 test statistic is declared the Q-factor with which the bitmap image had been historically compressed. The process is shown in the following figure.

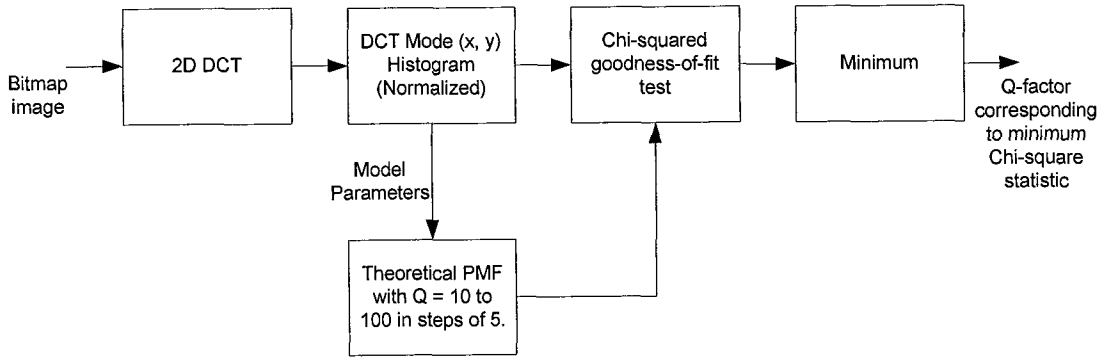

Figure 4.4 Proposed algorithm for Q-factor detection.

It may be recalled from Section 4.2.3 that the model parameters detected from the block DCT mode are approximations only. However they are sufficiently accurate to detect Q-factors of as low as 30 with a high rate of success.

4.3.2.2 Results

This detection process was carried out for a few arbitrary images from [29], with arbitrary Q-factors, as listed in the following table.

Table 4.9 Q-factors and χ^2 test statistics for Q-factor detection

Image	**Compression Q-factor**	**χ^2 statistic**	**Detected Q-factor**
Splash	95	1013	95
Tiffany	100	340	100
F-16	70	1233	70
Aerial	20	186	20
Boat	100	574	100
Elaine	50	359	50
House	40	326	40

The proposed Q-factor detection approach was run across 44 standard grayscale test images from the USC-SIPI database [29]. Every image was JPEG compressed with Q-factors ranging from 10 to 100 in steps of 5. The average success rate for each Q-factor was then calculated as a percentage. The obtained results are shown in the following table.

Table 4.10 Q-factors and Q-factor detection success rates

Compression Q-factor	Detection Success Rate
100	65%
95	83%
90	87%
85	83%
80	87%
75	87%
70	87%
65	90%
60	90%
55	90%
50	84%
45	81%
40	84%
35	84%
30	84%
25	75%
20	65%
15	49%
10	30%

This detection method works best for values of Q-factor in the range [30, 95]. At lower values of Q, the model parameters are significantly inexact, leading to low detection success rate for low values of Q-factor. At a Q-factor value of 100, the detected Q-factors were found to be in the range [96, 100], leading to lowered success rates. It has been observed in general that the error in detection is no greater than a Q-factor of 5 with the proposed approach.

The results from Table 4.10 are plotted as a graph, and compared against the results from the Fan and Queiroz approach.

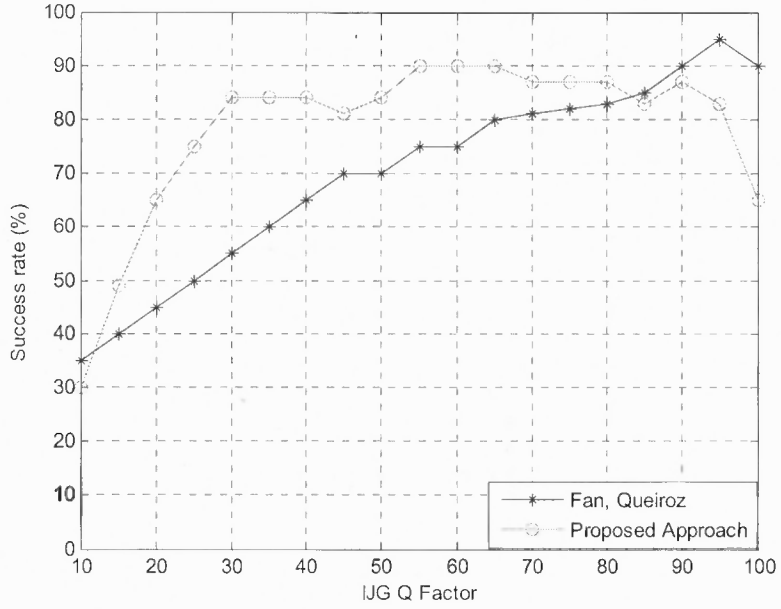

Figure 4.5 Q-factor detection success rate for the Fan and Queiroz approach and the proposed approach.

On average, the performance of the proposed method is better than that of the Fan and Queiroz approach. The performance of both approaches is fairly poor at very low Q-factors, i.e., [10, 20], but the performance of the proposed approach is better for the Q-factors in the range [30, 80]. The performance of the proposed approach is slightly worse than the Fan and Queiroz approach for Q-factor values close to 100, but as noted earlier, this error is only by a maximum Q-factor value of about 5.

The approach may be optimized to be computationally less intensive by using a divide-and-conquer algorithm, similar to Binary Search [35].

4.4 Leading Digit Distributions – Validating the Generalized Benford Law

In this application, the GN-QPMF will be shown to validate the Generalized Benford's Law for quantized AC Block DCT coefficients [27].

Leading digit probability distributions of block DCT data have been used in image forensics in the past decade [36][27][39]. Here, previous research pertaining to leading digit distributions in the context of block DCT coefficients is summarized, and an attempt is made to develop a model for the leading digit distribution of quantized AC block DCT coefficients using finite Generalized Normal mixtures.

4.4.1 Background Information

This subsection explores the theory of leading digit distribution and its relevance to block DCT data.

4.4.1.1 Leading Digits and Benford's Law

The leading digit distribution of a real data set is the PMF of the first digits of the numbers in the set. Certain naturally-occurring data sets which span multiple decimal scales, have been shown to display unique statistical properties in their leading digits [23]. These numbers have a leading digit distribution that follows a decimal-base logarithmic characteristic given as,

$$p_D(d) = \log_{10}\left(1 + \frac{1}{d}\right), 1 \leq d \leq 9, d \in Z^+. \tag{4.8}$$

The implication is that the digit 1 has the highest probability of occurrence as a leading digit, and subsequent digits have progressively lower probabilities. The following table lists the probability values.

Table 4.11 Probability values of leading digits for scale invariant natural data

d	1	2	3	4	5	6	7	8	9
$p_D(d)$	0.301	0.176	0.125	0.0969	0.0791	0.0669	0.057	0.051	0.046

This property of naturally occurring data was discovered by in 1881 by Simon Newcomb and was formalized by Frank Benford in 1932. For over sixty years, this law remained unproven, until it was analytically justified in Hill (1996) [51].

4.4.1.2 Benford's Law and Exponential Random Variables

The law is of relevance in this context owing to the fact that the floating point AC block DCT coefficients, i.e., block DCT coefficients before quantization, follow Benford's law in a *weak* fashion [36]. The implication of the term *weak* is that the AC block DCT coefficients, on average, follow Benford's law. This will become clearer subsequently.

The reason for AC block DCT to be weakly *Benford*[7] is twofold.

- Each mode of 2D DCT, assumed Laplace distributed, may be modeled as an infinite Gaussian mixture, with individual variance controlled by an exponential distribution [25].
- Exponential random variables are weakly Benford [26].

These two conditions are both necessary and sufficient for AC block DCT coefficients to be Benford since Property 3 in [36] states that a random variable whose PDF is modeled as an infinite Gaussian mixture with exponentially distributed variance control can be expressed as a product of the Gaussian random variable and the square-root of the variance control random variable. As noted earlier, according to [26],

[7] When a data set is said to be 'Benford', it implies that the set follows Benford's Law in either a weak or strong fashion.

caution (since the property is mostly valid for *strongly* Benford random variables), it may be asserted that random variables that are Laplace distributed could be considered weakly Benford.

A proof for the first assertion is available in Hjorunges, Lervik and Ramstad (1996) [25], where it is shown that if a stochastic process X has a probability defined as,

$$p_X(x) = \int_0^\infty \frac{1}{\sqrt{2\pi\sigma^2}} \exp\left(-\frac{x^2}{2\sigma^2}\right) \lambda \exp(-\lambda\sigma^2) d\sigma^2.$$

then the integral can be shown to evaluate to,

$$p_X(x) = (\sqrt{\lambda/2}) \exp(-\sqrt{2\lambda}|x|).$$

which is a Laplacian distribution [24].

The weak Benford nature of exponential random variable is explored in Engel and Leuenberger (2003) [26]. It is shown that for an exponential distribution $f(t)$ with shape parameter λ,

$$f(t) = \lambda \exp(-\lambda t) \qquad t > 0.$$

The probability of the leading digit being d is given as,

$$g_d(\lambda) = \sum_{k=-\infty}^{\infty} \exp(-\lambda d 10^k)\,(1 - \exp(-\lambda 10^k)).$$

Evidently, this probability is a function of λ. Furthermore,

$$g_d(10\lambda) = \sum_{k=-\infty}^{\infty} \exp(-10\lambda d 10^k)\,(1 - \exp(-10\lambda 10^k)).$$

$$= \sum_{k=-\infty}^{\infty} \exp(-\lambda d 10^{k+1})\,(1 - \exp(-\lambda 10^{k+1})).$$

$$= \sum_{k=-\infty}^{\infty} \exp(-\lambda d 10^k)\,(1 - \exp(-\lambda 10^k)) = g_d(\lambda).$$

$$= \sum_{k=-\infty}^{\infty} \exp(-\lambda d 10^k)\,(1 - \exp(-\lambda 10^k)) = g_d(\lambda).$$

In general,

$$g_d(10^x \lambda) = g_d(\lambda) \quad x \in Z.$$

Thus, $g_d(\lambda)$ is periodic in powers of 10. Considering then a new function,

$$h_d(x) = g_d(10^x).$$

It is easily seen that $h_d(x)$ is 1-periodic. [26] considers the Fourier series expansion of $h_d(x)$ and shows that it is sinusoidal with a single harmonic. $h_d(x)$ is plotted for $d \in [1, 9]$ in the following figure.

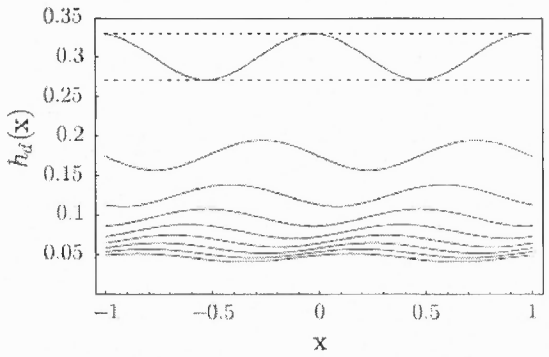

Figure 4.6 A plot of the leading digit probabilities, on a log-scale. The topmost sinusoid is for the digit 1, and subsequent sinusoids are for digits from 2 to 9. The mean value of the sinusoid is the strong Benford probability value.

Source: H. Engel and C. Leuenberger, "Benford's law for exponential random variables", Statistics & Probability Letters, vol. 63, no. 4, pp. 361-365, July 2003.

An important observation from Figure 4.6 is that the average value of each sinusoid is the corresponding digit probability according to Benford's Law (Table 4.11). That is, the average value of $h_1(x)$ is 0.301, the average value of $h_2(x)$ is 0.176, and so on.

the sinusoids would be replaced by flat lines positioned at the average value of each sinusoid. Ergo, exponential random variables are *weakly* Benford.

4.4.1.3 Benford's Law and AC Block DCTs

Perez-Gonzalez, Heileman and Abdallah (2007) [36] show that the 2D AC DCT coefficients, modeled with the Generalized Normal distribution are *weakly* Benford as well. Their paper employs the following property of random variables that follow Benford's law.

If X is a random variable that follows Benford's law *strongly*, the transformation,

$$Y = (log_{10}X)\ mod\ 1.$$

leads to a random variable Y that is Uniformly distributed [37].

The histogram of the DCT of Lena in $(log_{10}X)\ mod\ 1$ is shown in the following figure.

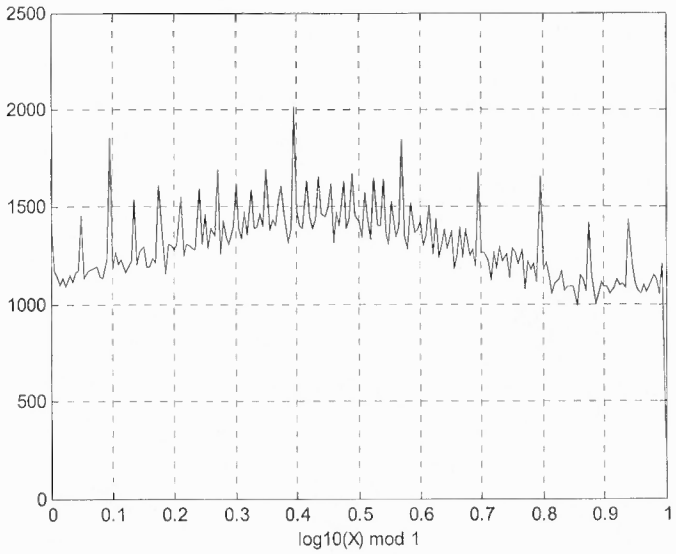

Figure 4.7 A plot of floating-point DCT coefficient histogram in $(log_{10}X)\ mod\ 1$ space.

Evidently, the histogram appears to be sinusoidal with diminishing harmonic amplitudes, and with some 'DC' component. This is proof that the 2D DCT is *weakly* Benford in a manner similar to the plots in Figure 4.6.

This property does not hold for the case of a quantized AC block DCT histogram, as shown in the following plot.

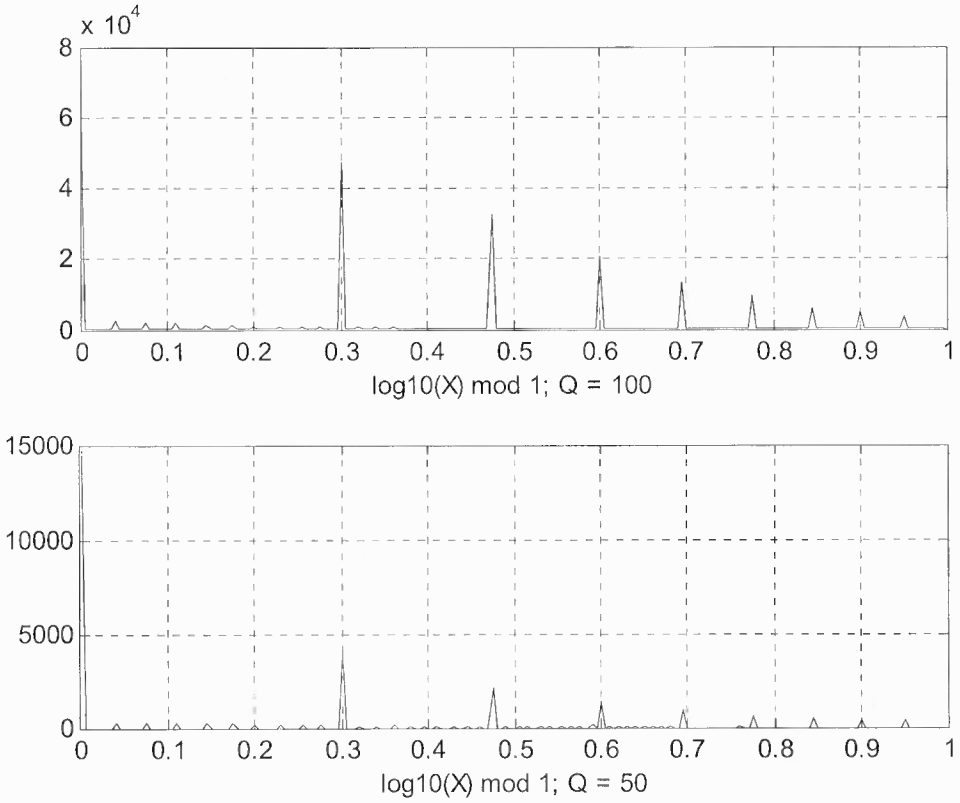

Figure 4.8 Plots of quantized DCT coefficients' histograms in $(log_{10} X)$ *mod* 1 space.

.

It is of note that the peaks in the above plots exist only at the logarithms of integers in [1, 9]. This is a consequence of quantization.

It follows from the above plots that quantized block DCTs do not follow Benford's law. This is true of individual modes of the quantized block DCT as well, as shown for the mode (1, 1) histogram in the following plot.

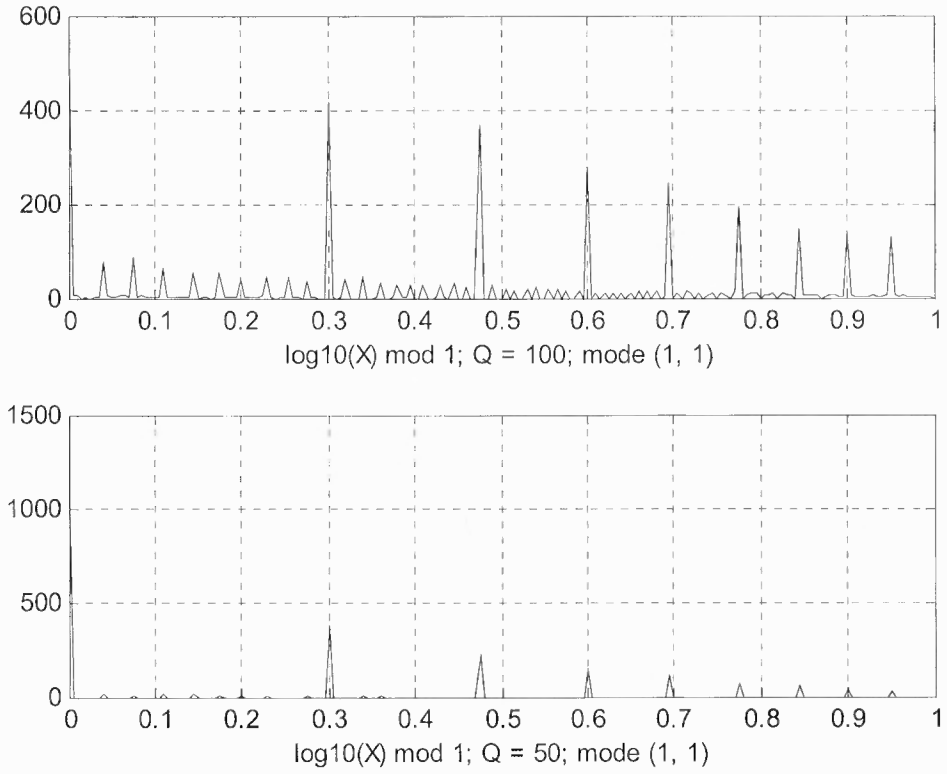

Figure 4.9 Plots of the (1, 1) mode histogram of quantized DCT coefficients in $(log_{10} X)$ *mod* 1 space.

4.4.1.4 The Generalized Benford's Law as per Fu *et al.*

Quantized block DCTs follow the *Generalized* Benford's Law, proposed by Fu, Shi and Su (2007) [27]. This model is shown in the following equation.

$$p(x) = N \log_{10}\left(1 + \frac{1}{s + x^q}\right), x = 1, 2, \ldots, 9. \tag{4.9}$$

The parameters N, s and q are empirically determined, and are listed in the following table for varying Q-factors.

Table 4.12 Model parameters for varying Q-factors, for the Generalized Benford model.

Q-factor	Model Parameters		
	N	q	s
100	1.456	1.47	0.0372
90	1.255	1.563	-0.3784
80	1.324	1.653	-0.3739
70	1.412	1.732	-0.337
60	1.501	1.813	-0.3025
50	1.579	1.882	-0.2725

Source: D. Fu, Y.Q. Shi, and W. Su, "A generalized Benford's law for JPEG coefficients and its applications in image forensics," in Proc. SPIE, Security, Steganography and Watermarking of Multimedia Contents IX, San Jose, USA, January 2007.

This distribution is for the first digits of *all* quantized AC DCT coefficients. To formally derive an equivalent model from the GN-QPMF[8], the concept of mixture distributions will first have to be used to develop a composite model for all quantized AC coefficients.

4.4.2 A Complete Model for all Quantized AC block DCT Coefficients

Considering that the quantized block DCT distributions derived in Chapter 3 models each mode of the DCT block as a distinct random variable, a complete quantized DCT distribution encompassing all AC modes must be derived from a combination of individual mode distributions.

4.4.2.1 Finite Mixtures

It is known that Discrete Cosine Transform coefficients have minimum cross-correlation for most natural images [2]. This form of linear independence may be exploited, to estimate a composite model for all quantized AC block DCT coefficients.

[8] Refer to Equation (3.38)

The aggregate quantized AC block DCT coefficient set may be seen as a mixture of 63 (AC) linearly independent variables. The PDF of a finite mixture of random variables is generally given as a convex combination of the PDFs of those individual random variables, as shown in Titterington, Smith and Makov (1985) [52]. In general, if X is a mixture of n component discrete random variables Y_i, the PDF of X, $f_X(x)$ is given as,

$$f_X(x) = \sum_{i=1}^{n} a_i f_{Y_i}(x). \tag{4.10}$$

Here,

$f_{Y_i}(x)$ is the PDF of the i^{th} random variable. a_i is the mixture proportion for the i^{th} random variable.

Furthermore, the following convex sum requirement has to be satisfied by the mixture proportions.

$$\sum_{i=1}^{n} a_i = 1. \tag{4.11}$$

In the specific case of AC DCT coefficients, the mixture proportions are equal. Therefore,

$$a_1 = a_2 = \cdots = a_n = \frac{1}{n}, n = 63. \tag{4.12}$$

4.4.2.2 Finite Mixtures and Quantized AC Block DCT Coefficients

While a composite model for non-quantized AC block DCT coefficients is empirically shown to be a Cauchy distribution by Eggerton and Srinath (1986) [32], there has been no model proposed for quantized AC block DCT coefficients. The remaining part of this section will attempt to develop such a model.

Recalling the Generalized Normal Quantized PMF (GN-QPMF) for the quantized AC block DCT coefficients from Equation (3.38) with the parameters of the PMF assumed to be known a-priori,

$$p_R(n \mid K, N, \Sigma)$$

$$= \begin{cases} \frac{k\vartheta\alpha(\vartheta)}{12\sigma\Gamma(1/\vartheta)}\left[\exp\left\{-\left[\alpha(\vartheta)\left(\frac{k}{2\sigma}\right)\right]^{\vartheta}\right\} + 4\exp\left\{-\left[\alpha(\vartheta)\left(\frac{k}{4\sigma}\right)\right]^{\vartheta}\right\} + 1\right] & n = 0. \\ \frac{k\vartheta\alpha(\vartheta)}{12\sigma\Gamma(1/\vartheta)}\left[\exp\left\{-\left[k\alpha(\vartheta)\left|\frac{2n+1}{2\sigma}\right|\right]^{\vartheta}\right\} + 4\exp\left\{-\left[k\alpha(\vartheta)\left|\frac{n}{\sigma}\right|\right]^{\vartheta}\right\} + \exp\left\{-\left[k\alpha(\vartheta)\left|\frac{2n-1}{2\sigma}\right|\right]^{\vartheta}\right\}\right] & n \neq 0, n \in Z. \end{cases} \quad (4.13)$$

From Equations (4.10), (4.11) and (4.12),

$$p_M(n \mid K, N, \Sigma) = \frac{1}{63}\sum_{i=1}^{63} p_i(n \mid K, N, \Sigma).$$

Where, $p_M(n)$ is the mixture distribution, $p_i(n)$ is the i^{th} mode's PMF. Using Equation (4.13),

$$p_M(n \mid K, N, \Sigma)$$

$$= \begin{cases} \frac{1}{63}\sum_{i=1}^{63} \frac{k_i \vartheta_i \alpha(\vartheta_i)}{12\sigma_i \Gamma(1/\vartheta_i)} \left[\exp\left\{ -\left[\alpha(\vartheta_i) \left(\frac{k_i}{2\sigma_i} \right) \right]^{\vartheta_i} \right\} + \right. \\ \left. 4\exp\left\{ -\left[\alpha(\vartheta_i) \left(\frac{k_i}{4\sigma_i} \right) \right]^{\vartheta_i} \right\} + 1 \right] & n = 0. \\ \frac{1}{63}\sum_{i=1}^{63} \frac{k_i \vartheta_i \alpha(\vartheta_i)}{12\sigma_i \Gamma(1/\vartheta_i)} \left[\exp\left\{ -\left[k_i \alpha(\vartheta_i) \left| \frac{n + 1/2}{\sigma_i} \right| \right]^{\vartheta_i} \right\} + \right. \\ 4\exp\left\{ -\left[k_i \alpha(\vartheta_i) \left| \frac{n}{\sigma_i} \right| \right]^{\vartheta} \right\} + \\ \left. \exp\left\{ -\left[k_i \alpha(\vartheta_i) \left| \frac{n - 1/2}{\sigma_i} \right| \right]^{\vartheta} \right\} \right] & n \neq 0. \end{cases} \quad (4.14)$$

ϑ_i, σ_i and k_i are the model parameters of the GN-QPMF of the i^{th} DCT mode.

Analytic computation of this summation is mathematically rigorous and is not of significant value in this context. Instead, the sum is solved numerically, and the fit of this model is visually and objectively measured as follows.

The Lena image is subjected to a 2D block DCT, followed by quantization with a range of Q-factors. KS tests are performed to measure the goodness of fit of the model in Equation (4.14) with the probability distribution of all quantized AC DCT coefficients. This is repeated for a select set of standard images from [29]. The plots for Lena with Q-factors of 100, 90 and 85 are shown.

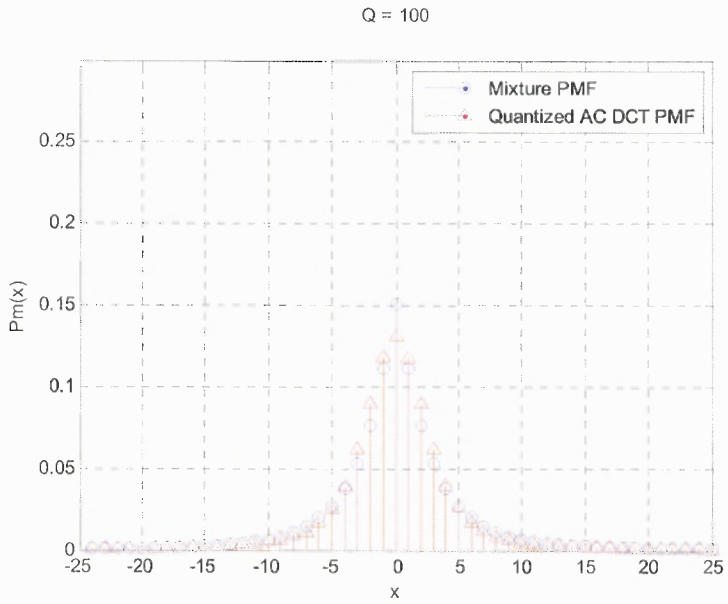

Figure 4.10 Plot of AC DCT PDF and Mixture PMF of Lena modeled as above, for Q = 100.

.

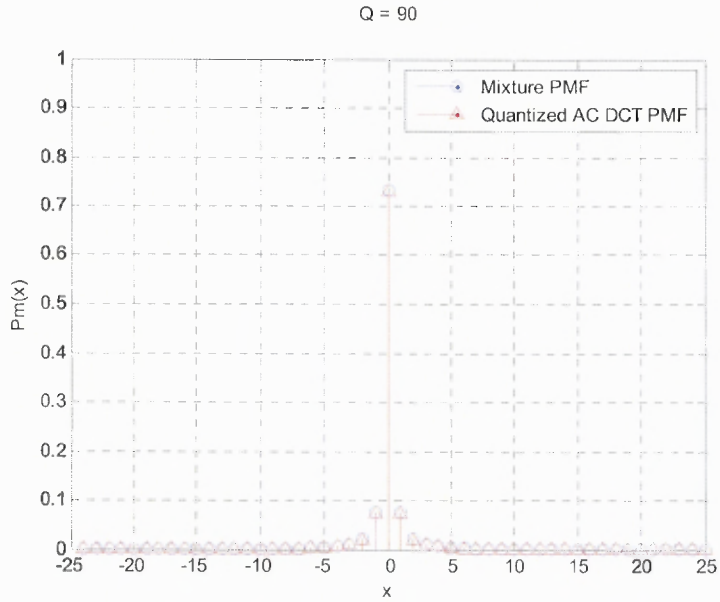

Figure 4.11 Plot of AC DCT PDF and Mixture PMF of Lena modeled as above, for Q = 90.

.

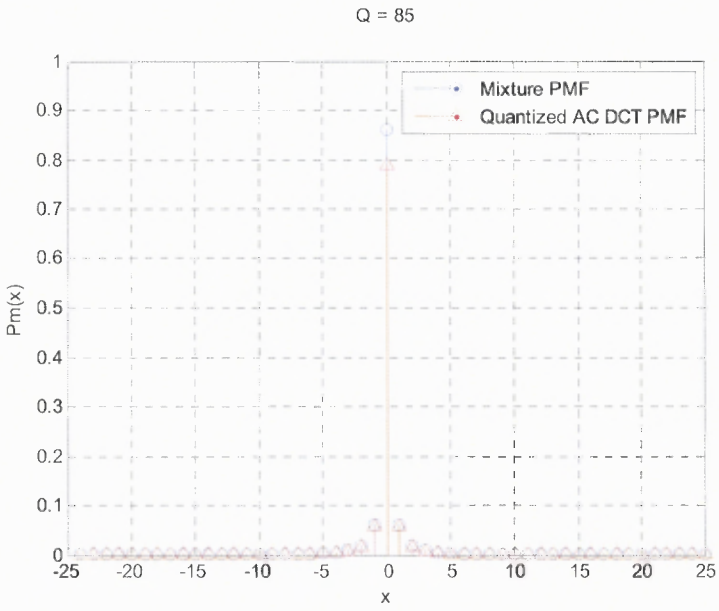

Figure 4.12 Plot of AC DCT PDF and Mixture PMF of Lena modeled as above, for Q = 85.

The corresponding KS test results are shown in the following table.

Table 4.13 KS test results for AC DCT coefficient histograms and the Mixture PMF.

Image	**Q-Factor**	**KS Test Statistic**
Splash	100	0.4326
F-16	90	0.7053
Aerial	100	0.2837
Stream and Bridge	95	0.6034
Boat	85	0.7892

Considering that all values of the KS test statistic in the table are significantly lower than 1, the model is a fairly close match to the empirical data sets.

4.4.3 A Model for First Digit Distribution – Validating the Generalized Benford's Law

The composite model for all quantized AC block DCT coefficients developed in Equation (4.14) may be used to derive the first digit distribution of quantized AC block DCT coefficients, by summing in decimal ranges, i.e., {[1, 9]}, {[10, 19], [20, 29], [30, 39], …, [90, 99]}, {[100, 199], [200, 299], …, [900, 999]} and so on.

Analytically therefore, the first digit distribution $p_D(n)$ is expressed as,

$$p_D(n) = \lim_{t\to\infty}\left[\sum_{k=0}^{t-1}\sum_{l=0}^{10^k-1} p_M(n10^k + l)\right] \qquad 1 \le n \le 9. \qquad (4.15)$$

Where $p_M(n)$ is there mixture PMF.

While computing the first digit probabilities using Equation (4.15) is mathematically rigorous, for practical purposes, a useful approximation to use the mixture probabilities in the range [1, 9] (t = 1 in Equation (4.15)) since a majority of values in the normalized histogram of the data lie in that range. Therefore,

$$p_{D'}(n) \cong \frac{p_M(n)}{\sum_{i=1}^{9} p_M(i)}, 1 \le n \le 9.$$

Where $p_{D'}(n)$ is an approximation to the first digit PMF and $p_M(n)$ is the mixture PMF.

This approximation is not a very good match for Q-factor of 100, since there are a significant number of values of quantized AC-DCT coefficients outside the range [1, 9]. This is evident in the following plot.

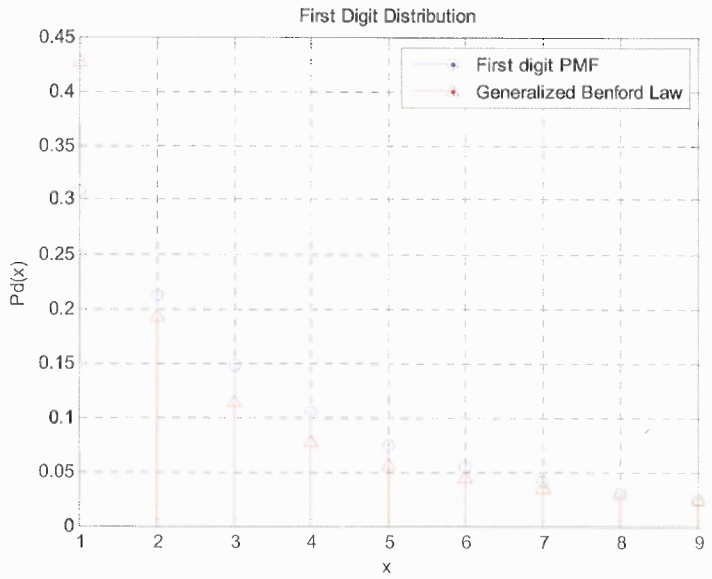

Figure 4.13 Plot of Generalized Benford's Law versus Mixture PDF in [1, 9], for Q = 100.

The fit may be improved by using t values of 2 or greater in Equation (4.15). The improved fit for a t value of 2 is shown in the following plot.

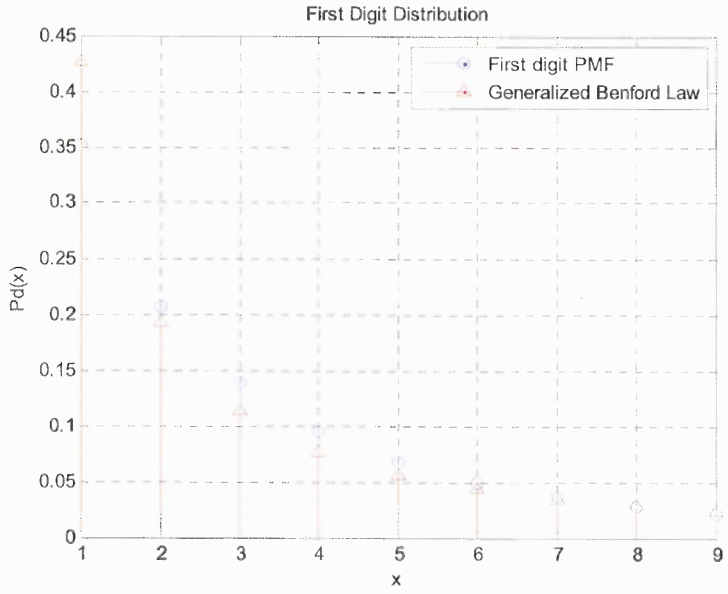

Figure 4.14 Plot of Generalized Benford's Law versus Mixture PDF in [1, 9], for Q = 100. (Additional samples of the PMF considered).

The plot in Figure 4.14 fits the Generalized Benford's Law better than the plot in Figure 4.13. This is especially visible at $x = 1$. For more aggressive quantization, i.e., with lower values of Q-factor, the approximation is more valid, since a higher percentage of values in the quantized AC block DCT histogram lie in the range [1, 9]. This is seen in the plots on the following page.

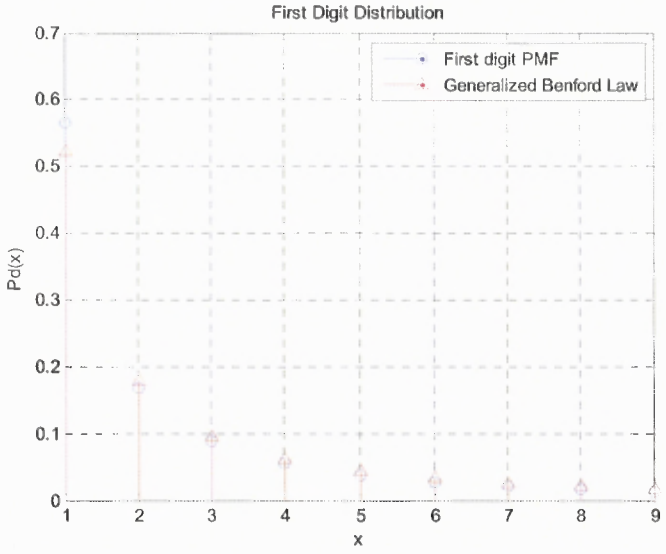

Figure 4.15 Plot of Generalized Benford's Law versus Mixture PDF in [1, 9], for Q = 90.

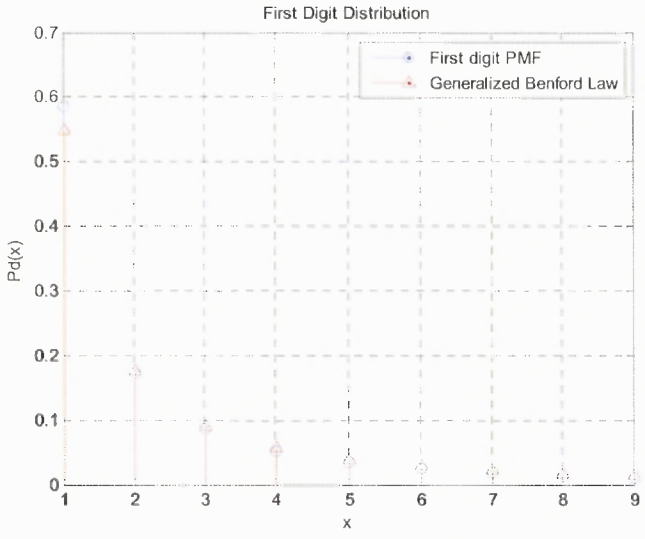

Figure 4.16 Plot of Generalized Benford's Law versus Mixture PDF in [1, 9], for Q = 80.

These results are valid across multiple images, as evidenced by the KS test results shown below. The KS tests compares the Generalized Benford's law PMF and the first digit distribution approximation, $p_D(n)$, derived above.

Table 4.14 KS test results for AC DCT coefficients' first digit distribution.

Image	Q-Factor	KS Test Statistic
Splash	90	0.2222
Tiffany	80	0.2112
F-16	70	0.2077
Aerial	60	0.2037
Elaine	70	0.2022

It is of note that the KS test statistics are uniformly low across all images, implying a very close fit between the distributions. Furthermore, the statistics are progressively lower for lower values of Q-factor, implying increasingly better fits.

Thus, the Generalized Benford's Law based model as suggested by Fu et al (2007) is validated in an approximate manner from the point of view of quantized distributions. The accuracy of the validation may be improved with a more compact expression for the mixture distribution. This would aid in evaluating the limit in Equation (4.15) in a considerably simpler and more accurate fashion. Indeed, this may be seen as follow-up work to this research.

CHAPTER 5

CONCLUSIONS AND SUMMARY

5.1 Summary

This thesis studies the various probability distributions of type-II 2D DCT coefficients in the context of JPEG compression. Block DCT distributions, full frame DCT distributions and DCT quantization error distributions have been studied from existing literature.

Literature survey shows that DC coefficients of block DCT are Gaussian distributed, while AC coefficients are Laplacian, Generalized Normal or Generalized Gamma distributed. The literature survey also shows that full-frame DCT coefficients are best modeled as Laplacian distributed and DCT quantization error distributions are either Laplacian or Uniform distributed depending on whether the DCT coefficient is quantized to a zero or a non-zero value respectively.

Models have been derived for the probability mass functions of quantized block DCT coefficients and de-quantized block DCT coefficients (QPMF and DQPMF respectively), starting from Laplacian, Generalized Normal and Generalized Gamma distributions. The corresponding PMFs are named,

- L-QPMF: The QPMF based on the Laplacian model for AC block DCT.
- GN-QPMF: The QPMF based on the Generalized Normal model for AC block DCT.
- GG-QPMF: The QPMF based on the Generalized Gamma model for AC block DCT.
- L-DQPMF: The DQPMF based on the Laplacian model for AC block DCT.
- GN-DQPMF: The DQPMF based on the Generalized Normal model for AC block DCT.
- GG-DQPMF: The DQPMF based on the Generalized Gamma model for AC block DCT.

The suitability of each QPMF and DQPMF has been evaluated across multiple images for specific, non-DC low-frequency subbands (modes) of the block DCT, using the χ^2-squared and Kolmogorov-Smirnov goodness-of-fit tests. It has been concluded that the GN-QPMF and GN-DQPMF are the most suitable distributions, since they have relatively low goodness-of-fit statistics when compared to L-QPMF and L-DQPMF respectively and only two model parameters as compared to three in the case of GG-QPMF and GG-DQPMF respectively. The expressions for GN-DQPMF and GN-QPMF and their corresponding first four moments are given in the following set of equations.

1. GN-DQPMF:

$$p_R(nq) = \begin{cases} \frac{q\vartheta\alpha(\vartheta)}{12\sigma\Gamma(1/\vartheta)}\left[\exp\left\{-\left[\alpha(\vartheta)\left(\frac{q}{2\sigma}\right)\right]^{\vartheta}\right\} + 4\exp\left\{-\left[\alpha(\vartheta)\left(\frac{q}{4\sigma}\right)\right]^{\vartheta}\right\} + 1\right] & n = 0. \\ \frac{q\vartheta\alpha(\vartheta)}{12\sigma\Gamma(1/\vartheta)}\left[\exp\left\{-\left[\alpha(\vartheta)\left|\frac{nq+q/2}{\sigma}\right|\right]^{\vartheta}\right\} + 4\exp\left\{-\left[\alpha(\vartheta)\left|\frac{nq}{\sigma}\right|\right]^{\vartheta}\right\} + \exp\left\{-\left[\alpha(\vartheta)\left|\frac{nq-q/2}{\sigma}\right|\right]^{\vartheta}\right\}\right] & n \neq 0, n \in Z. \end{cases} \quad (5.1)$$

Where σ is the square root of the variance of the distribution, ϑ is the shape parameter of the distribution, related to its kurtosis, q is the quantization step, and $\alpha(\vartheta) = \sqrt{\frac{\Gamma(3/\vartheta)}{\Gamma(1/\vartheta)}}$, where $\Gamma(\ldots)$ is the complete Gamma function, defined as,

$$\Gamma(z) = \int_0^{\infty} t^{z-1}e^{-t}dt.$$

The moments of a GN-DQPMF random variable x', with $E\{...\}$ being the expectation operator, are summarized as follows.

$$E\{x'\} = 0. \tag{5.2}$$

$$E\{x'^2\} = \sigma^2 + \left(\frac{1}{12}q^2\right). \tag{5.3}$$

$$E\{x'^3\} = 0. \tag{5.4}$$

$$E\{x'^4\} = \left[\frac{\Gamma(1/\vartheta)\Gamma(5/\vartheta)}{\Gamma^2(3/\vartheta)}\right]\sigma^4 + \left[\frac{q^2}{2}\sigma^2 + \left(\frac{1}{80}q^4\right)\right]. \tag{5.5}$$

2. GN-QPMF:

$$p_R(n) = \begin{cases} \frac{k\vartheta\alpha(\vartheta)}{12\sigma\Gamma(1/\vartheta)}\left[\exp\left\{-\left[\alpha(\vartheta)\left(\frac{k}{2\sigma}\right)\right]^{\vartheta}\right\} + 4\exp\left\{-\left[\alpha(\vartheta)\left(\frac{k}{4\sigma}\right)\right]^{\vartheta}\right\} + 1\right] & n = 0. \\ \frac{k\vartheta\alpha(\vartheta)}{12\sigma\Gamma(1/\vartheta)}\left[\exp\left\{-\left[k\alpha(\vartheta)\left|\frac{n+1/2}{\sigma}\right|\right]^{\vartheta}\right\} + 4\exp\left\{-\left[k\alpha(\vartheta)\left|\frac{n}{\sigma}\right|\right]^{\vartheta}\right\} + \exp\left\{-\left[k\alpha(\vartheta)\left|\frac{n-1/2}{\sigma}\right|\right]^{\vartheta}\right\}\right] & n \neq 0, n \in Z. \end{cases} \tag{5.6}$$

Where σ is the square root of the variance of the distribution, ϑ is the shape parameter of the distribution, related to its kurtosis, k is the quantization divisor for encoding, and $\alpha(\vartheta) = \sqrt{\frac{\Gamma(3/\vartheta)}{\Gamma(1/\vartheta)}}$, where $\Gamma(...)$ is the complete Gamma function, defined as,

$$\Gamma(z) = \int_0^{\infty} t^{z-1}e^{-t}dt.$$

The moments of a GN-DPMF random variable x', with $E\{...\}$ being the expectation operator, are summarized as follows.

$$E\{x'\} = 0. \tag{5.7}$$

$$E\{x'^2\} = \left(\frac{\sigma}{k}\right)^2 + \left(\frac{1}{12}\right). \tag{5.8}$$

$$E\left\{x'^3\right\} = 0. \tag{5.9}$$

$$E\{x'^4\} = \left[\frac{\Gamma(1/\vartheta)\Gamma(5/\vartheta)}{\Gamma^2(3/\vartheta)}\right]\frac{\sigma^4}{k^4} + \left[\frac{1}{2}\left(\frac{\sigma}{k}\right)^2 + \left(\frac{1}{80}\right)\right]. \tag{5.10}$$

The GN-QPMF and GN-DQPMF have been applied to,

1. Detecting the presence of JPEG compression history in a bitmap image. The approach and empirical thresholds for detection have been proposed. The approach has been compared against an established method proposed by Fan and Queiroz (2003), and has been found to outperform it.
2. Detecting the level of JPEG compression history in a bitmap image. The approach and algorithmic optimizations have been proposed. The approach has been compared against an established method proposed by Fan and Queiroz (2003), and is found to outperform it.
3. Developing a closed form summation for all quantized AC block DCT coefficients' distribution using finite Generalized Normal mixtures. The expression has been empirically tested for fit against quantized AC block DCT data from a set of images.
4. Validating the Generalized Benford's Law proposed by Fu, Shi and Su (2007) for leading digit distribution of quantized AC block DCT coefficients. An approximate expression for leading digit distributions of quantized AC block DCT coefficients has been compared against the Generalized Benford's Law model and has been found to validate it in an approximate sense.

5.2 Conclusions

The PMF models summarized in Equations (5.1) and (5.6) most suitably model quantized and de-quantized DCT coefficients respectively. Goodness-of-fit tests indicate that both the Generalized Normal de-quantized PMF and Generalized Normal quantized PMF are better than the Laplacian de-quantized PMF and Laplacian quantized PMF respectively. The Generalized Normal based PMFs have been preferred over the Generalized Gamma de-quantized PMF and Generalized Gamma quantized PMF respectively, since they offer comparable performance and have the advantage of requiring fewer model parameters. The Generalized Normal de-Quantized PMF has been employed to detect compression history in bitmap images to good effect. It is shown to outperform a classical compression history detection approach [22]. The Generalized Normal quantized PMF has finally served to validate the Generalized Benford's Law for first digit distributions [27].

APPENDIX A

CHI-SQUARED AND KOLMOGOROV-SMIRNOV GOODNESS-OF-FIT TESTS

A goodness-of-fit test is a statistical tool to determine how well an empirical data set fits a specified distribution. Pearson's χ^2 test and Kolmogorov-Smirnov test are two such tests which are popular due to their simplicity and general applicability.

Chi-Squared Goodness-of-Fit Test

The Chi-squared goodness-of-fit test establishes a χ^2 test statistic as follows:

$$\chi 2 = \sum_{i=1}^{k} \frac{(m_i - Np_i)^2}{Np_i}.$$

Where p_i is the probability of the i^{th} class of the standard distribution, m_i is the observed frequency in the i^{th} class of the input data set, k is the number of classes and N is the number of samples in the input set.

The limiting distribution of the $\chi 2$ statistic is a Chi-squared distribution, as proved by Pearson [30]. The value of the $\chi 2$ statistic is evidently lower for data that fits the theoretical distribution better.

A null-hypothesis in a goodness-of-fit test is a binary decision mechanism, by which the fit is either rejected or accepted. If the null-hypothesis is to be accepted, a derived statistic must be lower than a pre-designated threshold, and vice-versa. In the case of the Chi-squared goodness-of-fit test, the derived statistic is computed from the $\chi 2$ statistic as follows.

The derived statistic is called the *p-value*. It is computed by comparing the $\chi 2$ statistic to a $\chi 2$ distribution. The number of degrees of freedom is given as,

$$f = k - 1.$$

The value of the $\chi 2$ statistic is looked up in a Chi-squared distribution table for a specific degree of freedom. The value in the table closest to the $\chi 2$ statistic is the p-value. If p-value is above a pre-determined threshold, such as 0.05, then the null-hypothesis is accepted. If not, it is rejected.

In the context of this thesis, the p-value is not computed, since $\chi 2$ statistic is used more for comparison purposes, and less for fitting purposes.

Although MATLAB does not implement a Chi-squared test, open-source implementations of it are freely available [55].

Kolmogorov-Smirnov (KS) Goodness-of-Fit Test

The Kolmogorov-Smirnov goodness-of-fit described here is the two-sample KS test, since this thesis describes both the empirical distribution and the distribution against which to compare.

The 2-sample KS test compares a sample distribution function to a given distribution function. Analytically, the 2-sample KS test statistic is computed as follows.

A data set $X = \{x_1, x_2, \dots, x_M\}$ is considered and the sample distribution is derived,

$$F_X(z) = \begin{cases} 0, z < x_{(1)}. \\ \dfrac{n}{M}, x_{(n)} \leq z < x_{(n+1)}, \quad n = 1,2, \dots, M-1. \\ 1, z \geq x_{(M)}. \end{cases}$$

Where $x_{(n)}, n = 1,2, \dots, M$ are the order statistics of X.

The KS test statistic is defined as,

$$t = \max_{i=1,2,\ldots,M} |F_X(x_i) - F(x_i)|.$$

The KS test statistic, like the Chi-square test statistic implies a better match when it has a low magnitude.

The null-hypothesis is rejected at level α if,

$$\sqrt{\frac{N}{2}}t > K_\alpha.$$

Where N is the sample set size and K_α is determined from the specified threshold α.

MATLAB implements the 2-sample Kolmogorov-Smirnov test using the `kstest2(...)` function. It outputs the null-hypothesis, the asymptotic bound and the test statistic [56].

APPENDIX B

MATLAB CODE FOR ESTIMATION OF SHAPE PARAMETER OF GENERALIZED NORMAL USING DU'S EQUATION

The Generalized Normal distribution is guided by a shaping parameter, ϑ.

$$f(x;\sigma,\vartheta,\mu) = \frac{\vartheta\alpha(\vartheta)}{2\sigma\Gamma(1/\vartheta)}\exp\left\{-\left[\alpha(\vartheta)\left|\frac{x-\mu}{\sigma}\right|\right]^{\vartheta}\right\}.$$

Muller (1993) used Du's (1991) equation to estimate this parameter.

Du's equation:

$$\frac{\psi\left(\frac{1}{\vartheta}+1\right)+\log(\vartheta)}{\vartheta^2}+\frac{1}{\vartheta^2}\log\left(\frac{1}{n}\sum_{i=1}^{n}|x_i|^{\vartheta}\right)-\frac{\sum_{i=1}^{n}|x_i|^{\vartheta}\log(|x_i|)}{\vartheta\sum_{i=1}^{n}|x_i|^{\vartheta}}=0.$$

Where the symbols have their usual meaning, as defined in Section 2.1.2.

A MATLAB implementation of Du's equation is provided below.

```
%% This is the p-estimator as per Du

% Given a set of stochastic data, it should be possible to estimate
% the shaping factor of the Generalized Normal distribution using
% this.

function nu = EstimatePKnP(data_vector)

% We start off with a fixed moment parameter, m and the stochastic
% distribution itself.
incoming_data = data_vector;
moment = 3;
N = numel(incoming_data);

sum_x_log_x = 0;
e_m = 0;

% Estimate parameters - 1.
for i = 1:N
    if (incoming_data(i) ~= 0)
        sum_x_log_x = sum_x_log_x + (power(abs(incoming_data(i)),
moment) * log(abs(incoming_data(i))));
```

```
    end

    e_m = e_m + (power(abs(incoming_data(i)), moment));

end

idx = 0;
% estimate equation solutions for varying 'nu'
for shape_factor = 0.1:0.01:5

    factor_1 = (psi(1 + (1 / shape_factor)) + log(shape_factor)) /
        (shape_factor ^ 2);

    v_th_moment = 0;

    for j = 1:N
        v_th_moment = v_th_moment + abs(incoming_data(j)) ^
shape_factor;
    end

    v_th_moment = v_th_moment / N;

    factor_2 = (1 / shape_factor ^ 2) * log(v_th_moment);

    numerator = 0;

    for j = 1:N
        if (incoming_data(j) ~= 0)
            numerator = numerator + (abs(incoming_data(j)) ^
shape_factor) * log(abs(incoming_data(j)));
        end
    end

    factor_3 = numerator / (v_th_moment * N * shape_factor);
    should_be_zero(idx + 1) = factor_1 + factor_2 - factor_3;
    idx = idx + 1;
end

% Find the smallest of the lot.
set = 0.1:0.01:5;
nu = set(1); % Error
minimum = min(abs(should_be_zero));
for i = 1:numel(should_be_zero)
    if (minimum == abs(should_be_zero(i)))
        nu = set(i);
        break;
    end
end
```

APPENDIX C

GENERATION OF GENERALIZED NORMAL RANDOM VARIABLES WITH SHAPE PARAMETER OF 1/2 USING THE LAMBERT-W FUNCTION

Generalized Normal random variables with shape parameters other than 1, 2 and ∞ need to be generated using specialized functions. This is because neither linear, nor non-linear transformations of Uniform random variables can be used to generate them. A specific random variable with a shape factor of 0.5 can be generated using Lambert W functions as derived in Chapeau-Blondeau and Monir (2002) [31].

A Uniform random variable, $U(0,1)$, is transformed into a Generalized Normal random variable using the following transformation.

$$G(x) = \begin{cases} -\frac{1}{2\sqrt{30}}\left[1 + W_{-1}\left(-\frac{2x}{e}\right)\right]^2 & for\ 0 < x \leq \frac{1}{2}. \\ \frac{1}{2\sqrt{30}}\left[1 + W_{-1}\left(-\frac{2(1-x)}{e}\right)\right]^2 & for\ \frac{1}{2} \leq x < 1. \end{cases}$$

Where $W_{-1}(x)$ is the branch of the Lambert W function defined for $-\frac{1}{e} \leq x < 0$.

The following plot shows the Lambert W function.

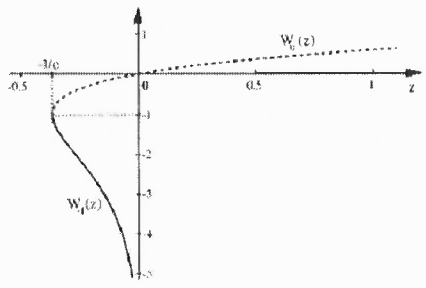

Figure C.1 Lambert W function

Source: F. Chapeau-Blondeau, A. Monir, "Numerical evaluation of the Lambert W function and application to generation of generalized Gaussian noise with exponent 1/2"; IEEE Transactions on Signal Processing 50, 2160-2165 (2002).

An implementation of the Lambert W function is available for MATLAB [57] where the branch to the function must explicitly be specified as -1.

The MATLAB code implementing this generation is fairly simple, as listed below.

```
%GENERALIZEDNORMAL05   Generate generalized normal random variables
with shape factor of 0.5.
%
%   R = GENERALIZEDNORMAL05(LAMBDA, N) returns a 1-by-N array of
%   Generalized Normal (Gaussian) random variables with a fixed mean of
0
%   and a variance specified via LAMBDA. LAMBDA is related to the
variance
%   as follows:
%
%   LAMBDA = sqrt(gamma(3 / 0.5) / (gamma(1 / 0.5) * variance));
%   => LAMBDA = sqrt(120 / variance);
%   => variance = 120 / LAMBDA^2;
%
%   This implementation uses the transformation established by
%   Chapeau-Blondeau and Monir in,
%   "Numerical Evaluation of the Lambert W Function and Application to
%   Generation of Generalized Gaussian Noise With Exponent 1/2"
%   available at
%   http://www.istia.univ-angers.fr/~chapeau/papers/lambertw.pdf
function gg_rand_05 = GeneralizedNormal05(lambda, n_el)

% Generate uniform randoms
u_rand = rand(1, n_el);
% Allocate array
gg_rand_05 = zeros(1, n_el);
% Generate randoms
for i = 1:n_el
    % Left branch
    if (u_rand(i) < 0.5)
        gg_rand_05(i) = -(1 / (1 * lambda)) * ...
            (1 + lambertw(-1, -2 * u_rand(i) / exp(1)))^2;
    % Center
    elseif (u_rand(i) == 0.5)
        gg_rand_05(i) = -(1 / (1 * lambda)) * ...
            (1 + lambertw(-1, -2 * u_rand(i) / exp(1)))^2;
        gg_rand_05(i) = gg_rand_05(i) + (1 / (1 * lambda)) * ...
            (1 + lambertw(-1, -2 * (1 - u_rand(i)) / exp(1)))^2;
    % Right branch
    else
        gg_rand_05(i) = (1 / (1 * lambda)) * ...
            (1 + lambertw(-1, -2 * (1 - u_rand(i)) / exp(1)))^2;
    end
end
```

REFERENCES

[1] N. Ahmed, T. Natarajan, and K. R. Rao, "Discrete Cosine Transform," *IEEE Transactions on Computers*, 90-93, Jan 1974.

[2] Akansu, Ali N. and Haddad, Richard A., *Multiresolution Signal Decomposition, Transforms, Subbands, Wavelets,* Second Edition, San Diego, CA, Academic Press, 2001.

[3] W.-H. Chen, C. H. Smith, and S. Fralick, "A Fast Computational Algorithm for the Discrete Cosine Transform," *IEEE Transactions on Communications* 25, 1004–1009, Sep 1977.

[4] M. J. Narasimha and A. M. Peterson, "On the computation of the discrete cosine transform," *IEEE Transactions on Communications* 26 (6), p. 934–936 (1978).

[5] Y. Arai, T. Agui, and M. Nakajima, "A fast DCT-SQ scheme for images," *Transactions of the IEICE* 71 (11), 1095–1097 (1988).

[6] E. Feig, S. Winograd. "Fast algorithms for the discrete cosine transform," *IEEE Transactions on Signal Processing* 40 (9), 2174-2193 (1992).

[7] J. Makhoul, "A fast cosine transform in one and two dimensions," *IEEE Transactions on Acoustic Speech Signal Processing* 28 (1), 27-34 (1980).

[8] Jain, Anil K., *Fundamentals of Digital Image Processing,* Englewood Cliffs, NJ, Prentice Hall, 1989.

[9] ISO/IEC 10918-1:1994, Information technology -- Digital compression and coding of continuous-tone still images: Requirements and guidelines, February 15, 1994.

[10] W. C. Fong, S. C. Chan, and K. L. Ho, "Designing JPEG quantization matrix using rate-distortion approach and human visual system model," *Proceedings of the IEEE International Conference on Communications*, 1997.

[11] M. Robertson and R. Stevenson, "DCT quantization noise in compressed images," *IEEE Transactions on Circuits and Systems for Video Technology*, vol. 15, pp. 27–38, Jan. 2005.

[12] R. Reininger and J. Gibson : "Distribution of the two-dimensional DCT coefficients for images," *IEEE Transactions on Communications* 31 (6) 1983.

[13] F. Benford, "The Law of Anomalous Numbers," *Proceedings of the American Philosophical Society* 78, 551-572, 1938.

[14] E. W. Weisstein, "Kolmogorov-Smirnov Test." From *MathWorld*--A Wolfram Web Resource. http://mathworld.wolfram.com/Kolmogorov-SmirnovTest.html, retrieved March 22, 2010.

[15] F. Muller, "Distribution Shape of Two-Dimensional DCT Coefficients of Natural Images," *Electronics Letters*, 29, Oct. 1993, 1935–1936.

[16] E. Lam, J. A. Goodman, "A Mathematical Analysis of the DCT Coefficient Distributions for Images," in *IEEE Transactions on Image Processing* 9(10), 1661-1666 (2000).

[17] J.-H. Chang, J. W. Shin, N. S. Kim, S. K. Mitra, "Image Probability Distribution Based on Generalized Gamma Function," *IEEE Signal Processing Letters*, 2005.

[18] M. Barni, F. Bartolini, A. Piva, and F. Rigacci, "Statistical modeling of full frame DCT coefficients," in *Proceedings of EUSIPCO'98*, Rhodes, Greece.

[19] J. E. Gray, "An Exact Determination of the Probability Density. Function Under Coordinate Transformations," *The First IEEE conference on Aerospace Control Systems*, 1993.

[20] B. Widrow, I. Kollár, and M.C. Liu, "Statistical theory of quantization," *IEEE Transactions on Instrumentation and Measurement*, 45(2):353-361, April 1996.

[21] Gerald, Curtis F. and Wheatley, Patrick O., *Applied Numerical Analysis,* Seventh Edition, Addison Wesley, 2003.

[22] Z. Fan and R. de Queiroz, "Identification of bitmap compression history: JPEG detection and quantizer estimation," *IEEE Transactions on Image Processing*, vol. 12, pp. 230–235, Feb. 2003.

[23] E. W. Weisstein, "Benford's Law." From *MathWorld*--A Wolfram Web Resource. http://mathworld.wolfram.com/BenfordsLaw.html, retrieved March 22, 2010.

[24] E. W. Weisstein, "Laplace Distribution." From *MathWorld*--A Wolfram Web Resource. http://mathworld.wolfram.com/LaplaceDistribution.html, retrieved March 22, 2010.

[25] A. Hjorungnes, J. Lervik, and T. Ramstad, "Entropy coding of composite sources modeled by infinite Gaussian mixture distributions," in *IEEE Digital Signal Processing Workshop* pages 235--238, 20-24 January 1996.

[26] H. Engel and C. Leuenberger, "Benford's law for exponential random variables," *Statistics & Probability Letters*, vol. 63, no. 4, pp. 361-365, July 2003.

[27] D. Fu, Y.Q. Shi, and W. Su, "A generalized Benford's law for JPEG coefficients and its applications in image forensics," in *Proceedings of SPIE, Security, Steganography and Watermarking of Multimedia Contents IX*, San Jose, USA, January 2007.

[28] F. Zou, Z. Lu and H. Ling, "Statistical model of quantized DCT coefficients," in *Proceedings of the ICSP '04, 7th International Conference on Signal Processing* 2004.

[29] *USC SIPI Image Database.* http://sipi.usc.edu/database/database.cgi?volume=misc, retrieved March 30, 2010.

[30] E. W. Weisstein, "Chi-Squared Test." From *MathWorld*--A Wolfram Web Resource. http://mathworld.wolfram.com/Chi-SquaredTest.html, retrieved March 30, 2010.

[31] F. Chapeau-Blondeau, A. Monir, "Numerical evaluation of the Lambert W function and application to generation of generalized Gaussian noise with exponent ½," *IEEE Transactions on Signal Processing* 50, 2160-2165 (2002).

[32] J. D. Eggerton, M. D. Srinath, "Statistical distributions of image DCT coefficients," *Computers & Electrical Engineering*, Volume 12, Issues 3-4, 1986, Pages 137-145, ISSN 0045-7906, DOI: 10.1016/0045-7906(86)90005-4.

[33] Z. Lin, J. He, X. Tang, and C. Tang, "Fast, automatic and fine-grained tampered JPEG image detection via DCT coefficient analysis," *Pattern Recognition.* 42, 11 (Nov. 2009), 2492-2501.

[34] R. Neelamani, R. L. de Queiroz, Z. Fan, R. G. Baraniuk, "JPEG compression history estimation for color images," *International Conference on Image Processing* (3) 2003.

[35] E. W. Weisstein, "Binary Search." From *MathWorld*--A Wolfram Web Resource. http://mathworld.wolfram.com/BinarySearch.html, retrieved March 31, 2010.

[36] F. Perez-Gonzalez, G. Heileman, and C. T. Abdallah, "Benford's law in image processing," in *Proceedings of the IEEE International Conference on Image Processing*, San Antonio, TX, USA, September 2007, pp. 169-176.

[37] P. Diaconis, "The distribution of leading digits and uniform distribution mod 1," *The Annals of Probability*, vol.5, pp. 72–81, 1977.

[38] E. W. Weisstein, "Lambert W-Function." From *MathWorld*--A Wolfram Web Resource. http://mathworld.wolfram.com/LambertW-Function.html, retrieved April 05, 2010.

[39] J. Wang, B.-H. Cha, S. Cho, and C.-C. Jay Kuo, "Understanding Benford's Law and its vulnerability in image forensics," in *Proceedings of the IEEE International Conference on Multimedia and Expo, MSATC*, New York City, NY, Jun. 2009, pp. 1568—1571.

[40] M. Püschel and J. M. Moura, "The Algebraic Approach to the Discrete Cosine and Sine Transforms and Their Fast Algorithms," *SIAM Journal on Computing,* 32, 5 (May. 2003), 1280-1316.

[41] G. Strang, "The Discrete Cosine Transform," *SIAM Review*, 41 (1999), pp. 135-147.

[42] W. K. Pratt, *Digital Image Processing*, New York: Wiley-Interscience, 1978, chapter 10.

[43] A. G. Tescher, "Transform image coding," in *Advances in Electronics and Electron Physics.* Suppl. 12. New York: Academic, 1979, pp. 113-115.

[44] H. Murakami, Y. Hatori, and H. Yamamoto, "Comparison between DPCM and Hadamard transform coding in the composite coding of the NTSC color TV signal," *IEEE Transactions on Communications*, vol COM-30, pp. 469-479, Mar. 1982.

[45] S. Nadarajah, "A generalized normal distribution," *Journal of Applied Statistics*. 32(7), pp. 685-694, 2005.

[46] E. W. Stacy, "A Generalization of the Gamma Distribution," *The Annals of Mathematical Statistics*. Vol. 33, No. 3, pp. 1187-1192, September, 1962.

[47] I. J. Cox, J. Kilian, F. T. Leighton, T. Shamoon, "Secure spread spectrum watermarking for multimedia," *IEEE Transactions on Image Processing*, Vol. 6, pp. 1673-1687, 1997.

[48] Titchmarsh, Edward C., Heath Brown, David R., *The Theory of the Riemann-Zeta function*, Second Edition, Oxford University Press, Oxford, 1986.

[49] Kay, Steven M., *Intuitive probability and random processes using MATLAB*, First Edition, Springer Science and Business Media, New York, NY, 2005.

[50] Kreyszig, Erwin, *Differential Geometry,* First Edition (Paperback), Dover Publications, 1991.

[51] T. P. Hill, "A Statistical Derivation of the Significant-Digit Law," *Statistical Science*, Vol. 10, pp. 354-363, 1996.

[52] Titterington, D., Smith, A. F. M, and Makov, U.E., *Statistical Analysis of Finite Mixture Distributions*, First Edition, John Wiley & Sons, 1985.

[53] S. Kakade, G. Shaknarovich, "Dimensionality Reduction,", *http://ttic.uchicago.edu/~gregory/courses/LargeScaleLearning/lectures/kl_pca.pdf*, retrieved April 08, 2010.

[54] *Critical Values of the Chi-square Distribution.* http://www.itl.nist.gov/div898/handbook/eda/section3/eda3674.htm, retrieved April 24, 2010.

[55] *Pearson Chi Square Hypothesis Test.* http://www.mathworks.com/matlabcentral/fileexchange/3596-pearson-chi-square-hypothesis-test, retrieved April 22, 2010.

[56] *Two Sample Kolmogorov Smirnov Test.* http://www.mathworks.com/access/helpdesk/help/toolbox/stats/kstest2.html, retrieved April 10, 2010.

[57] *Lambert W Function.* http://www.mathworks.com/matlabcentral/fileexchange/6909, retrieved March 3, 2010.